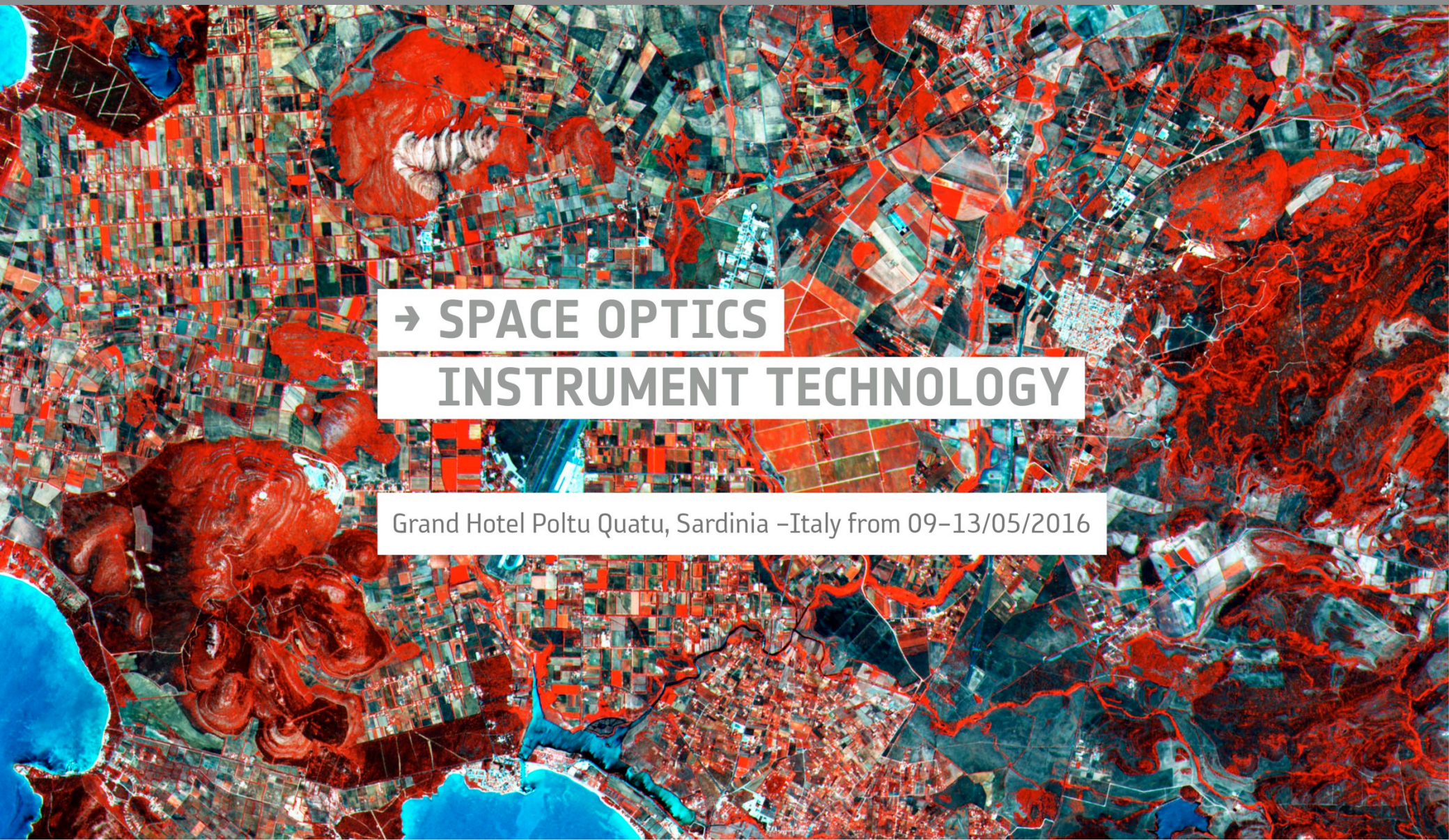

→ SPACE OPTICS INSTRUMENT TECHNOLOGY

Grand Hotel Poltu Quatu, Sardinia –Italy from 09–13/05/2016

ACTIVE OPTICS AND LARGE MIRROR TECHNOLOGIES

David Redding
JPL Fellow
Jet Propulsion Laboratory, California Institute of Technology

Overview of this lecture

- Part 1
  - Prologue: Adaptive optics for compensating atmospheric turbulence effects; active optics for space telescopes
  - Modeling and wavefront control: establishing notation
  - Large ULE mirrors
  - Active mirrors, small and large
  - Wavefront sensing and control: initializing a segmented space telescope
- Part 2
  - Wavefront sensing and control: fine phasing for segmented and monolithic space telescopes
  - Metrology and wavefront control
  - Conclusion: Looking to the future at NASA

Off-Axis WF Control with a DM: Angle Error 1

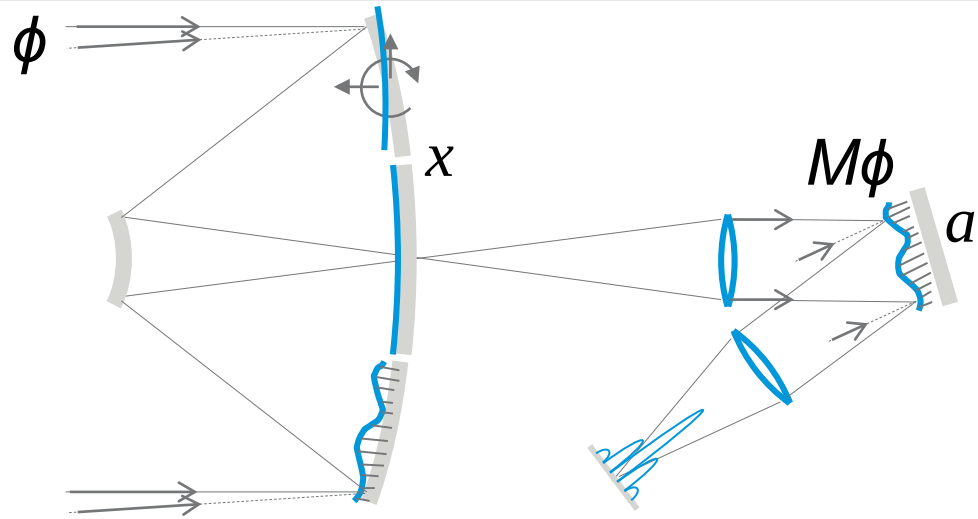

- A simplified model of a DM-controlled telescope:
  - DM is at a pupil imaging the PM, and is perfectly registered to the PM
  - PM (only) aberrations are x
  - DM actuator controls are a
  - Magnification is $M = D_{PM}/D_{DM}$
- From the earlier discussion, the on-axis WF w is:

$$w = \frac{\partial w}{\partial x} x + \frac{\partial w}{\partial a} a$$

- For a field angle ϕ at the PM, the angle of incidence at the DM is $M\phi$
  - The analysis of McComas and Friedman (2002) shows that an increasing angle of incidence ϕ decreases the impact of a mirror deflection by $\cos(\phi)$
  - Thus the WF w becomes:

$$w = \cos(\phi)\frac{\partial w}{\partial x} x + \cos(M\phi)\frac{\partial w}{\partial a} a$$

Off-Axis WF Control with a DM: Angle Error 2

– The WF control to null w at a (single) field point ϕ_1 is:

$$a = -\frac{\cos(\phi_1)}{\cos(M\phi_1)}\left[\frac{\partial w}{\partial a}\right]^{+} w = -\frac{\cos(\phi_1)}{\cos(M\phi_1)}\left[\frac{\partial w}{\partial a}\right]^{+}\frac{\partial w}{\partial x}x$$

– The post-control WF at ϕ_1:

$$w_{\phi_1} = \left\{\cos(\phi_1)I - \cos(M\phi_1)\frac{\cos(\phi_1)}{\cos(M\phi_1)}\frac{\partial w}{\partial a}\left[\frac{\partial w}{\partial a}\right]^{+}\right\}\frac{\partial w}{\partial x}x \cong 0$$

– The post-control WF at some other ϕ_2:

$$w_{\phi_2} = \left\{\cos(\phi_2)I - \cos(\phi_1)\frac{\cos(M\phi_2)}{\cos(M\phi_1)}\frac{\partial w}{\partial a}\left[\frac{\partial w}{\partial a}\right]^{+}\right\}\frac{\partial w}{\partial x}x$$

$$\cong \left[\cos(\phi_2) - \cos(\phi_1)\frac{\cos(M\phi_2)}{\cos(M\phi_1)}\right]w$$

– If the control is on-axis case, $\phi_1 = 0$, and:

$$w_{\phi_2} \cong \left(\cos(\phi_2) - \cos(M\phi_2)\right)w$$

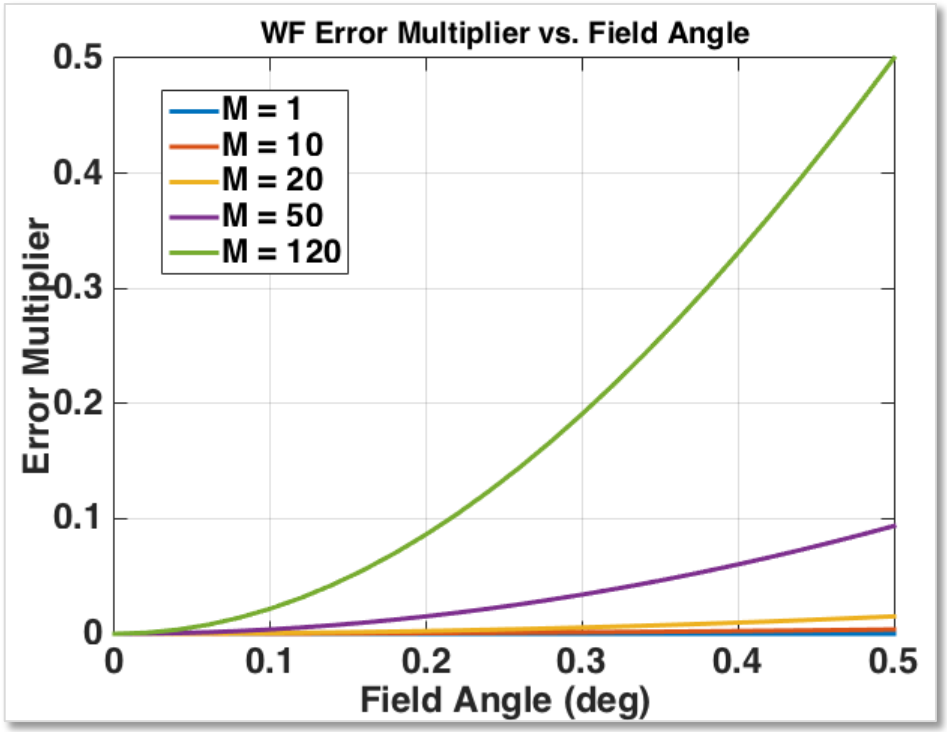

– Thus, for field angles away from the control point, the initial error leaks back in by ~ the factor $(\cos(\phi_2) - \cos(M\phi_2))$

Wavefront Sensing and Control:

Fine Phasing for Segmented and Monolithic Space Telescopes

WF Sensing for Fine Phasing and Figure Control

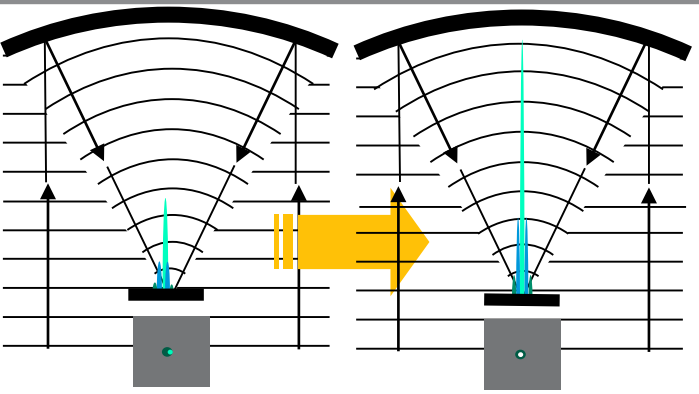

WFS&C Modes			Segmented Telescope		Monolithic Telescope		TRL
Initialization	Coarse Phasing	Dispersed-Fringe Sensing	>100 um piston error	<200 nm piston error	–	–	6
		Shack-Hartmann Sensing	>10 um figure error	<50 nm figure error	5 um	20 nm piston error	6
	Fine Phasing	Image-based WFS: MGS	>15 um	<3 nm	>15 um	<3 nm	6
		WFC	>15 um	<10 nm	>15 um	<10 nm	6

Image-based WF sensing has high accuracy

Shack-Hartmann WF sensing has high dynamic range

} *Use both*

Method	Instrument	Common mode reject	Accuracy	Range	Spatial resolution	Noise & jitter	Resolves piston?
Image-based	Any camera, any field	Yes	Excellent	Med (50 um)	High	Robust	Yes (multi-color)
Hartman sensor	Dedicated or flip-in	No	Good	High (1 mm)	Med	Robust	No
Shearing interf.	Dedicated	No	Good	Med	High	Robust	Maybe
Phase-shifting interf.	Dedicated	No	Excellent	Med	High	Sensitive	Yes (multi-color)

Shack-Hartmann WF Sensing

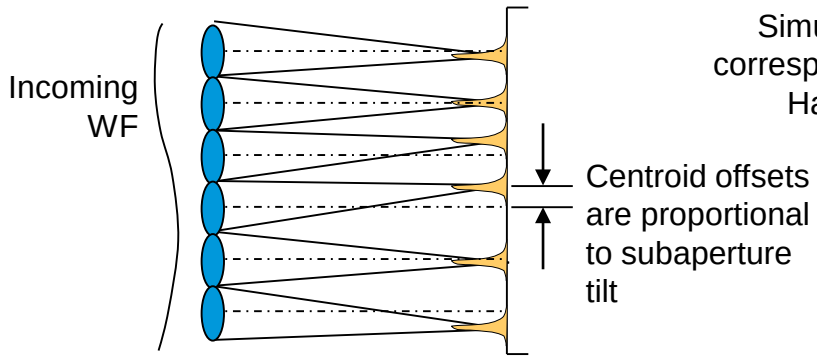

Simulated WF with corresponding Shack-Hartmann image

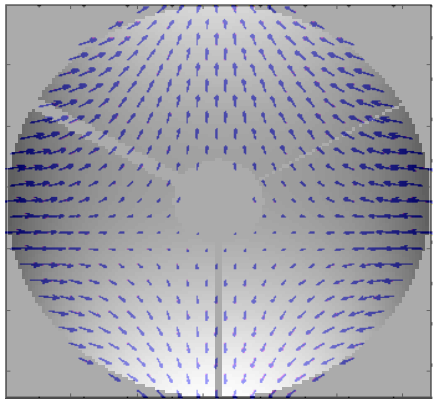

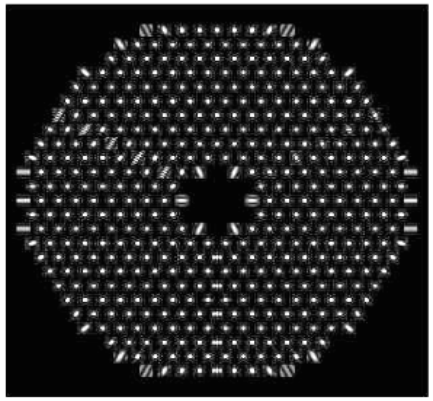

- A Shack-Hartmann sensor places a lenslet array at a plane conjugate to the WF error source -- the PM in our case -- and focused on a detector
- Each subaperture lenslet samples the WF in the corresponding patch of the WF
- Lenslet spot image shifts are proportional to the average tilt in the subaperture
- The WF control calculations invert actuator “poke” patterns to map WF error to actuator space
- New actuator commands are computed to restore ideal spot pattern

AHM Wavefront Sensing and Control "Ops" Demonstration

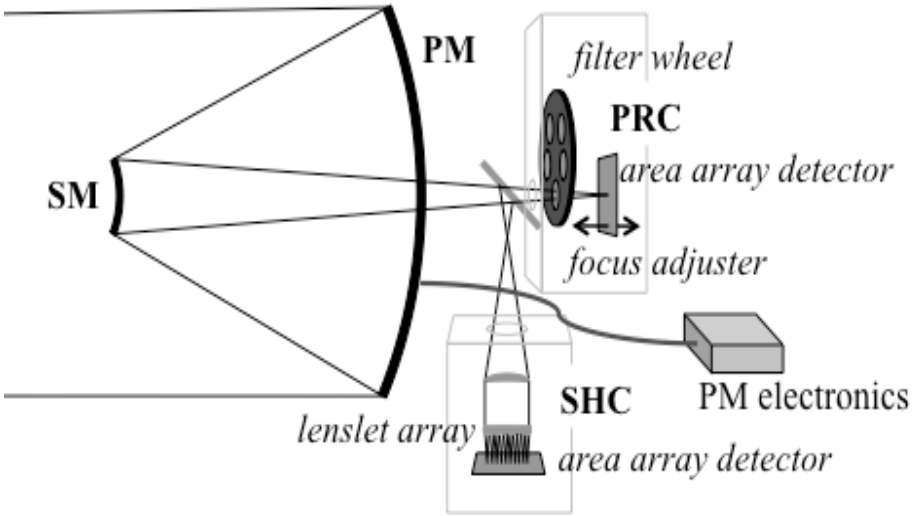

- WFS&C Elements
  - Imaging Camera ("PRC") with area array detector and narrow-band filter
  - Focus adjust mechanism
  - PM actuator electronics
  - Shack-Hartmann Camera ("SHC"), with area array detector, pupil imaging lens and lenslet array

- WFS&C Operations are performed while observing a "star" – a broad-band fiber-fed source
  - *Initialization WFS&C* uses SHC for large WF capture range (> 30), and PRC for high resolution and high accuracy
    - Use of PRC Imaging Camera "science camera" avoids non-common path WFE
  - *Maintenance WFS&C* uses PRC only, with minimal/no impact on science ops
    - Run periodically (1/day to 1/week rate) to keep WFE within spec
- Image-based WF sensing uses the Modified Gerchberg-Saxton (MGS) phase retrieval software

SHC Large Capture Example

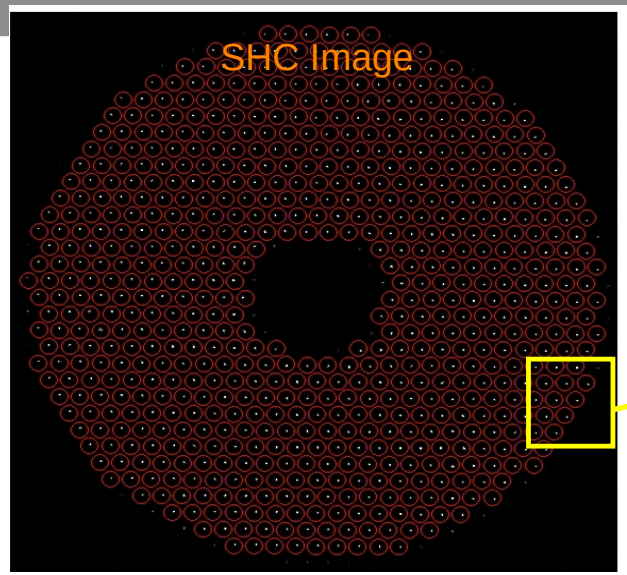

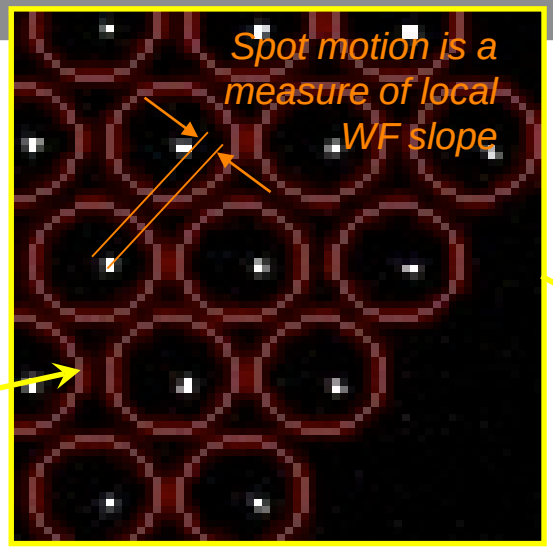

– *Data taken using white light source and open filter*

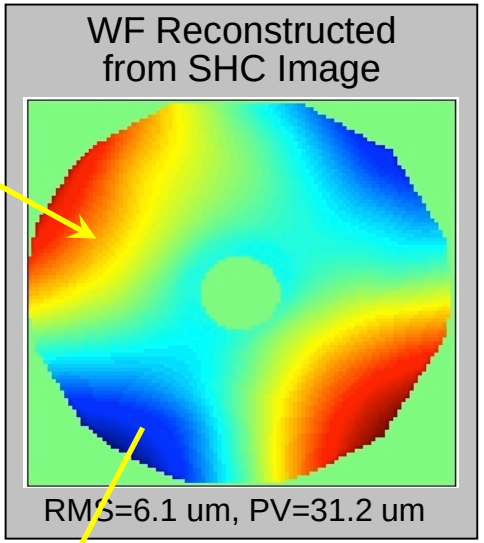

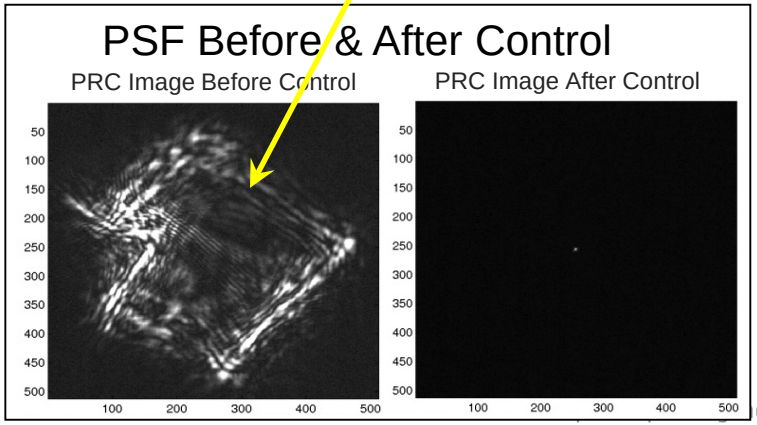

- *WFS&C Experiment* used an AHM, portable SHC and PRC, and autocollimating flat
- SHC results show large capture range WF control
  - Initial SHC WF error was 31 um (P-V), 6 um (RMS), double-pass
- After SHC control, WF error was 80 nm RMS in the SHC, 116 nm in the PRC

WF Sensing Using Defocussed Images

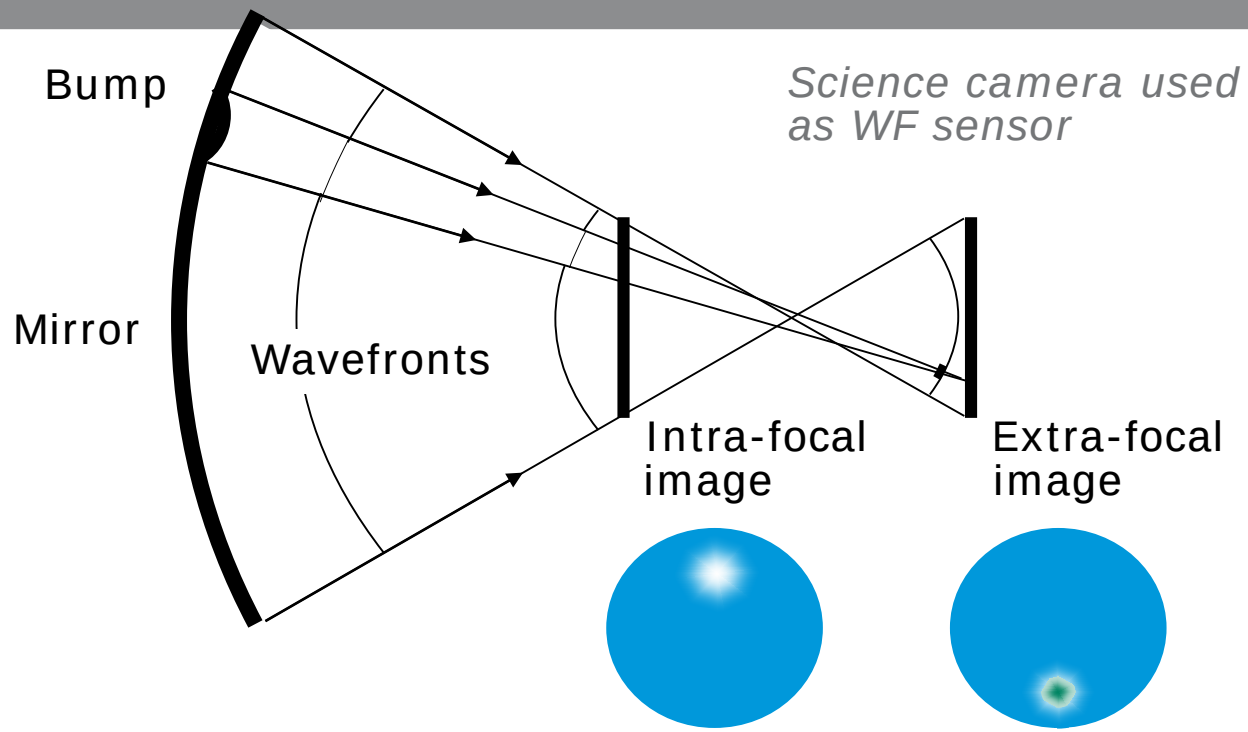

- Bumps on a mirror surface shift the focus of patches of the beam
- These show up as bright spots on one side of focus and dark spots on the other
- The pupil and defocussed images are related by Fourier transforms
- Iterative processing of multiple defocussed images correlates the intensity variations in each, derives common WF phase map

Gerchberg-Saxton Iterative-Transform PR

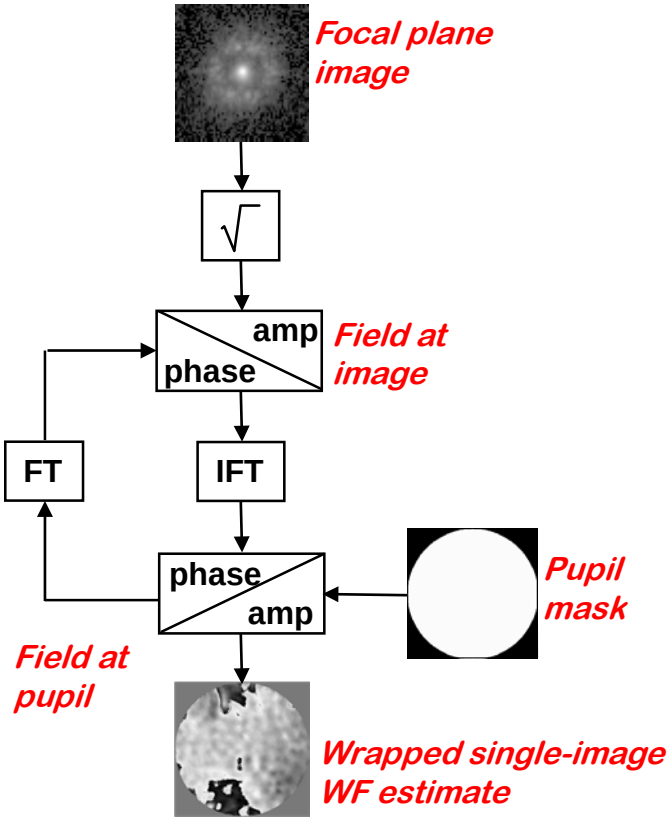

- Imaging system *f*/no., pixel size, aperture mask, λ: all known
- Starts with a random guess at the phase in the exit pupil
- Iterates on pupil complex field until changes between iterates are small
- Pupil phase is angle of pupil field
- Produces high-resolution pupil map which matches image

But…

- Solution non-unique
- In-focus image susceptible to noise

Modified Gerchberg-Saxton Inner Loop

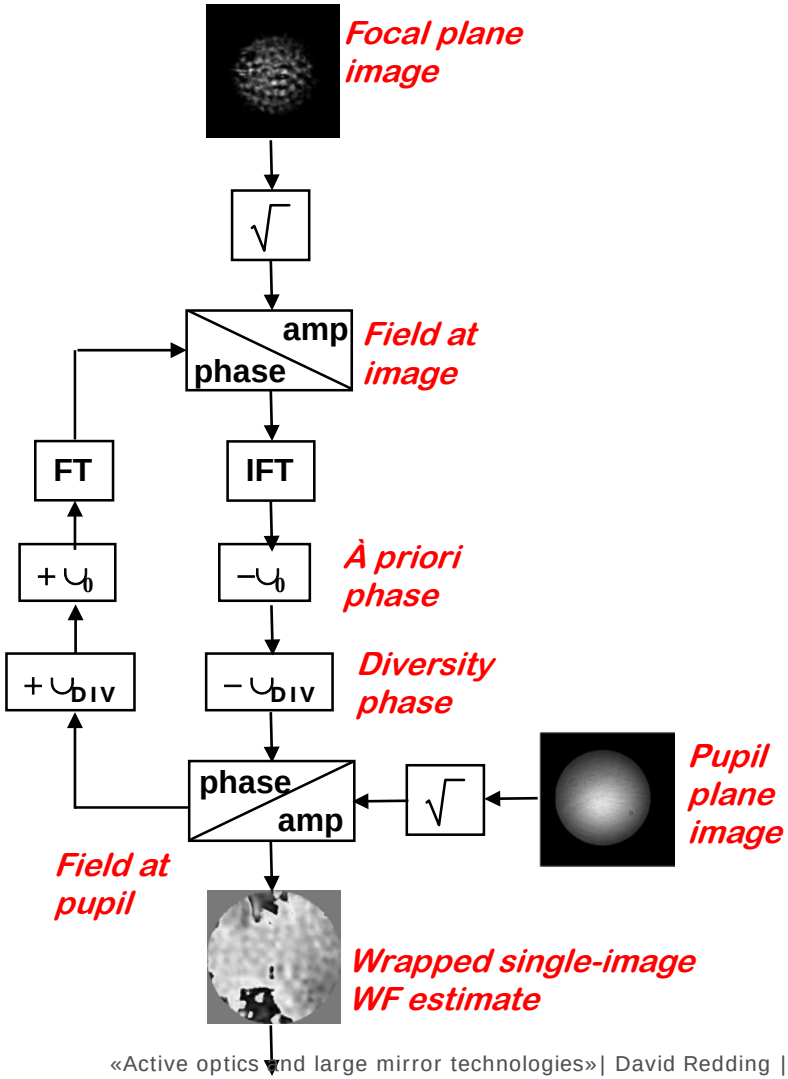

- Pupil image data can replace mask, if available
  - Important if obscurations not precisely known
- Defocussed images improve visibility of aberrations
  - Spread out effects over many pixels
  - Reduce impact of jitter, other blurring
  - Reduce contrast between low, high-f effects
- Subtract known phase (ψ_0, ψ_{DIV}) from the phase iteration
  - ψ_0 is systematic across all images, ψ_{DIV} is difference between images
  - Reduces the iteration dynamic range
  - Provides port for other feedback loops

MGS Outer Loop

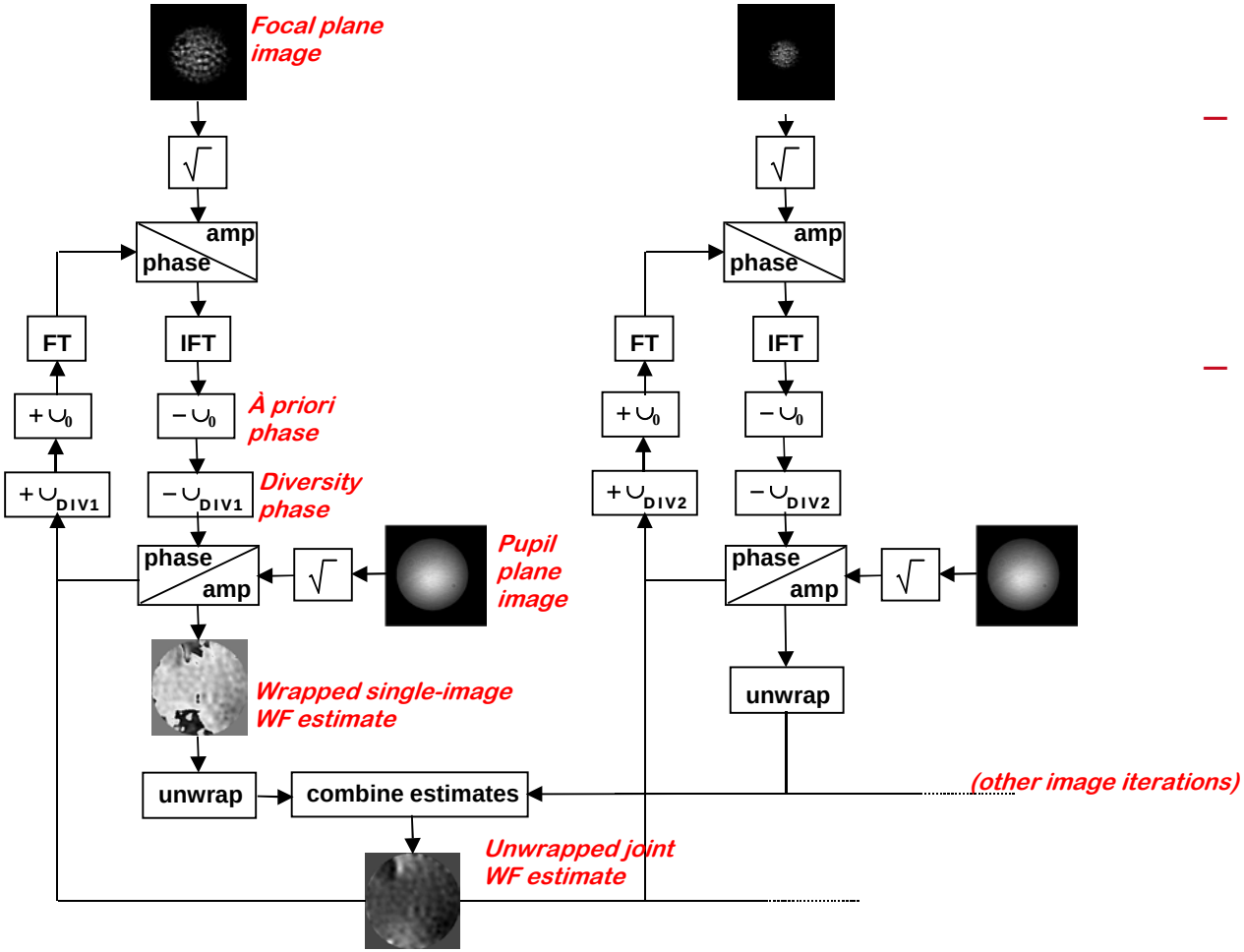

- Multiple images provide more data without introducing new unknowns, provided υ_{DIV} is accurately known
- Phase unwrapping helps estimation when WFE > $\lfloor$
  - Joint unwrapping allows use of "voting" between multiple single-image estimates to help resolve unwrapping artifacts
  - Unwrapping can also occur at the next level of iteration…

MGS Outer-Outer Loop "Feedback"

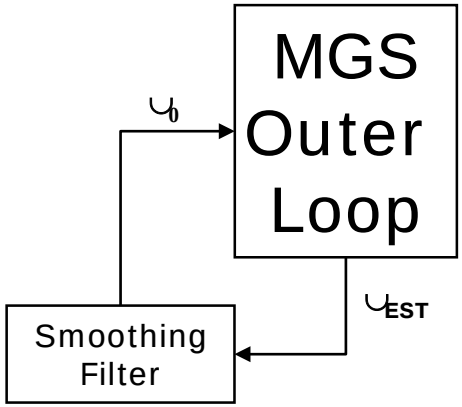

- "Outer-outer loop" restarts the MGS Outer Loop, with a new random starting guess, but an updated à priori phase Θ_0
- Allows an opportunity to "clean up" the phase unwrapping errors that may have crept into the phase estimate
  - By smoothing the prior and restarting
    - By hand if necessary – MGS has a GUI to facilitate making new Θ_0
- Successively replacing à priori phase with previous estimates reduces range of iterating phase
  - Turns MGS into a null-seeking algorithm
- Improves overall accuracy and convergence

Outer-Outer Loop, Illustrated

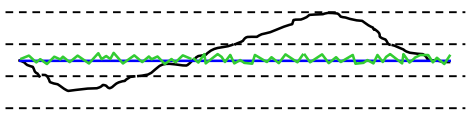

- Initial state
  - The as-yet unknown true phase is the black curve
  - Iterating phase (green curve) initialized to random values
  - Prior phase Θ_0(blue curve) initialized to 0

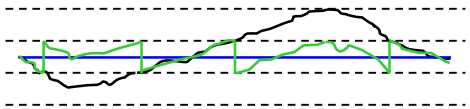

- After convergence of the inner loops (first iteration of the outer loop)
  - Iterating phase approximates the wrapped true phase

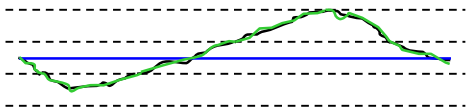

- After unwrapping the iterating phase (first iteration of the outer loop)
  - Iterating phase approximates the true phase

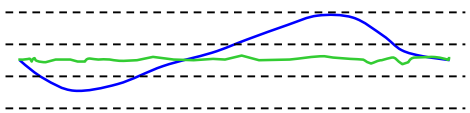

- After convergence of the outer loop (first iteration of the outer-outer loop)
  - Prior Θ_0 phase is set equal to the smoothed, unwrapped iterating phase
  - Iterating phase is now much smaller, << 1 wave

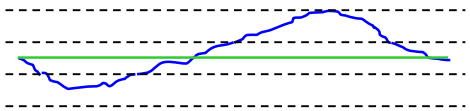

- After convergence of the outer-outer loop
  - Prior phase is equal to the true phase
  - Iterating phase is zero

Modified Gerchberg-Saxton (MGS) Algorithm

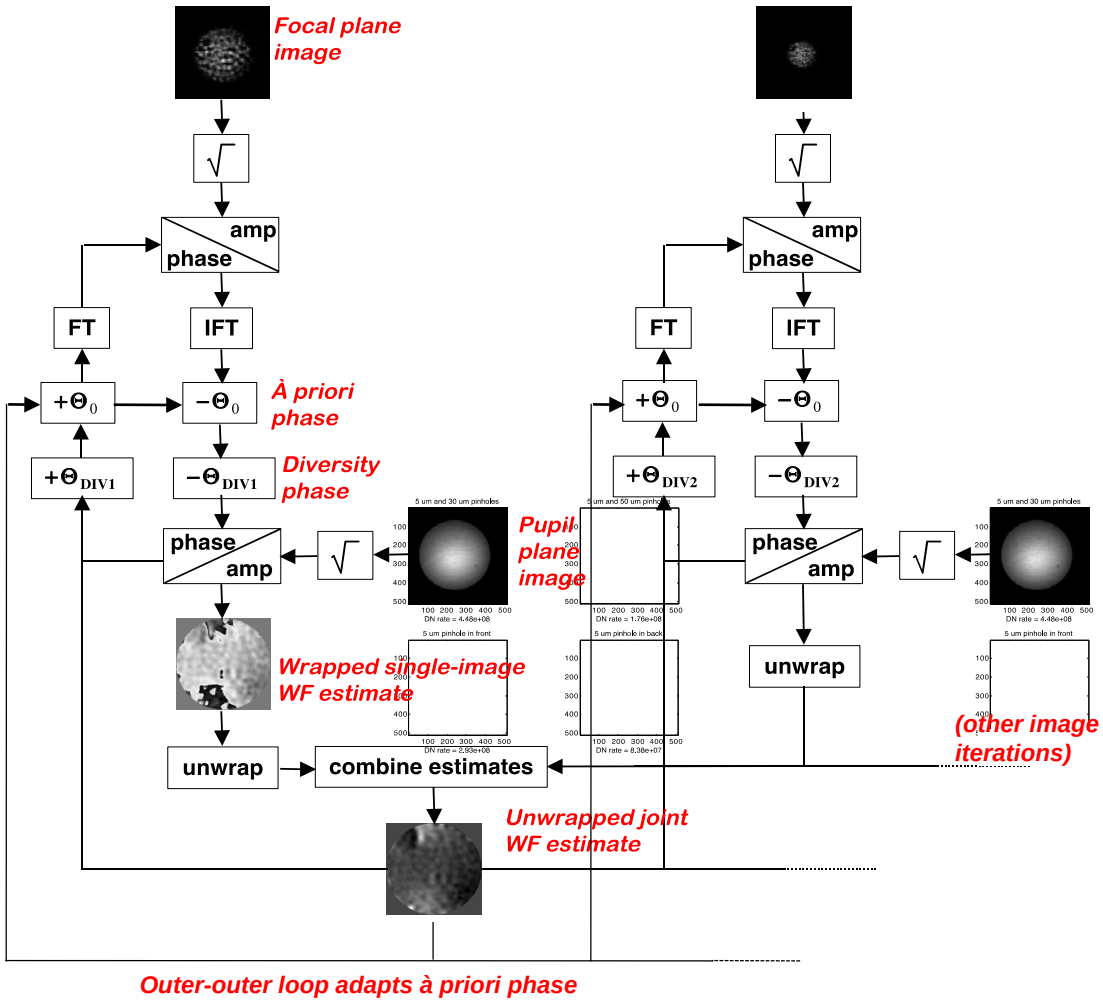

- Solves for a WF estimate
- Inputs:
  - n images, taken at different known focus and field locations, at known monochromatic wavelengths
  - Pupil image or equivalent
- Algorithm:
  - Image pre-processing assures model consistency
  - Iterates phase between pupil and the various focal planes
- Output:
  - Estimated WF OPD w_{est}
- Next step: use w_{est} to determine u

Fine Phasing Example: MGS Phase Retrieval

- This example uses a 9-segmented “petal” aperture
- Three simulated images are used, 1 in-focus and 2 defocused
- Top row of the figure are simulated data exposures
- Second row shows the estimates, being driven to match the data
- Third row shows the differences, decreasing with each iteration
- Pupil OPD estimate converges in ~10 iterations

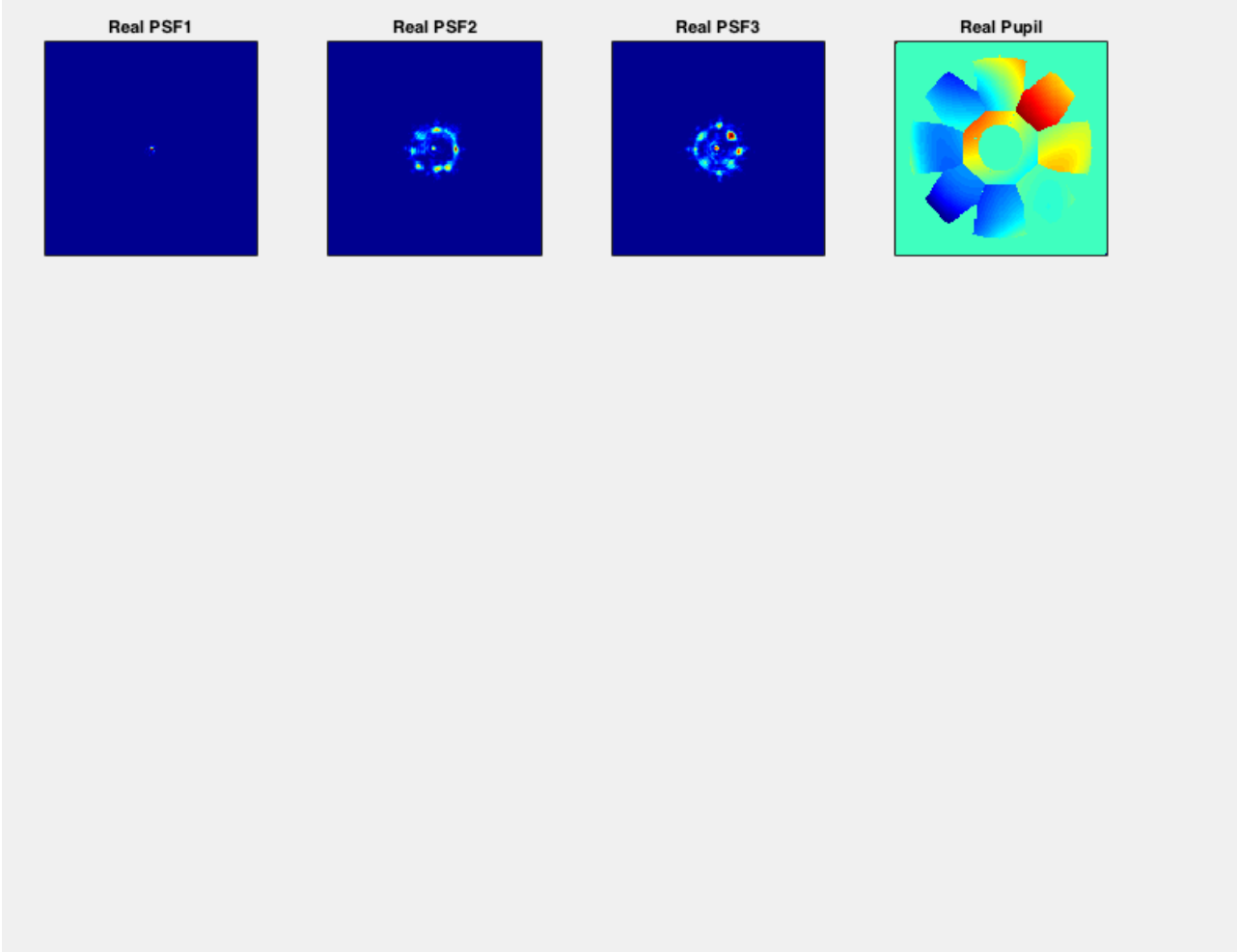

Fine Phasing Example: RB and DM Control

- WF Control uses the converged WF estimate first to set PM segment RBAs
- RB control solution uses both RB and DM sensitivities
- Result matches segment edges well
- Then DM-only control completes the job

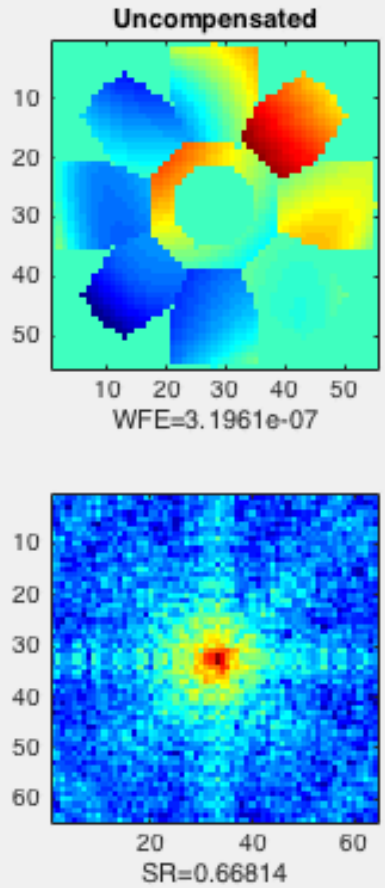

PRC Fine Control Example

Defocussed PRC Images

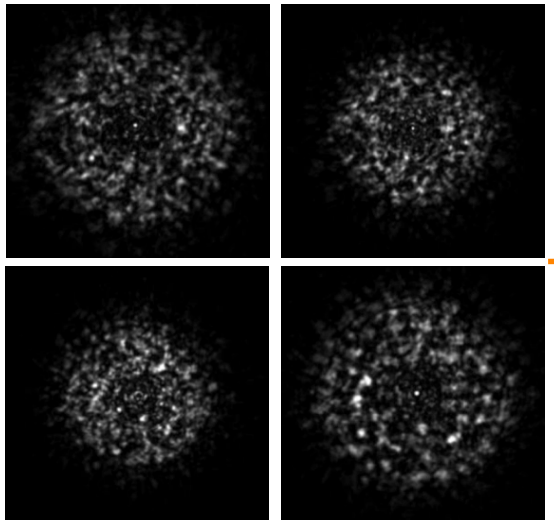

– *Data taken using white light source*
– *Narrow-band Filter*

Control used 18% of capacity,9 V on average

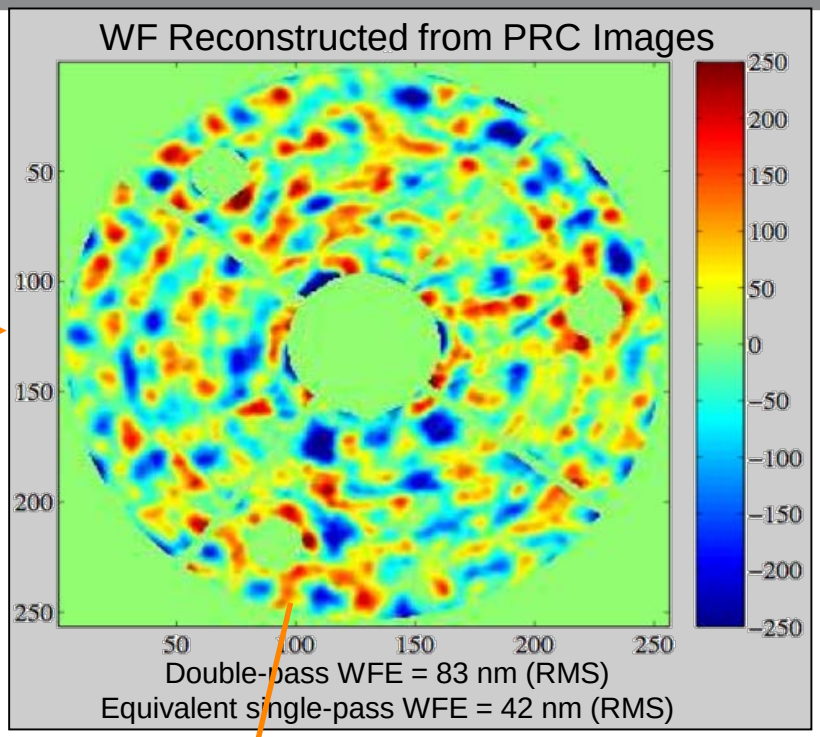

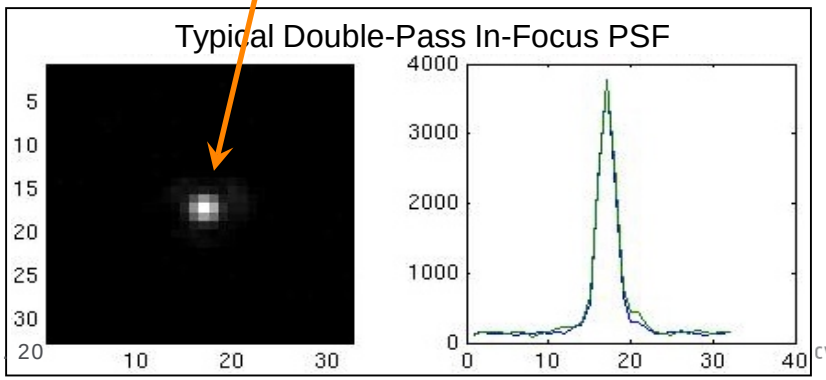

- *WFS&C Experiment* continues using the PRC imaging camera for *image-based WF sensing*
- One or more iterations of control to achieve diffraction-limited WFE
- Performance is confirmed by the high-quality "single-pixel" in-focus PSF

Active Mirror PSFs

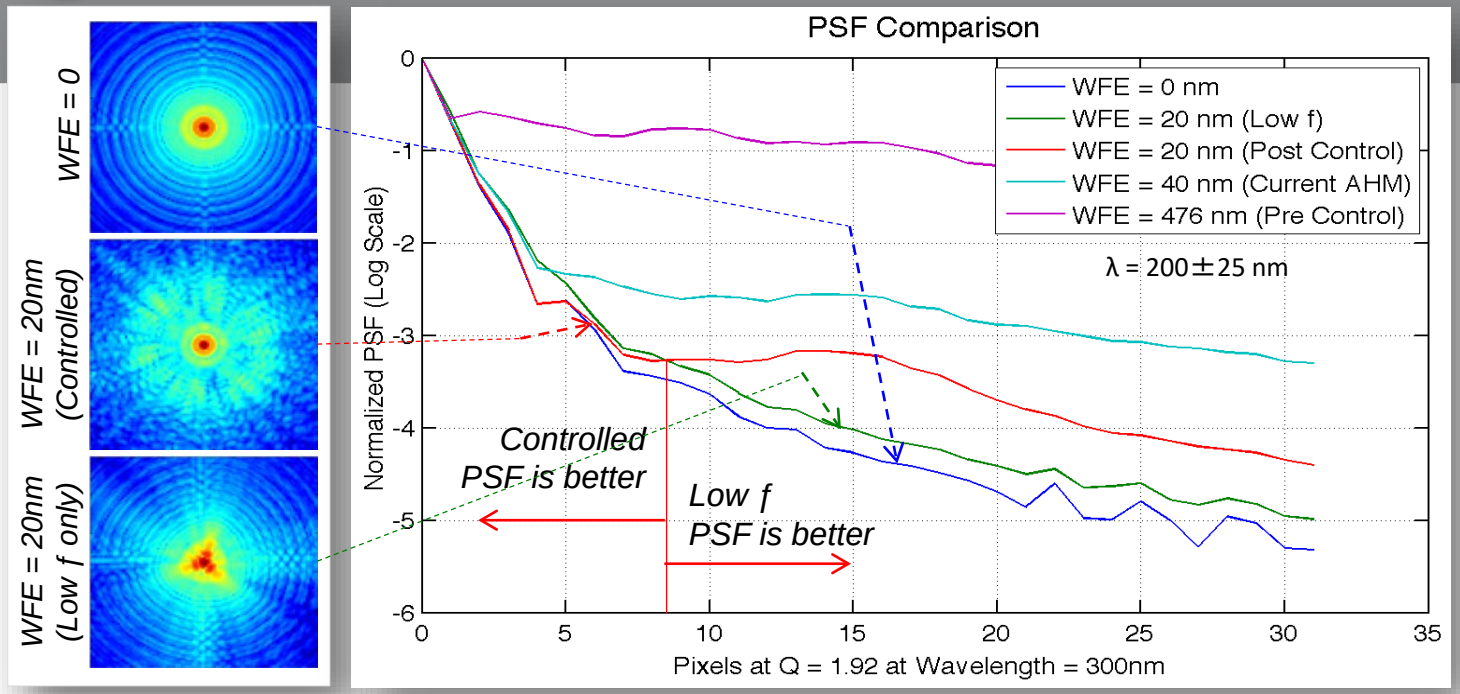

Simulated narrow-band PSFs at 200nm wavelength, for a UV telescope optimized for 300nm wavelength

- *Nominal WFE = 20nm*
- *Detector is critically sampled at λ = 300nm*
- *400 actuators for control case*

PSFs are plotted with a log stretch

- AHMs, like Deformable Mirrors generally, have a different distribution of WFE vs. *f*, compared to conventional optics
  - Lower error in the low spatial frequencies – and much smaller absolute error
  - Higher error at and beyond the actuator spatial frequency
- This results in a tighter PSF core, but a raised “halo” in the sidebands
- Post-control PSF quality is a function of actuator density and initial WFE, and can be engineered to meet science requirements

Sparse 3-Segment Testbed Fine Phasing

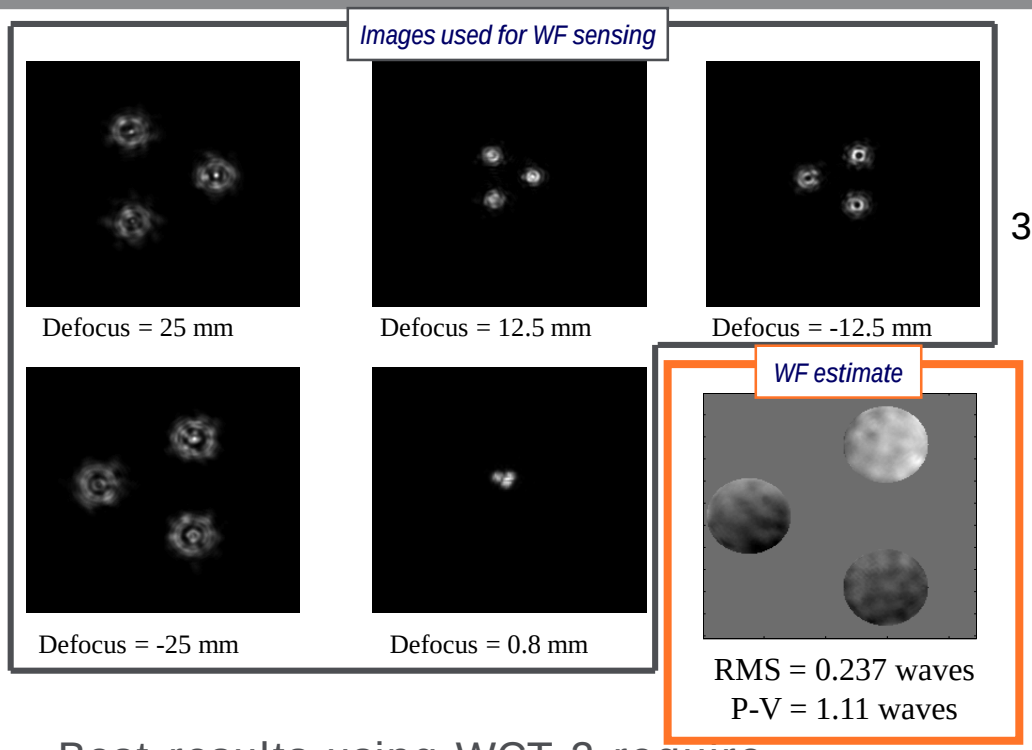

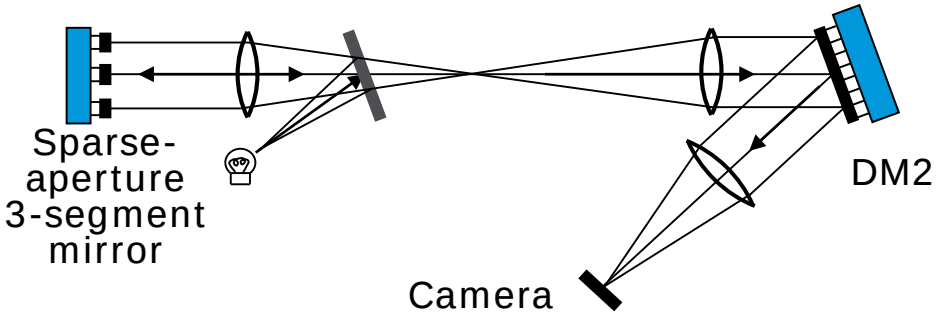

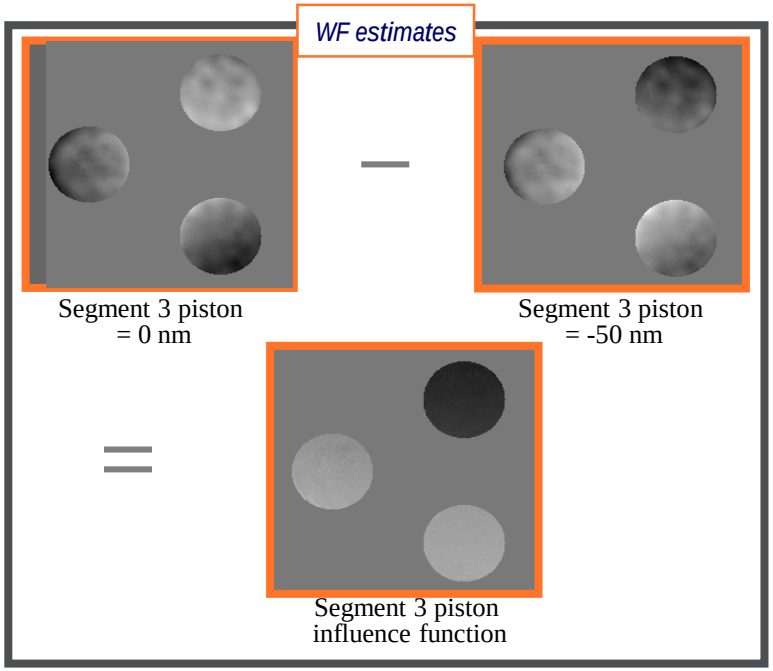

- Best results using WCT-2 require inclusion of at least 1 nearly in-focus image
- Goal: Measure segment piston influence function by “poking” actuators and subtracting WFs

DM Control of Segment SFE

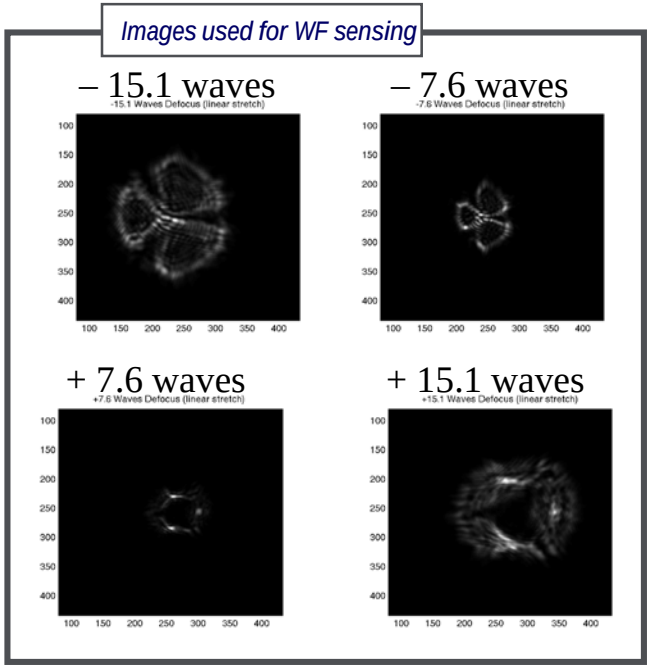

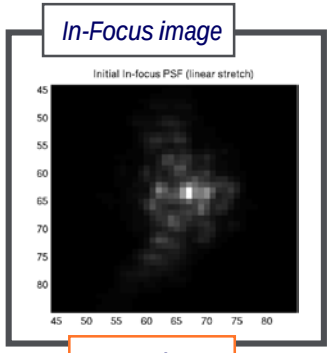

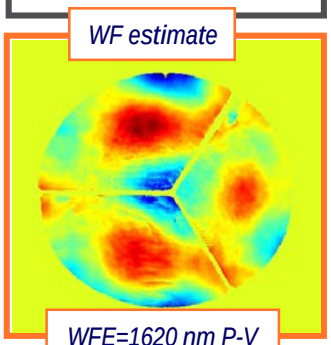

WFE=1620 nm P-V
(270 nm RMS)

- Goal: to correct segment Surface Figure Errors (SFE) using a DM
- Initial WFE 1620 nm peak-to-valley, 270 nm RMS
- After DM and segment control, WFE reduced to 54 nm RMS

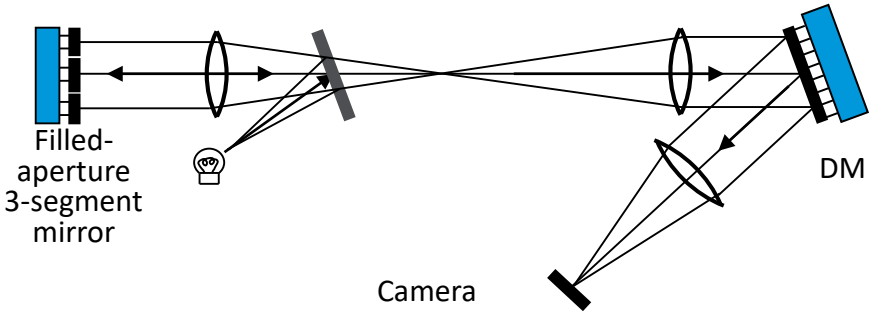

- JWST project WCT-3 testbed

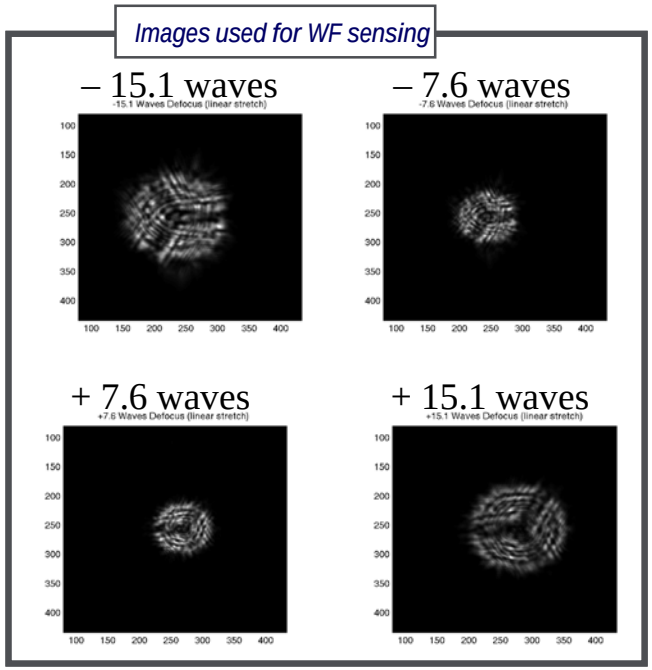

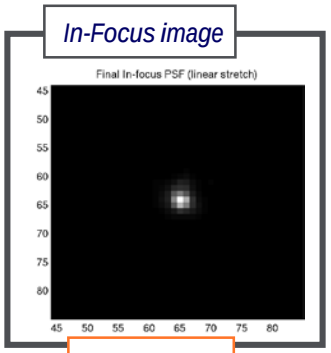

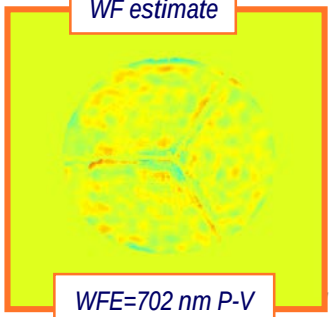

WFE=702 nm P-V
(54 nm RMS)

MGS Image-Based WFS&C is Highly Accurate

- Experiment using the TPF High Contrast Imaging Testbed, which is used to develop coronagraphy for planet hunting
- HCIT features (in this example) a 572 actuator DM
- HCIT is run in vacuum and is seismically isolated
- Data below shows a sequence of MGS WFS&C iterations leading to a WF corrected to λ/5000 within the DM spatial f bandpass
  - MGS algorithmic accuracy limits are <λ/5000

Sequence of Wavefront Estimates

Sequence of WFE Power Spectral Densities

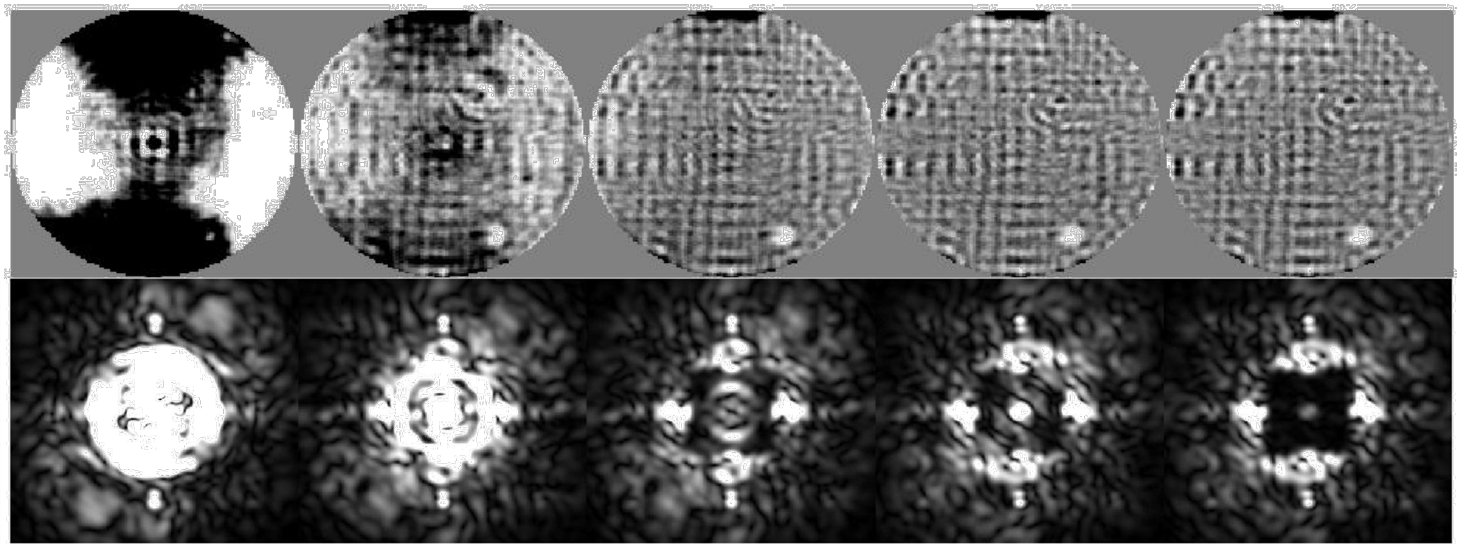

Focus-Diverse Measurements

WFSC Iteration 1 | WFSC Iteration 8

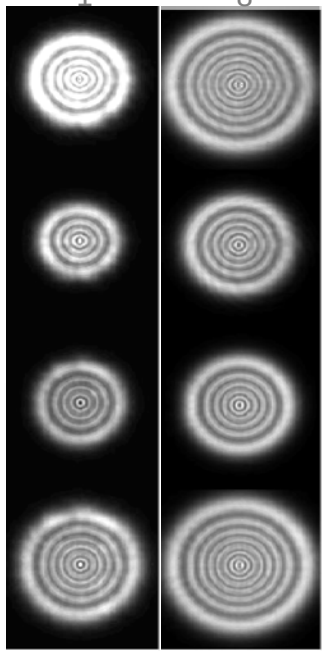

J. Green, S. Basinger, D. Cohen, A. Neissner, D. Redding, S. Shaklan and J. Trauger, "Demonstration of Extreme Wavefront Sensing Performance on the TPF High Contrast Imaging Testbed," Proc. SPIE 5170 (2003)

Image-Based WFS has Large Capture Range

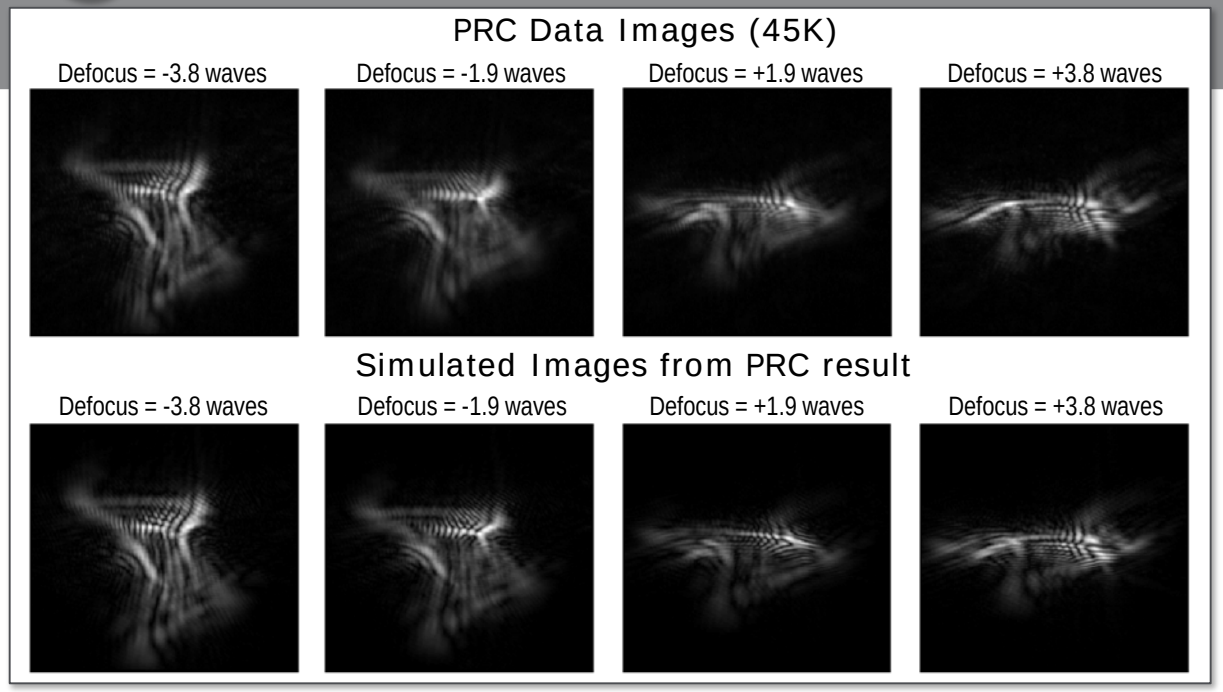

- PRC/AMSD testing succeeded at >10λ peak-to-valley WFE
- Sources of difference include
  - Alignment of PRC to IPI (0.1λ)
  - Alignment drift (0.1λ)
  - Non-common path optics
  - Different spatial *f* response (0.06λ)
- Difference is much smaller than the measured WF

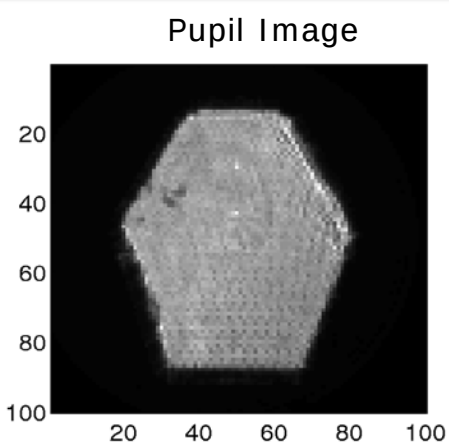

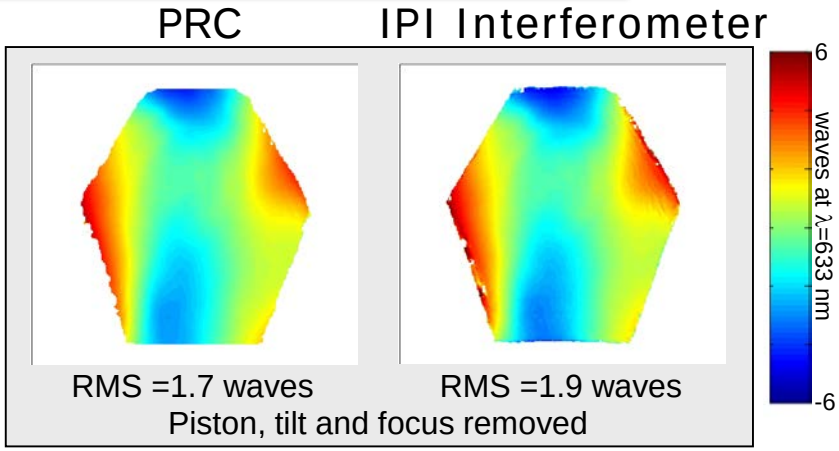

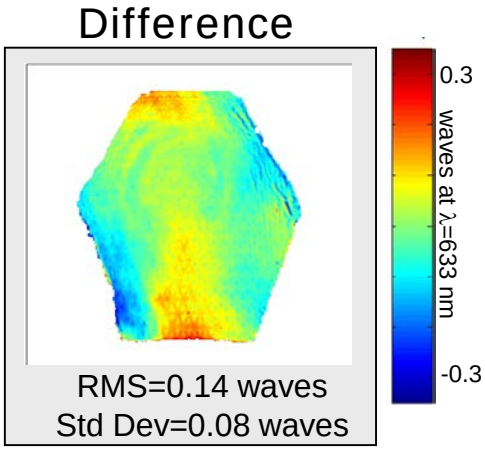

C. Ohara, J. Faust, A. Lowman, J. Green, D. Redding, S. Basinger, D. Cohen, F. Shi, "Phase retrieval camera testing of the Ball Advanced Mirror System Demonstration," Proc. SPIE 5487 (2004).

Simulated 36-Segment Fine Phasing

Images used for WF sensing

– 5 waves defocus

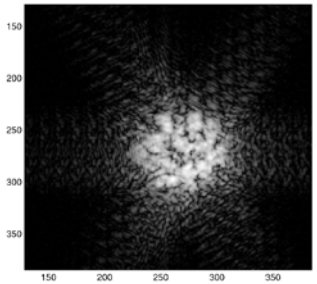

– 2 waves defocus

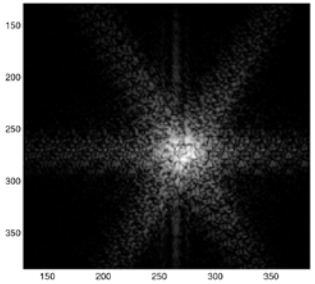

+ 2 waves defocus

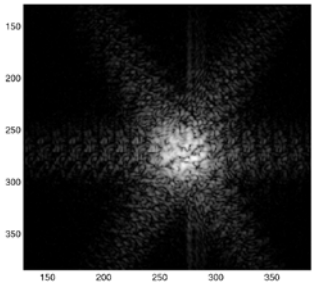

+ 5 waves defocus

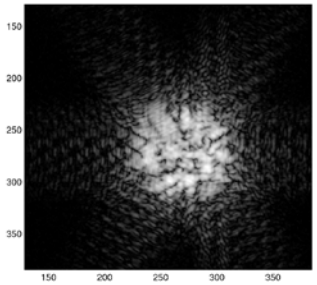

In-Focus image

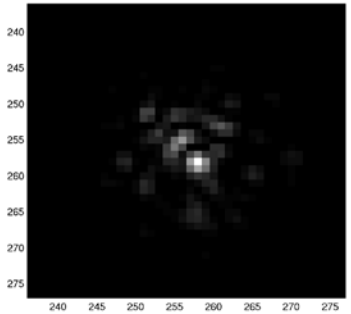

WF estimate

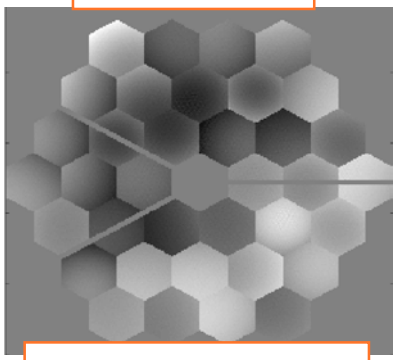

WFE=480 nm RMS

– Post-control WF meets 150 nm objective

In-Focus image

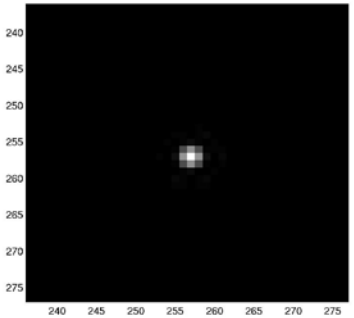

WF estimate

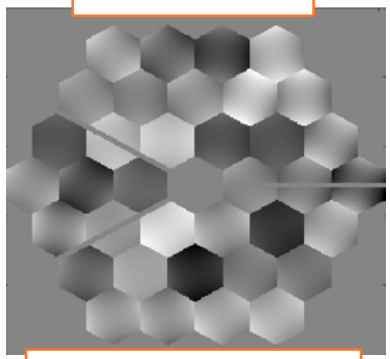

WFE= 35 nm RMS

– MGS Phase Retrieval is used to estimate WF

– WF control is applied using segment RB and RoC actuators

Prescription Retrieval: Model-Based, Parametric Phase Retrieval

- Like Phase Retrieval, Prescription Retrieval (R_xR) is an image-matching WF sensing technique…
- …but one using a ray-trace/diffraction model parameterized by optical prescription parameters
  - Model is driven to match images by an optimizer – like a design code

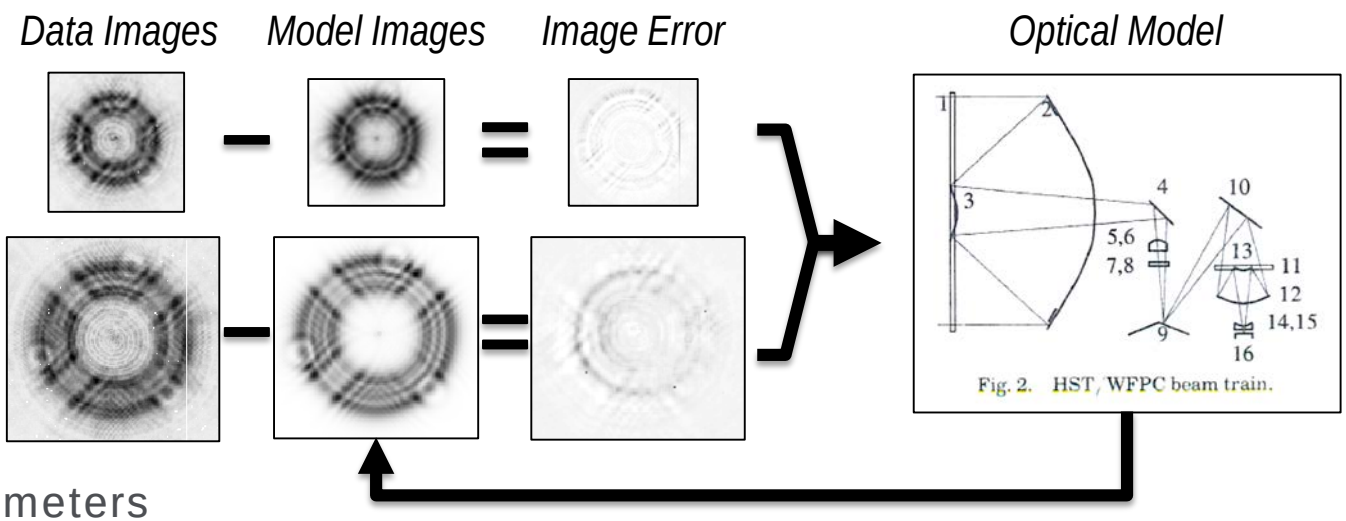

- Prescription Retrieval was one of several techniques developed to diagnose the Hubble Space Telescope aberrations, which it did successfully
  - Using field and focus-diverse images, we were able to match the data in terms of PM figure errors, but also SM and repeater camera figure and alignment errors – allowing separation of those effects and correct ID of the PM errors
  - Results agreed with diagnoses based on analysis of ground test equipment
  - Results were confirmed by success of the HST replacement cameras

Predicting HST PSFs from Prescriptions

- We also used retrieved prescriptions to predict the Point Spread Function (PSF) for arbitrary field points, in any of the WF/PC-2 cameras and filters
  - For image restoration and PSF subtraction
- This met with only limited success, as the predicted PSFs did not capture subtleties in the WF/PC-2 images
  - Aperture support function imperfectly known (only 4 on-axis defocused images were available for retrievals)
  - PM and SM high-spatial *f* errors imperfectly known
  - "Breathing" means significant PSF variation over each orbit
    - 5-20 nm WFE from focus, coma and astigmatism
  - Detector effects: CTE, charge diffusion

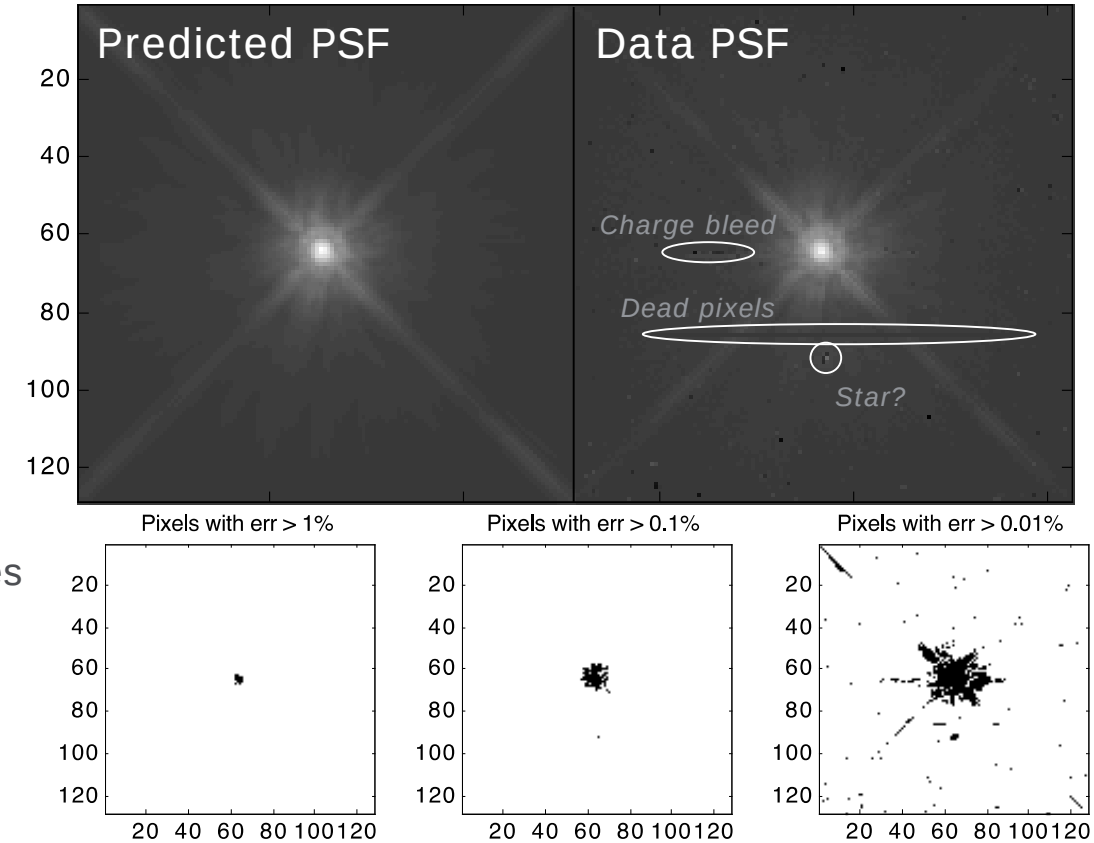

Predicting HST PSFs from PSFs

- Better PSF matches are now achieved, not by measuring the WF and predicting the PSF, but by drawing on large libraries of measured PSFs and using neural net techniques to match in-image stars

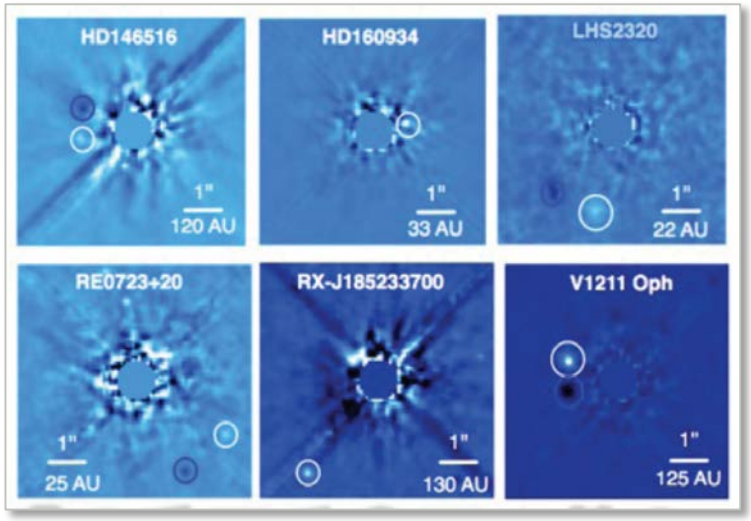

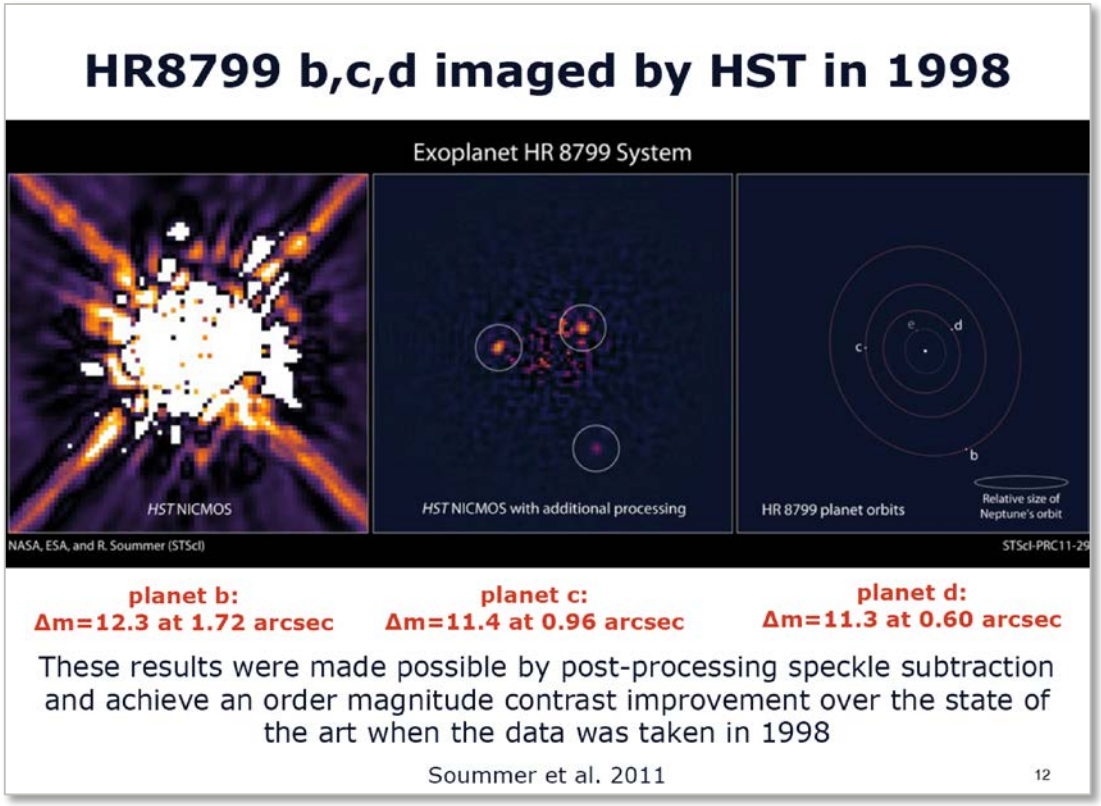

- These exoplanet images were made using archival NICMOS coronagraph data, reprocessed using LOCI and KLIP algorithms (Lafrenière et al, Soummer et al)

Prescription Retrieval for WFSC

- Model-based prescription retrieval has great utility for WFSC
  - Continuous optical surface models do not need phase unwrapping
  - Forward-only propagation: no need for inverse propagation
    - Broad-band light is correctly handled
    - Far-field vignetting is correctly handled
  - Tolerant of noise and poor sampling
    - Smooths over / interpolates to find consistent fits to small number of degrees of freedom
- Model-based and iterative-transform approaches are complementary
  - Iterative-transform has higher accuracy and resolution
  - Model-based has higher dynamic range and better noise tolerance
  - Iterative-transform requires multiple focus-diverse images
  - Model-based can work well with only a single image
  - The combination is very powerful…

In-Focus PSF Optimizer (IPO) for WFSC

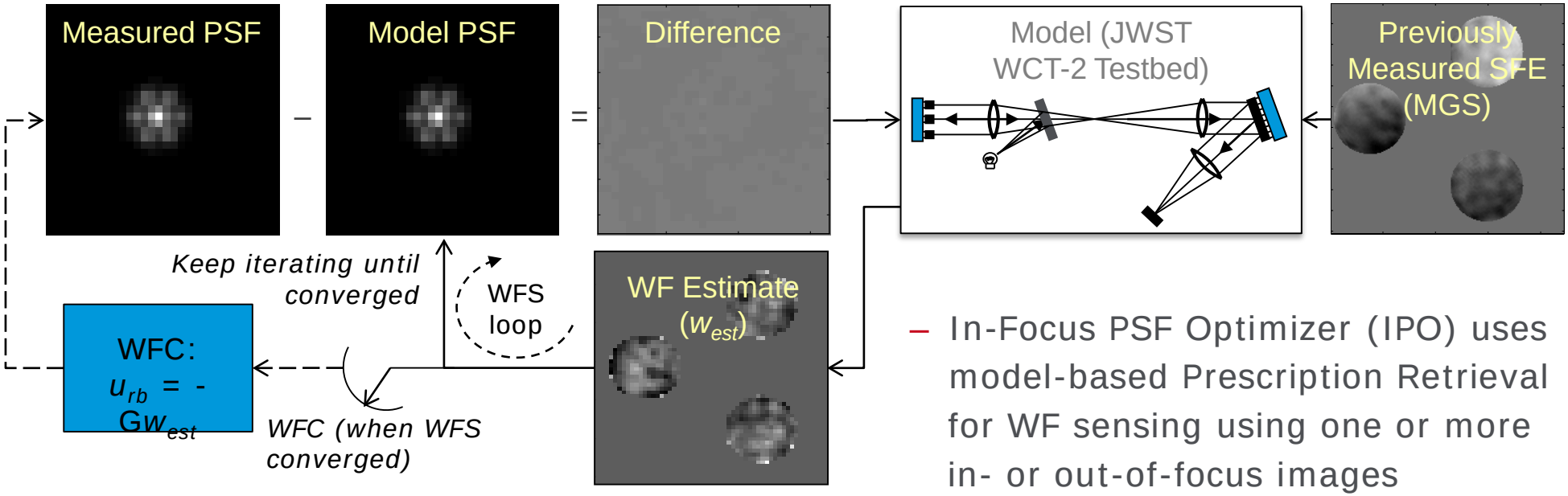

– In-Focus PSF Optimizer (IPO) uses model-based Prescription Retrieval for WF sensing using one or more in- or out-of-focus images

- IPO senses the WF by varying model prescription parameters to match measured PSFs
  - Model incorporates figure data from previous MGS measurements
  - Optimizer drives tip, tilt and piston of 3 segments to drive Difference image to null
- Converged WF estimate is used for WF control
  - RB controls are determined as u_{rb} = -pinv(dw/dx_{rb})*w_{est}, plus constraints

IPO Accuracy on WCT-2

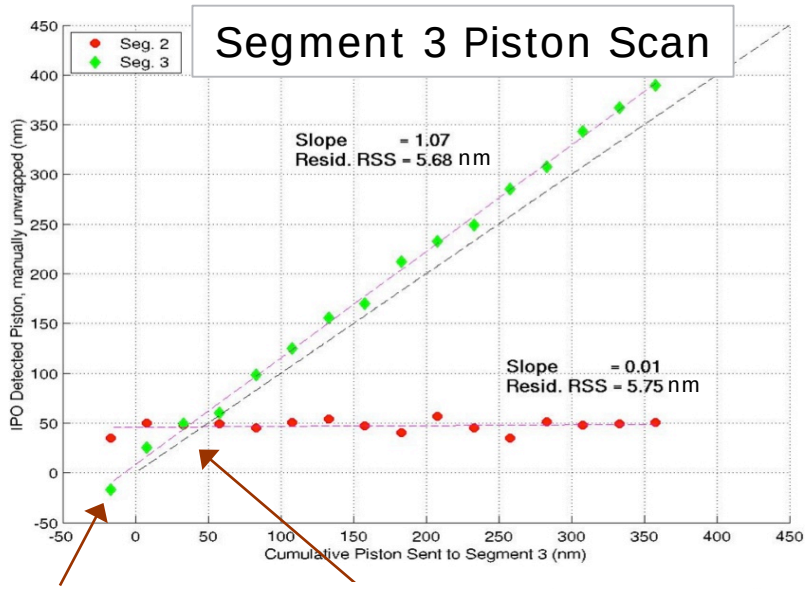

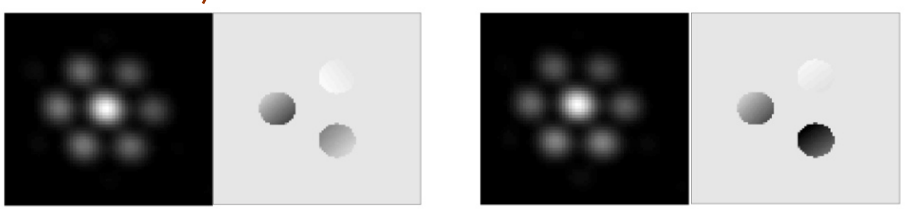

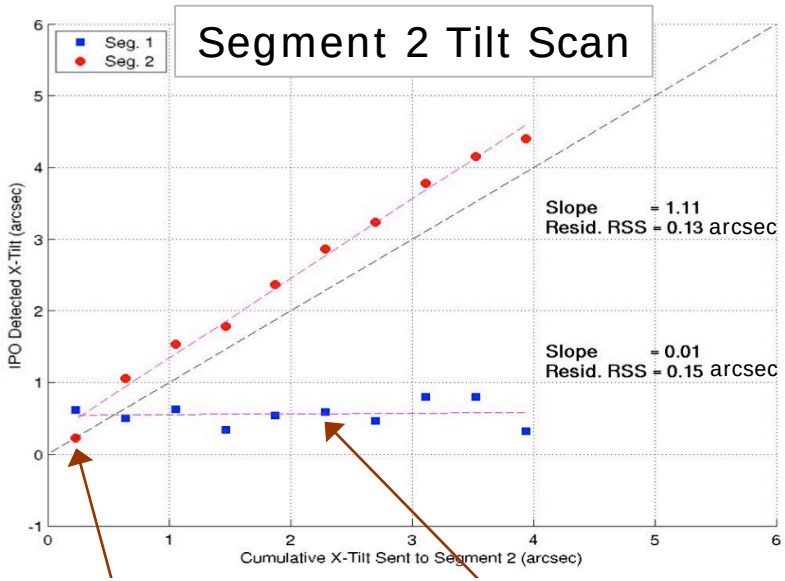

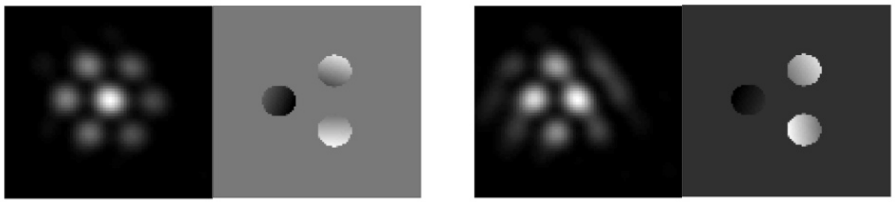

- Sensed piston compares to commanded piston to ~5.7 nm RMS
  - Consistent with 5 nm actuator accuracy
- Sensed tilt compares to commanded tilt to ~0.15 arcsec
  - Also consistent with actuator accuracy

Data from June 29, 2001
WCT-2 with λ = 900 and PSF magnifier

Multi-Color IPO Resolves Piston Ambiguity

Data

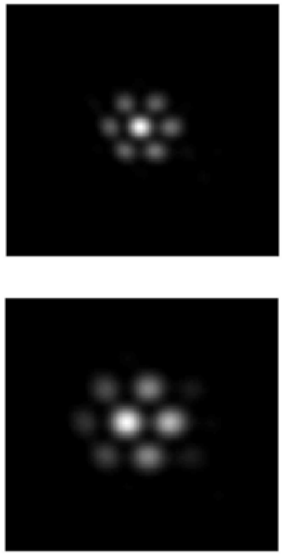

Phased at 633 nm, but not at 900 nm: Segment 1 off by (633/2) nm in piston

Segment 1 Piston Scan,
900 nm data only

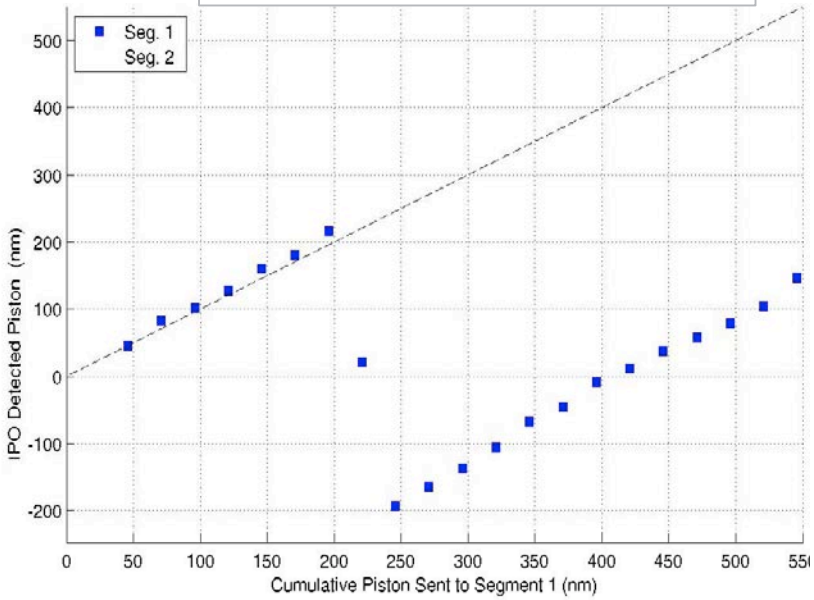

Segment 1 Piston Scan,
633 and 900 nm data

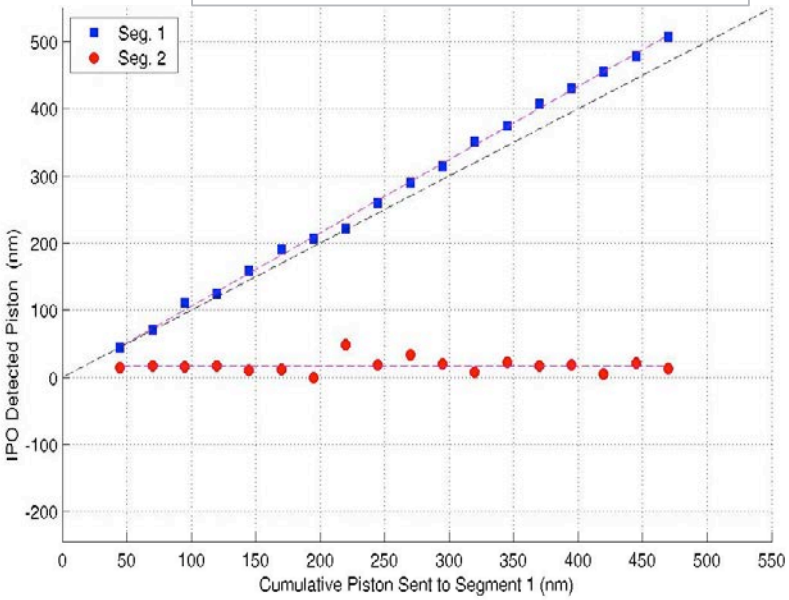

- Segment 1 was scanned in piston steps of +25 nm
- In-focus images were taken with both 633 and 900 nm filters at each step.
  - Piston was unwrapped using both images wavelengths.
  - Residual scatter (RSS) is consistent with 5 nm actuator accuracy

IPO for a 36-Segment Telescope

- The Fourier transform of a symmetric pupil, and so the in-focus image forming process, is symmetric
- IPO can match the in-focus image from a symmetric pupil with symmetric – but wrong – simulated aberrations
- Using accurate, high resolution à priori SFE knowledge in the IPO model appears to overcome the symmetrical ambiguity in most cases
  - Keeping initial estimate error and sensing noise small also important
- Other simple method to break symmetry: use 2 or more defocussed images

IPO Solution for a 36-Segment Telescope

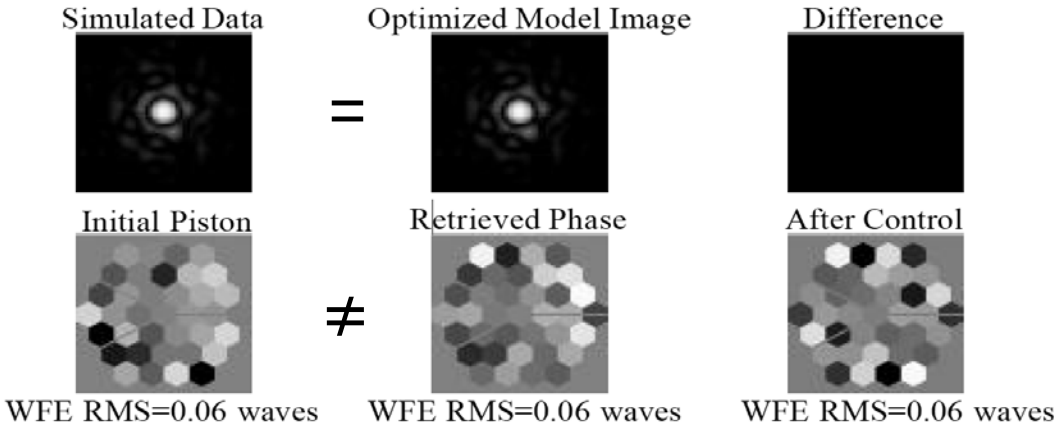

The Model image matches the Data image, but the WFE is different due to pupil symmetry

Adding the high spatial f features of the segments to the IPO model helps break the symmetry and leads to the correct solution

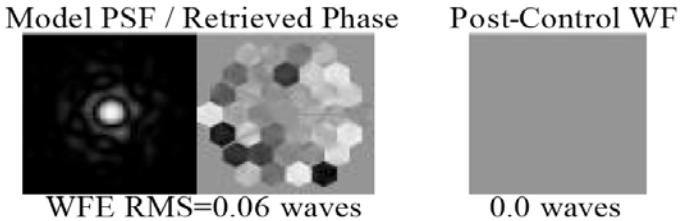

Multi-Field WF Control Performance

Perturbed WFE at 5 field points (worst case of 20)

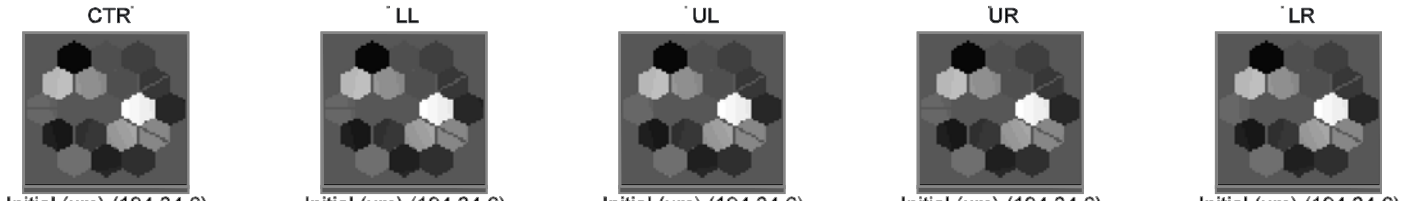

WFE after Single-Field WFSC at 5 fields (nm RMS) (worst case of 20)

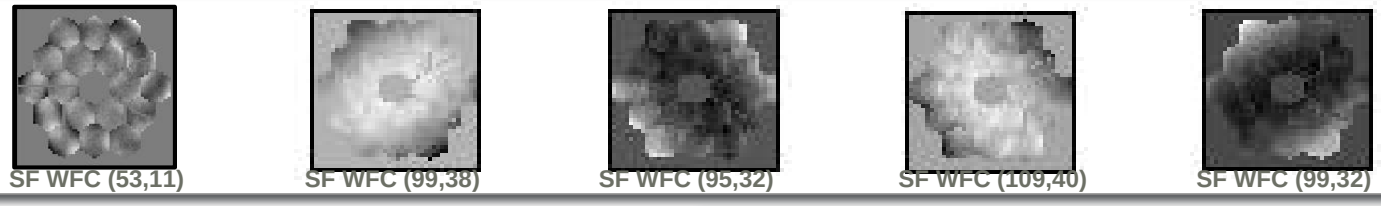

WFE following Multi-Field WFSC at 5 fields (worst case of 20)

OPD maps correspond to worse-case WFE of 20 trials. The (mean, std_dev) of residual WFE at each field position (nm) are shown.

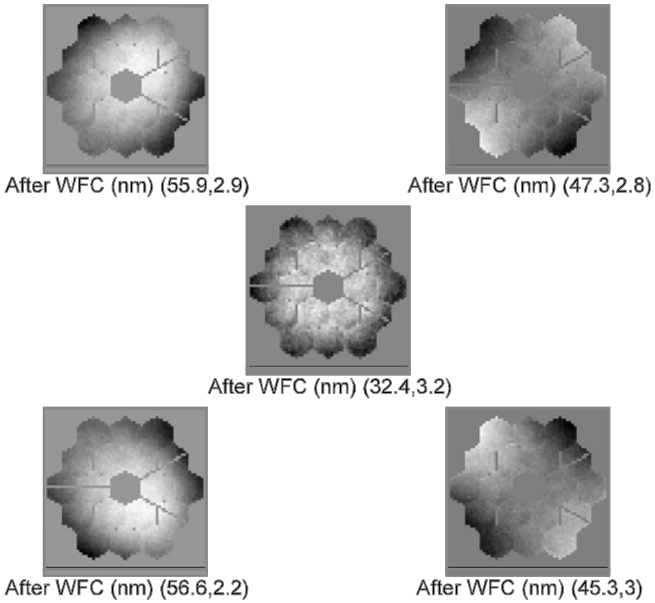

- Single-field WFSC corrects the WF only for the field in which the data was taken
- By measuring at multiple field points and solving for the joint optimum, the telescope can be fully collimated and corrected

Bibliography – Wavefront Sensing and Control: Fine Phasing for Segmented and Monolithic Space Telescopes

25. D. Redding, et al, “Performance of the NGST Wavefront Control System as tested on DCATT,” NGST Science and Technology Exposition, ASP Conference Series, Vol. 207 (2000).
26. D. Scott Acton, et al, “Wavefront Sensing and Controls for the James Webb Space Telescope,” SPIE 8442 (2012).
27. http://www.techbriefs.com/component/content/article/23-ntb/features/feature-articles/3123-nasa-awards-2007-software-of-the-year?limitstart=0.
28. D. Redding, et al, “Performance of the NGST Wavefront Control System as tested on DCATT,” NGST Science and Technology Exposition, ASP Conference Series, Vol. 207, E. Smith and K. Long, eds. (2000).
29. J. Green,et al, “Demonstration of Extreme Wavefront Sensing Performance on the TPF High Contrast Imaging Testbed,” Proc. SPIE 5170 (2003).
30. C. Ohara, D. Redding, F. Shi, J. Green and S. Basinger, “PSF Monitoring and In-Focus Wavefront Control for NGST,” Proc. SPIE 4850 (2002).
31. C. Ohara, et al, “Phase retrieval camera testing of the Ball Advanced Mirror System Demonstration,” Proc. SPIE 5487 (2004).
32. Remi Soummer, et al, “Orbital Motion of HR 8799 b,c, d using Hubble Space Telescope data from 1998: Constraints on Inclination, Eccentricity and Stability,” arXiv:1110.1382 [astro-ph.EP].
33. Lafrenière, D., Marois, C., Doyon, R., Nadeau, D., and Artigau, É., “A New Algorithm for Point-Spread Function Subtraction in High-Contrast Imaging: A Demonstration with Angular Differential Imaging,” ApJ 660, 770–780 (May 2007).

Metrology and Wavefront Control

A Laser Distance Gauge

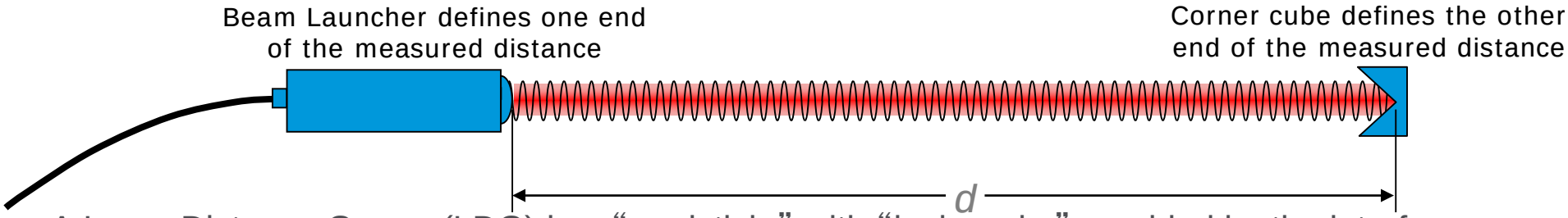

- A Laser Distance Gauge (LDG) is a "yardstick," with "inchmarks" provided by the interference fringes of the laser beam
  - Changes in the distance ***d*** between the Beam Launcher (BL) and the Corner Cube (CC) are measured as phase shifts between probe and reference beams
    - Intrinsic relative mode accuracy is better than 1 nm – with care could approach 1 pm
    - "Count fringes" to track large changes in ***d***
    - Optional "Absolute mode" using 2 colors gives micron absolute accuracy within cm range
- We can keep the BL and CC the same distance apart, by position feedback control of the BL and/or CC to keep *d* constant
  - LDG runs at high BW (nominally 1 kHz), but closed-loop position control BW can be very low
- A SIM Mission-derived technology application funded by JPL R&TD

Heterodyne Metrology Concept

- Laser light at λ = 1.55 um is split into 2 optical signals, with frequencies 77.00 & 77.04 MHZ (local & measurement)
- One set of signals is combined within the beam launcher (Reference signal)
- The second set is combined after traveling to the target (Target signal)
- Electronic comparators convert Reference and Target heterodyne signals to square waves
- Lag between edges of the Reference and Target signals measures phase
- Displacement is proportional to phase
- Accumulator keeps tracks of total number of waves displaced

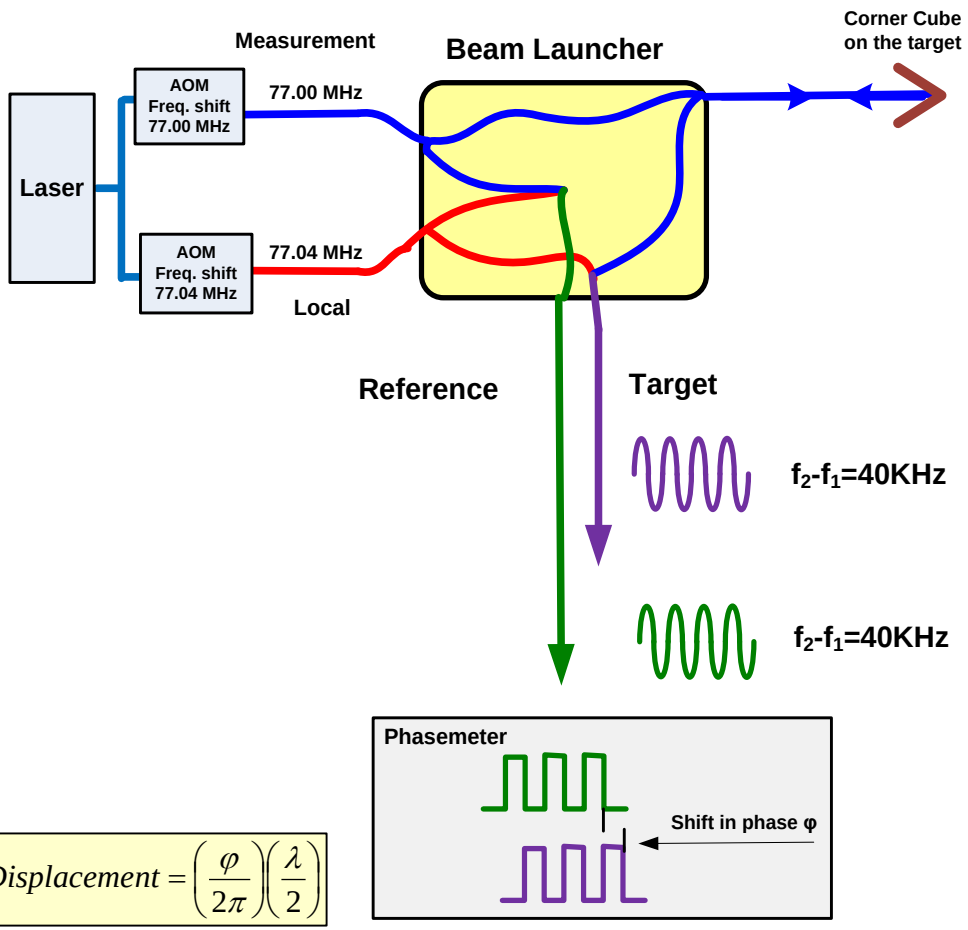

$$Displacement = \left(\frac{\varphi}{2\pi}\right)\left(\frac{\lambda}{2}\right)$$

Laser Truss Metrology Architecture

- Multiple LDGs are fed by a single laser split into multiple paths
- Compact, lightweight components facilitate integration with lightweight optics and structures
- Compact electronics

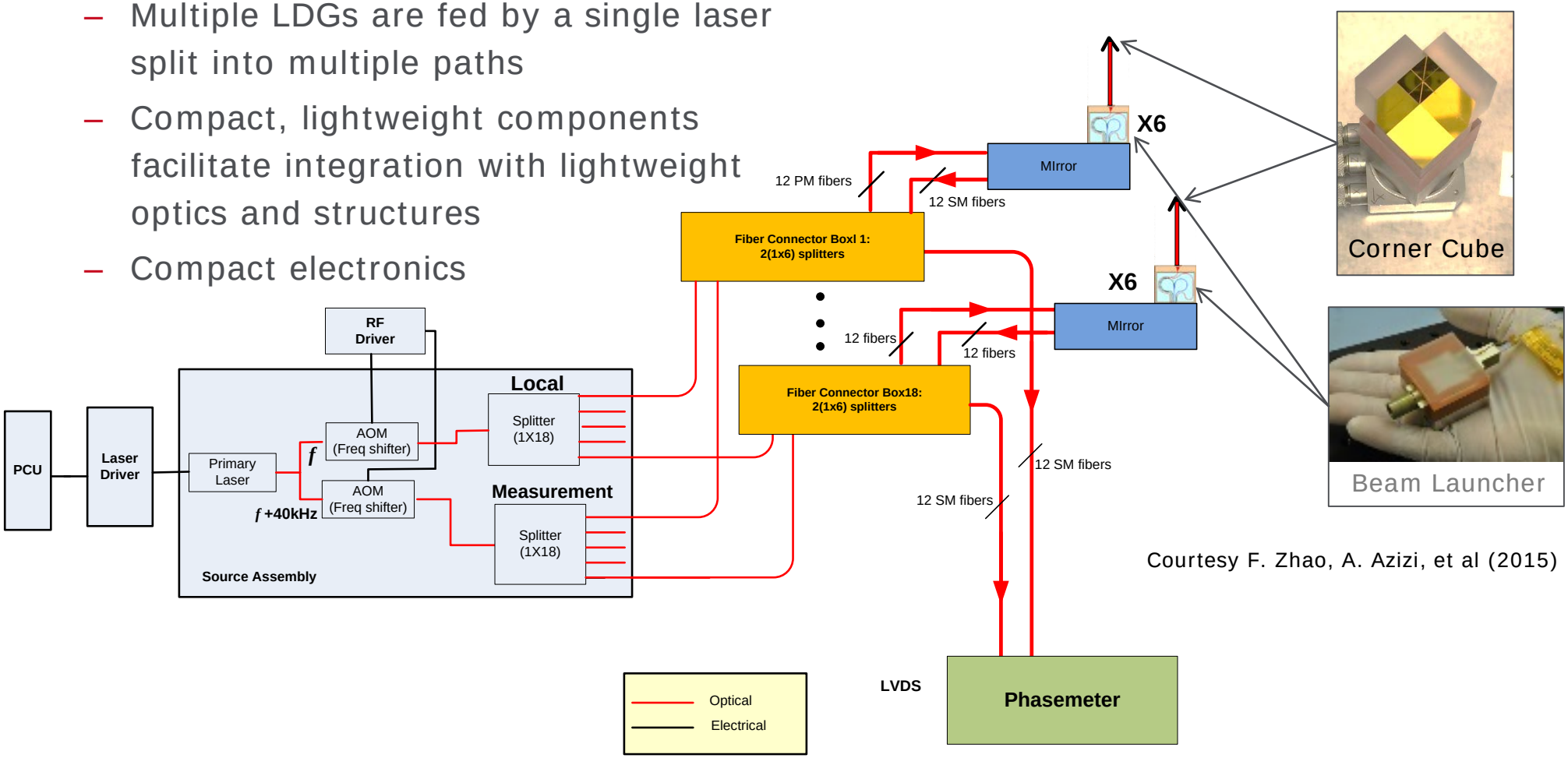

Courtesy F. Zhao, A. Azizi, et al (2015)

Metrology Capabilities

– Beam launcher utilizes integrated optics for compact form, light weight, and high performance

PLC* beam launcher

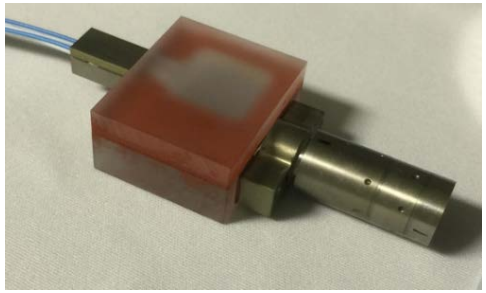

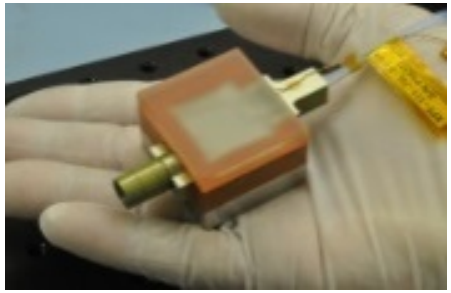

*PLC -- planar light-wave circuit
Silica-on-silicon waveguide technology

Courtesy F. Zhao, A. Azizi, et al (2015)

Performance Capabilities

Parameter	Performance
Mode of operation	Relative only
Technology	Heterodyne
Heterodyne frequency	10-100 KHz
Laser wavelength	1500-1600 nm
Number of channels	8-110
Precision	<1 nm
Working distance	0-50 m
Data rate	100-2000 Hz
Max slew rate	+/-5 mm/sec
Laser power from beam launcher in free space	<5uW (eye safe)
Phase meter technique	Zero crossing
Laser- external cavity	20 mW

The Laser Truss

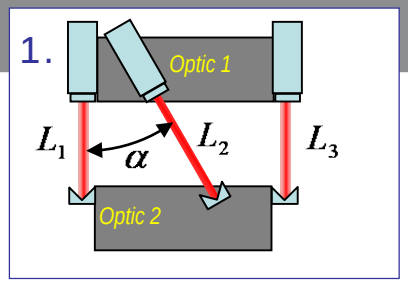

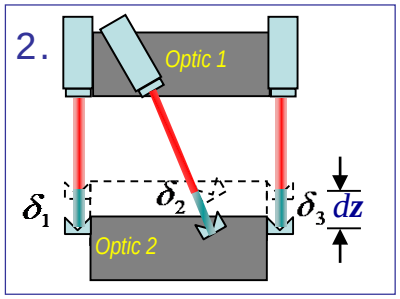

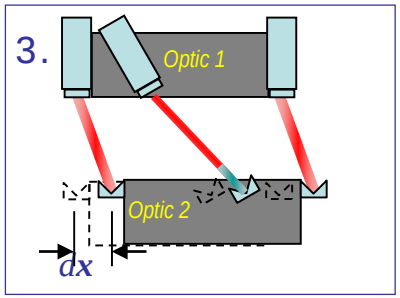

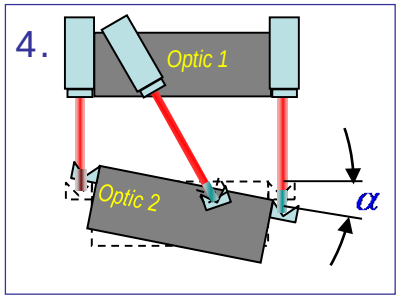

- This 2-D example illustrates use of LDG measurements to estimate rotational as well as translational DOFs between bodies
  1. Nominal geometry. There are 3 relative DOFs – x and z translation, and rotation θ
  2. Changes in LDG measurements due to a z translation:

     $$\delta_1 = dz; \qquad \delta_2 = \cos(\alpha)dz; \qquad \delta_3 = dz;$$

  3. Changes in LDG measurements due to an x translation:

     $$\delta_1 = 0; \qquad \delta_2 = \sin(\alpha)dx; \qquad \delta_3 = 0;$$

  4. Changes in LDG measurements due to a θ rotation:

     $$\delta_1 = r_1\theta; \qquad \delta_2 = r_2\sin(\alpha)\theta; \qquad \delta_3 = r_3\theta;$$

- The measurement in matrix form

$$\delta = \begin{bmatrix} \delta_1 \\ \delta_2 \\ \delta_3 \end{bmatrix} = \begin{bmatrix} 0 & 1 & r_1 \\ \sin(\alpha) & \cos(\alpha) & r_2\sin(\alpha) \\ 0 & 1 & r_3 \end{bmatrix} \begin{bmatrix} dx \\ dz \\ \theta \end{bmatrix} = Cx$$

- A simple state estimator

$$x = C^{-1}\delta$$

- Feedback control based on the δ measurements can keep the truss aligned

A 3-Dimensional Laser Truss

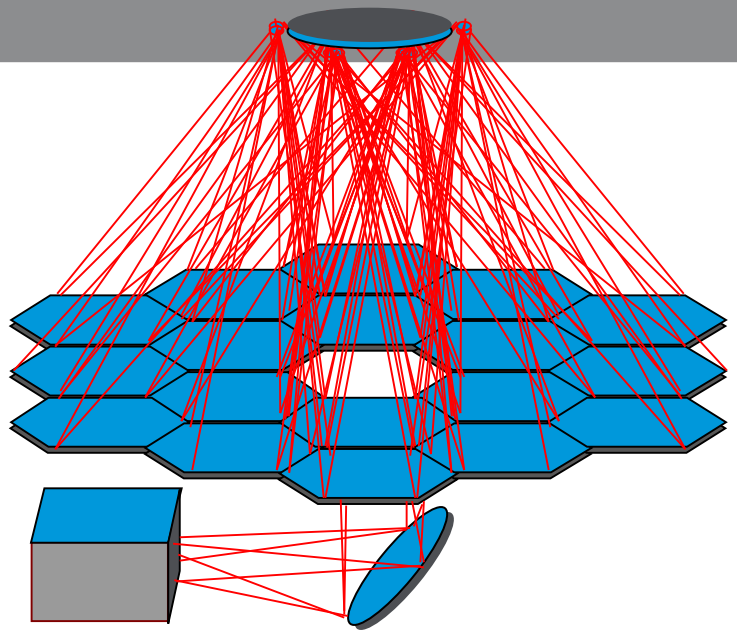

- The same approach is extended for the full 3-D LT
  - 6 LDGs per segment measure all relative RB DOFs in the entire OTA
    - All PM segments, the SM, FF, TM and OBA
  - The IRS is attached to the OBA, providing measurements of 6 more absolute DOFs wrt inertial space
- Same measurement equation: $\delta = Cx$
  - Sensitivities computed from model kinematics

- Measurement is invertible: $x = C^{-1}\delta$ is full rank
- Optical State Estimator: uses a Kalman Filter to estimate the RB state using LDG measurements
  - Balances measurement vs. prior knowledge for optimal estimate
  - Predicts WF and Boresight from state estimate
- Feedback control using RB actuators and optimal control laws keeps performance in spec

Control Block Diagram

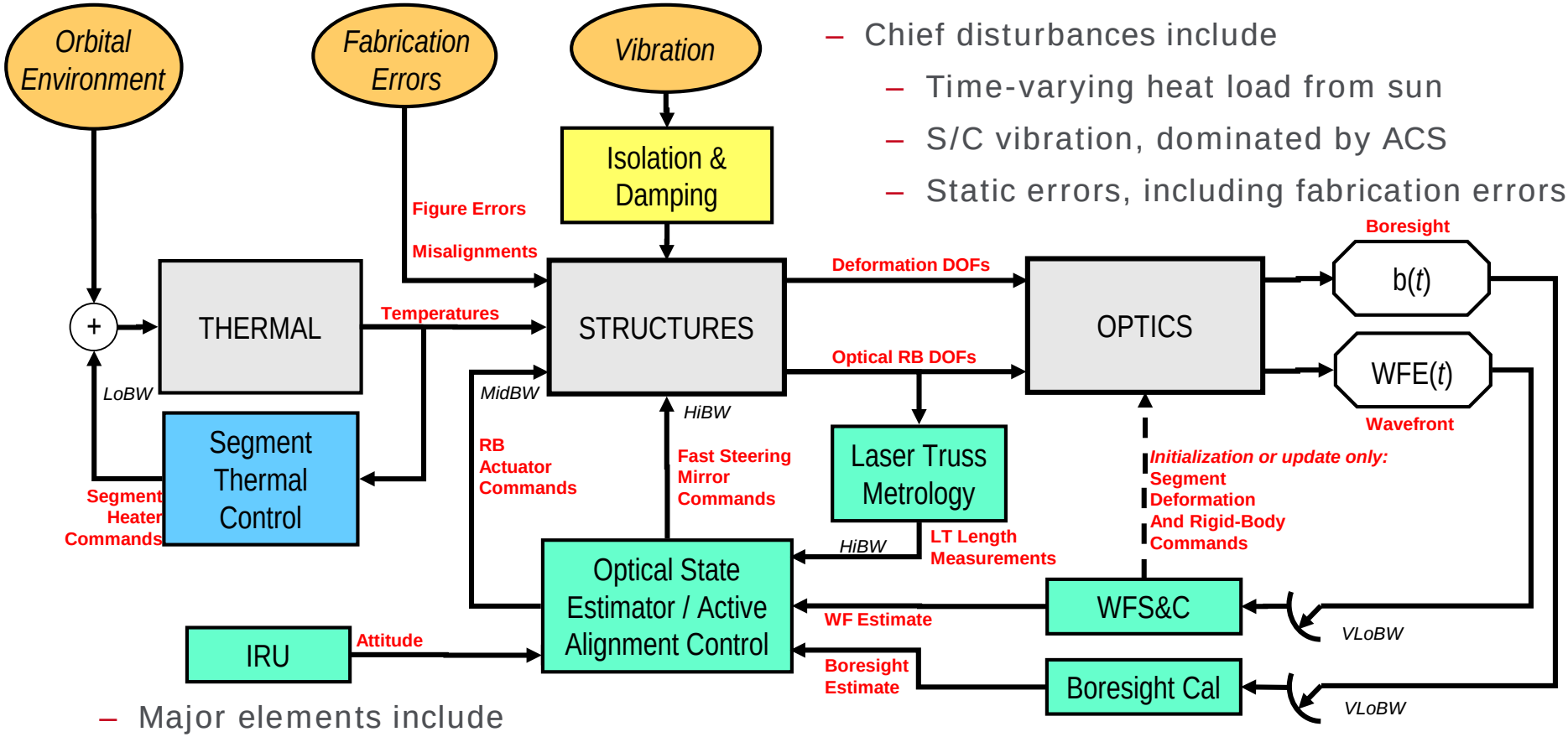

- Chief disturbances include
  - Time-varying heat load from sun
  - S/C vibration, dominated by ACS
  - Static errors, including fabrication errors

- Major elements include
  - Wavefront Sensing and Control
  - Laser Truss Active Alignment: active WF compensation and LOS pointing control
  - Segment Thermal Control to stabilize optical figure
  - Isolation and Damping to attenuate vibration disturbances

WFS&C

- Wavefront Sensing & Control sets segment figure and alignment
  - Initially, and then periodically during ops
  - Update frequency will depend on figure and Laser Truss drift rates

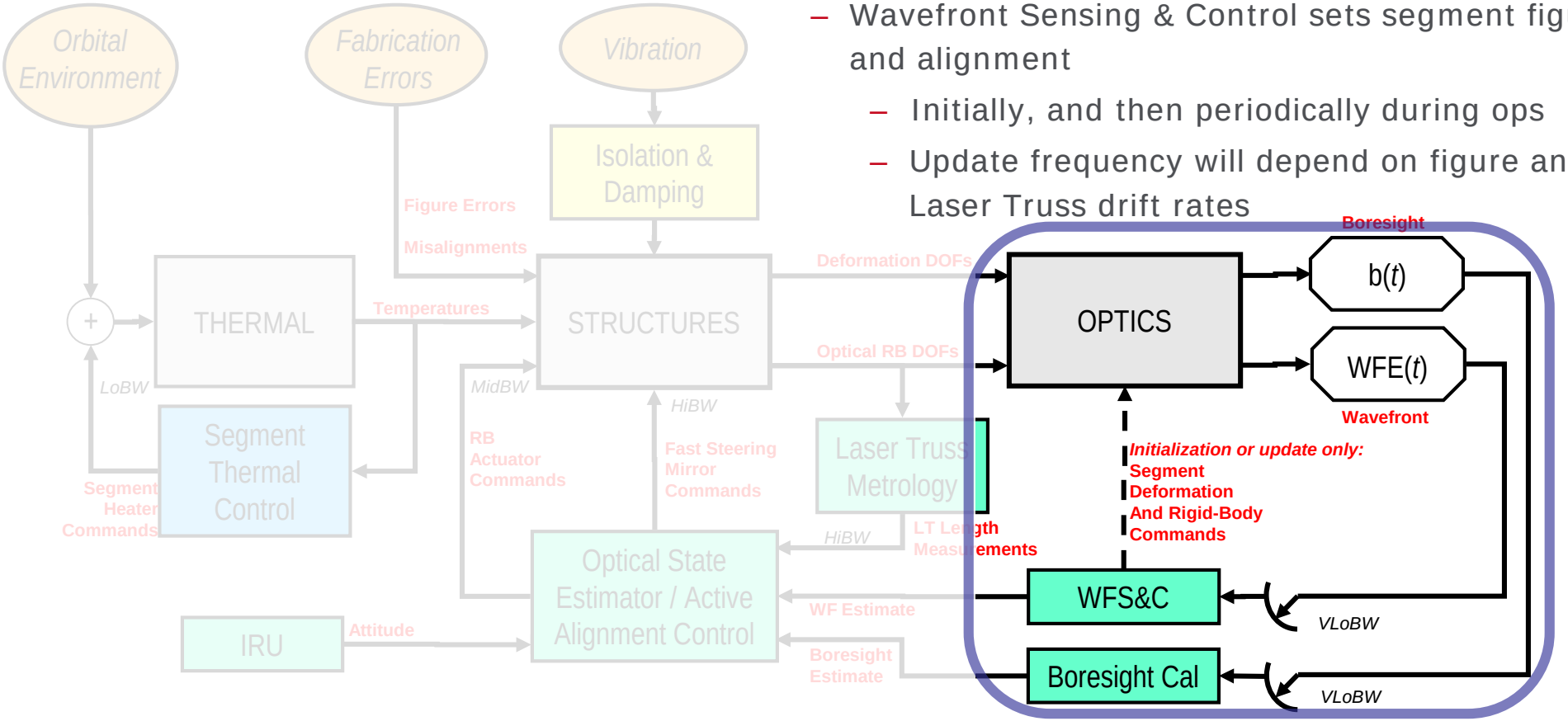

Thermal Control Preserves PM Figure

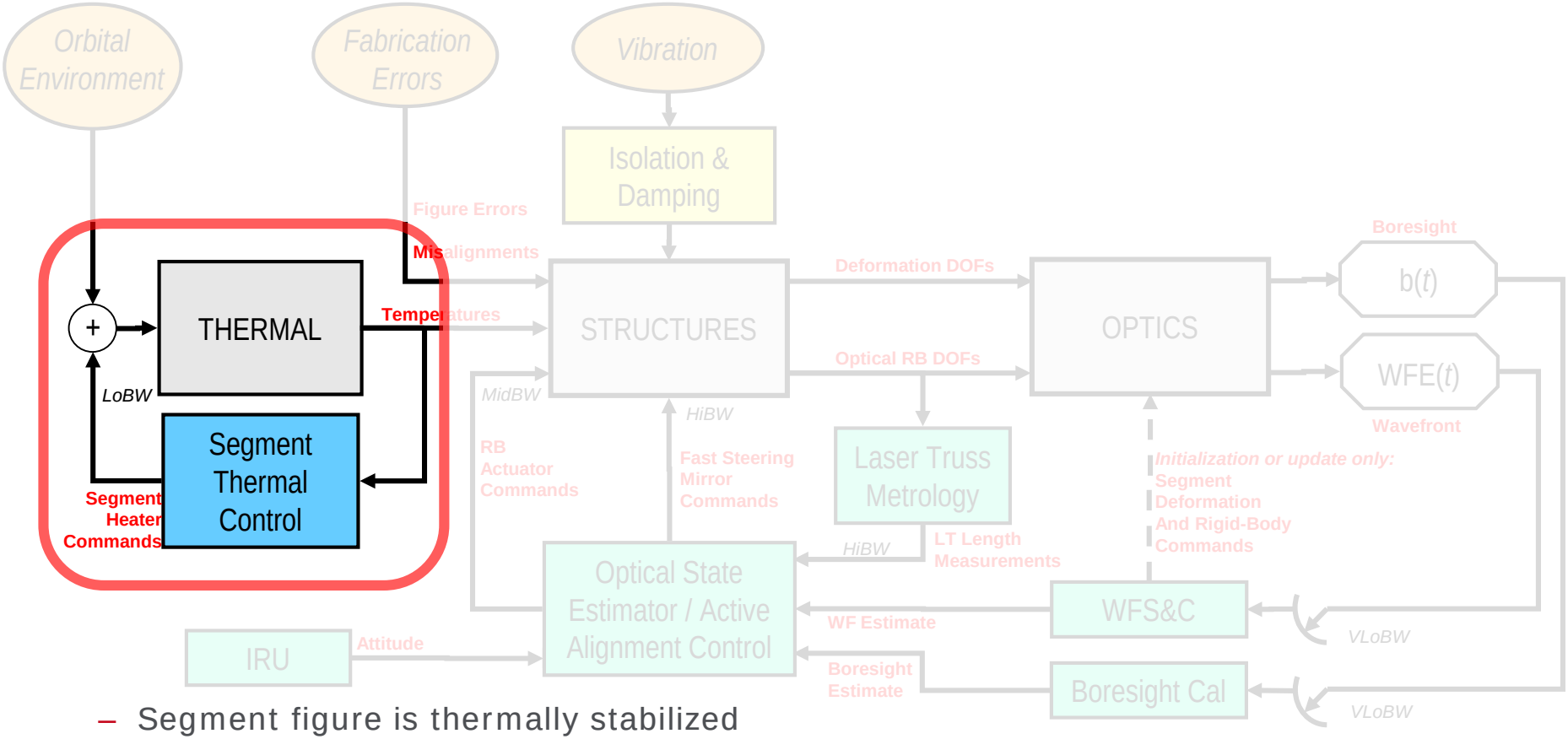

- Segment figure is thermally stabilized
  - Passive Athermalization: keeps WFE/° C very low
  - Passive Thermal Control: sunshade, operations constraints
  - Local Segment Thermal Control: PM segment temperatures are kept constant using heaters integrated with segment structure

Laser Truss Metrology Maintains Alignments

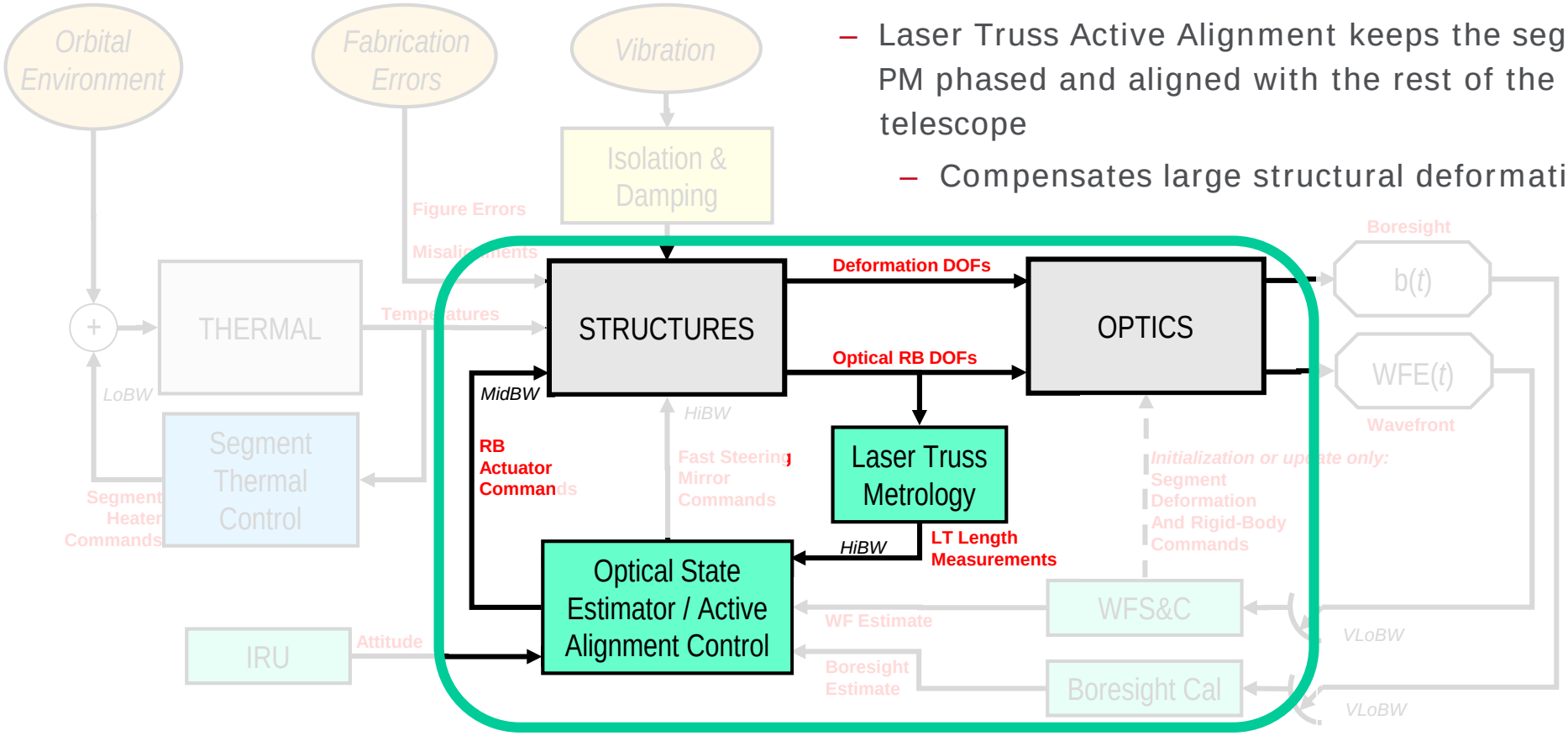

- Laser Truss Active Alignment keeps the segmented PM phased and aligned with the rest of the telescope
  - Compensates large structural deformations

- Laser Truss measurements at high BW are processed in the Optical State Estimator to estimate the perturbation state of all the optics
- Estimated state is fed back to control WFE using RBAs at low BW, and boresight at high BW using the Fast Steering Mirror

Laser Truss Stabilizes Line of Sight

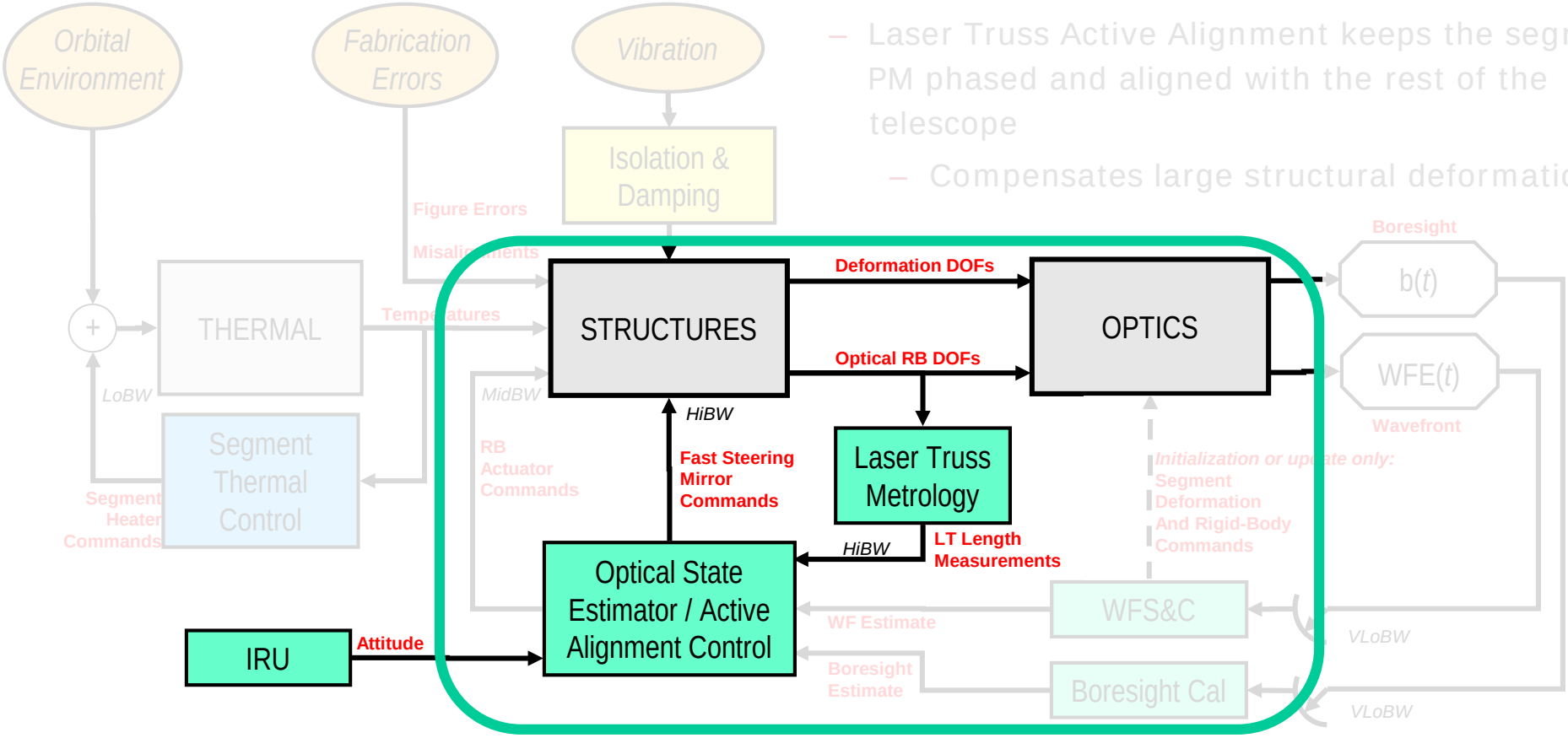

- Laser Truss Active Alignment keeps the segmented PM phased and aligned with the rest of the telescope
  - Compensates large structural deformations

- Laser Truss measurements at high BW are processed in the Optical State Estimator to estimate the perturbation state of all the optics
- Estimated state is fed back to control WFE using RBAs at low BW, and boresight at high BW using the Fast Steering Mirror

Control Block Diagram

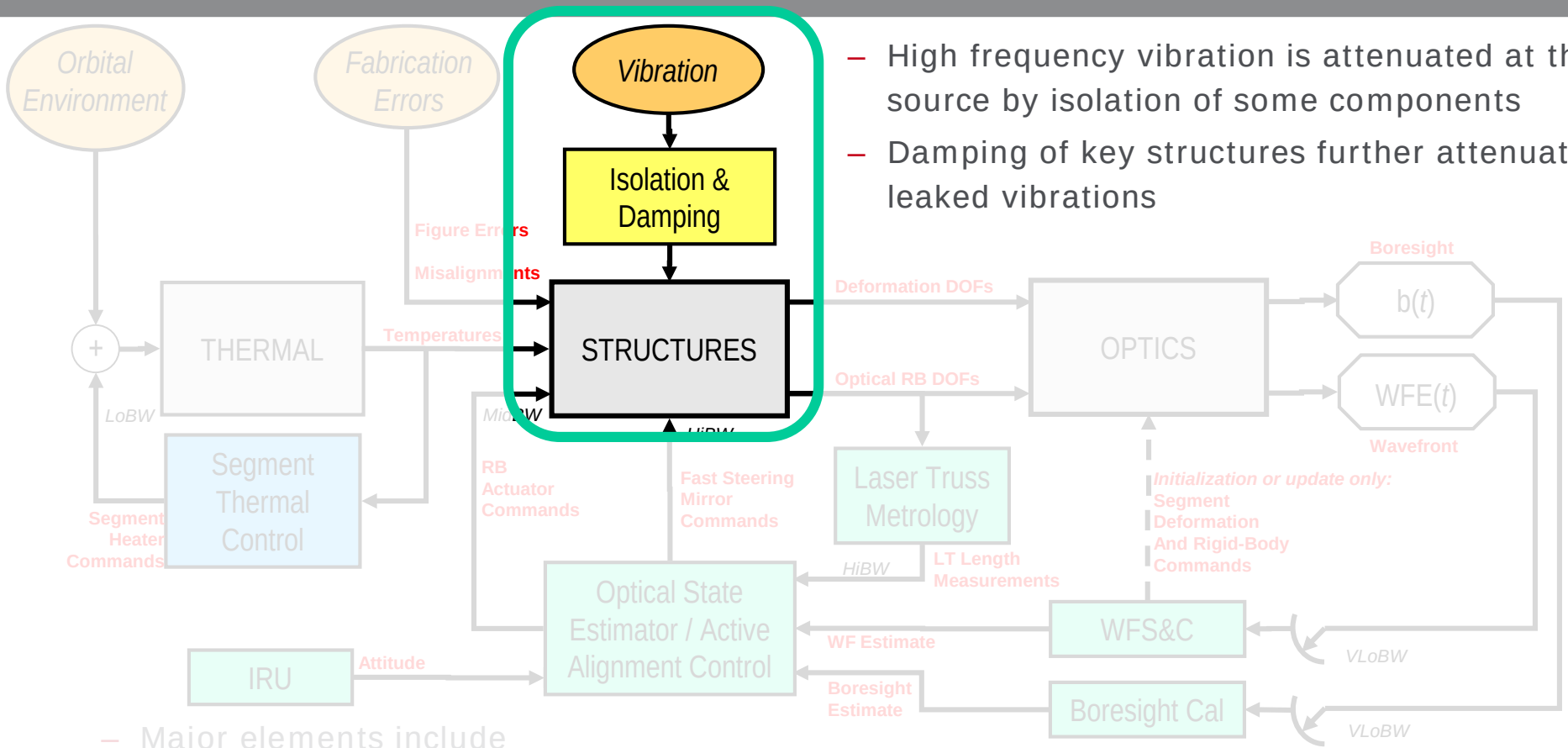

- High frequency vibration is attenuated at the source by isolation of some components
- Damping of key structures further attenuates leaked vibrations

- Major elements include
  - Wavefront Sensing and Control
  - Laser Truss Active Alignment: active WF compensation and LOS pointing control
  - Segment Thermal Control to stabilize optical figure
  - Isolation and Damping to attenuate vibration disturbances

Laser Truss Pros and Cons

- Pros
  - High accuracy – < 1 nm per LDG when Δ angle is small
  - Observes all important RB states – including Primary and Secondary Mirrors, and Optical Bench
  - Low drift – with 1 laser feeding all LDGs, require WFS update once per day
  - Light weight beam launchers
  - No on-segment power dissipation
  - Does not require segments to be close together
  - Does not require any particular gap geometry
  - Works with missing segments (no degradation for the segments that remain)
  - Useful for I&T
  - Degrades gracefully if individual LDGs go out
- Cons
  - Affected by lab seeing

CCAT Telescope – as was

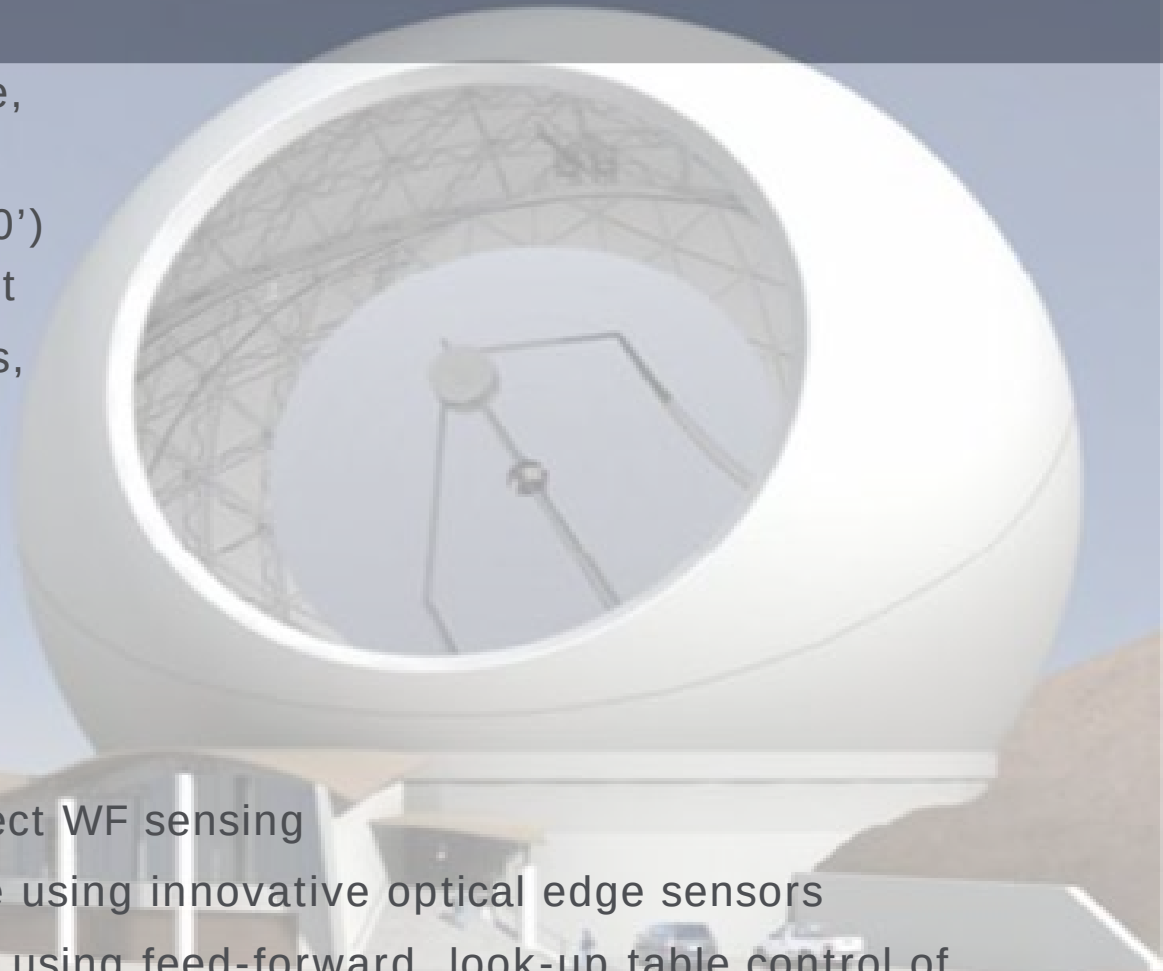

- Planned submillimeter-wave telescope, covering 200um to 2mm wavelengths
  - Was to be sited at 5,612m (18,410') altitude in the high Atacama desert
- 25 m aperture, with 162 PM segments, supported on composite structure
  - 3DOF actuation for segments
  - 5DOF actuation for SM
  - Telescope pointing and tracking
- Active control to compensate thermal and gravity-induced errors
  - Initialize telescope figure using direct WF sensing
  - Maintain Primary Mirror (PM) figure using innovative optical edge sensors
  - Compensate for gravity sag effects using feed-forward, look-up table control of Secondary Mirror (SM) position and pointing

CCAT Control Elements

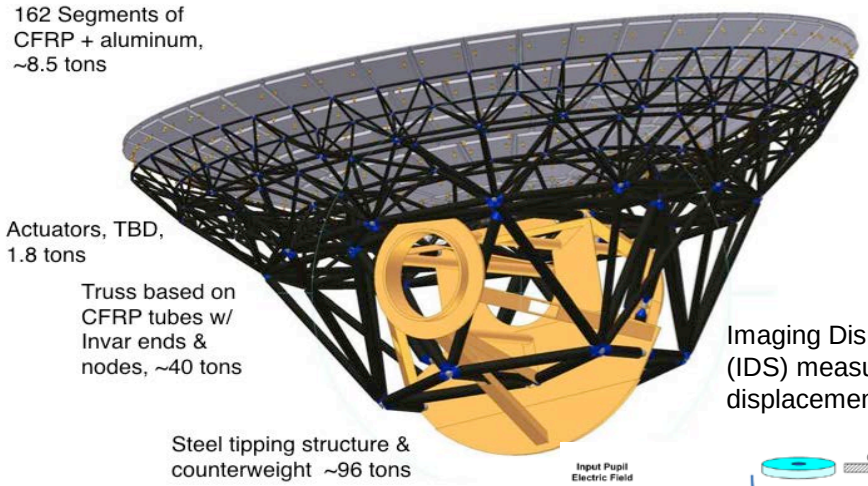

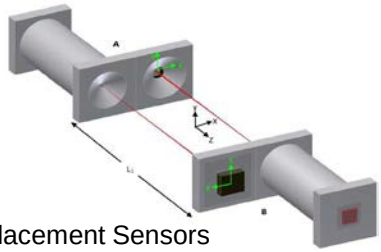

Imaging Displacement Sensors (IDS) measure PM segment displacements

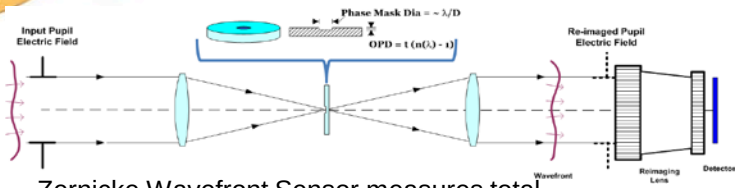

Zernicke Wavefront Sensor measures total system WF error

CFRP / Al honeycomb plate 'raft' is connected to truss by 3 linear actuators providing 3DOF of control

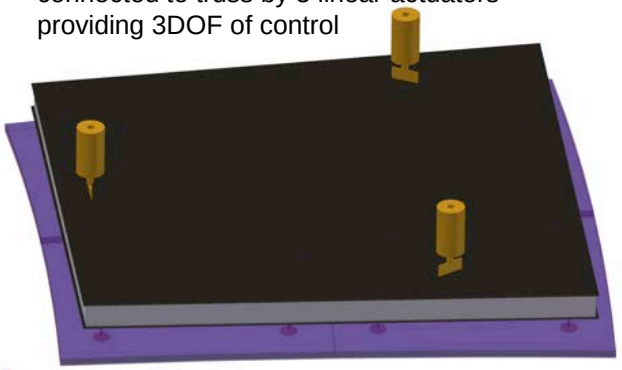

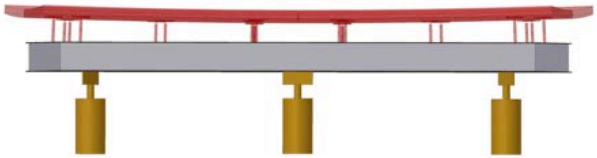

Machined aluminum tiles form reflecting surfaces, 4 per raft, mounted with five invar screw adjustors.

- CCAT telescope design utilizes CFRP truss structure
- Supports 162 segments, each about 2 meters in size
- Each segment is a CFRP/Al "raft" structure supporting 4 machined Al reflecting panels
- Three actuators per segment provide tip/tilt/piston control
- Secondary Mirror has 6DOF rigid body control as well

Imaging Displacement Sensors (IDS)

- IDS are optical edge sensors
  - "Projector" on 1st segment sends beam to "detector" on 2nd segment
  - Relative motions of segments move the beam centroids on the detectors

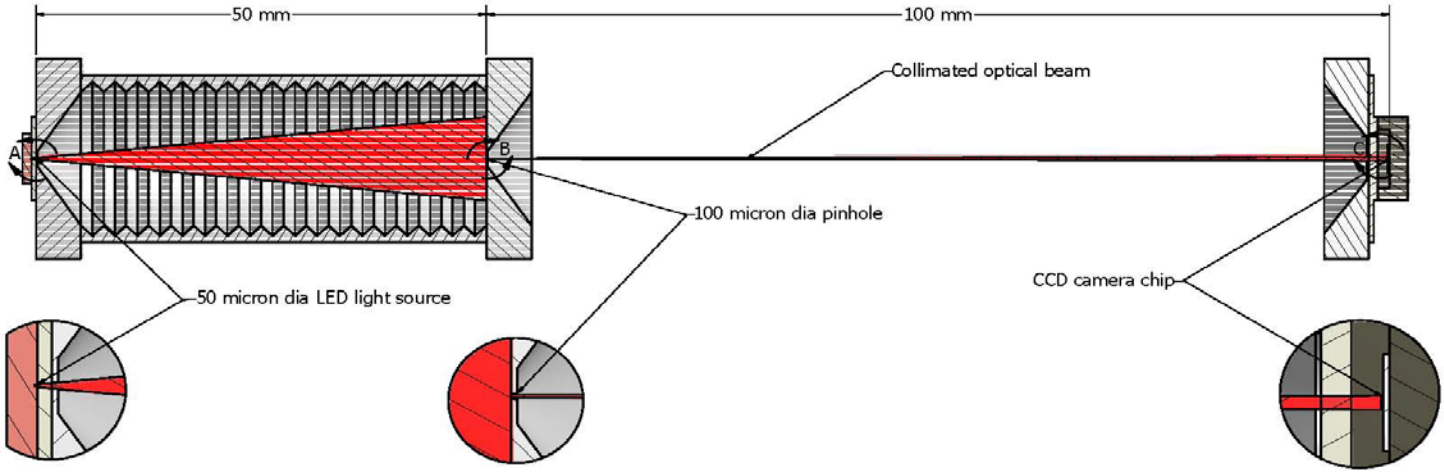

- IDS meets CCAT requirements
  - <0.1 micron sensor noise
    - < 1 nm for integration times >40 and <1000 sec
  - <0.3 microns RMS error over 20 C temperature range (Al prototype)
  - Inexpensive

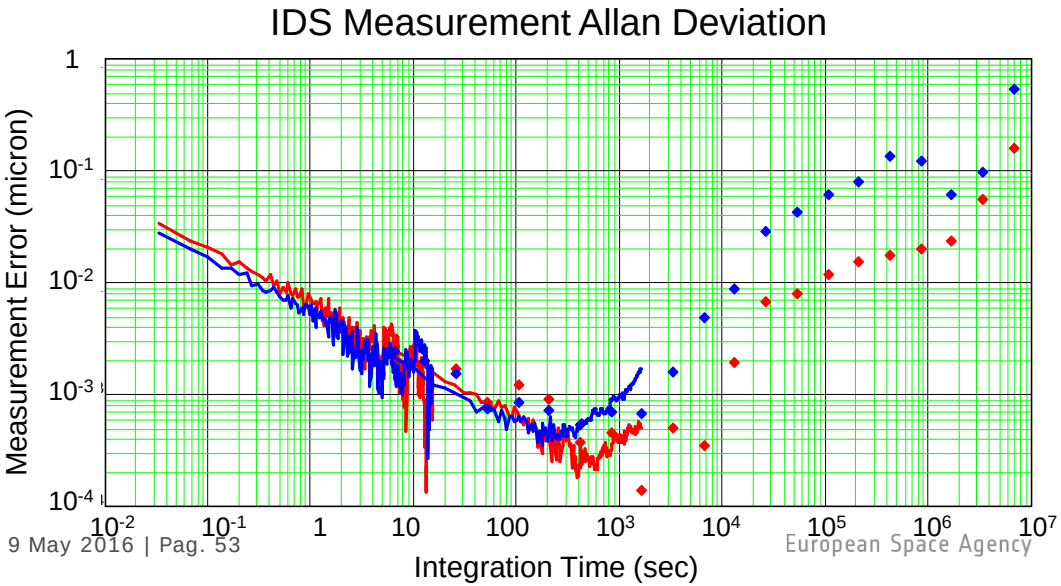

IDS Configuration

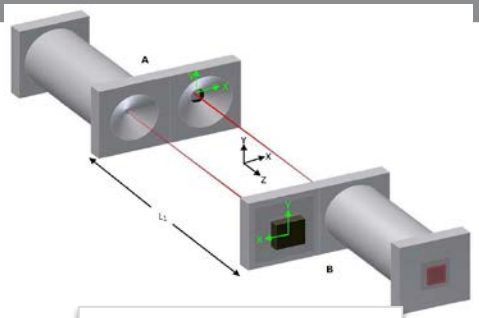

CCAT IDS Sensor Pair

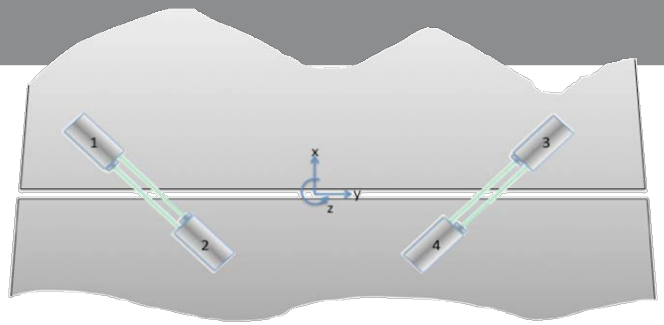

2 Sensor Pairs are used at each segment-to-segment edge

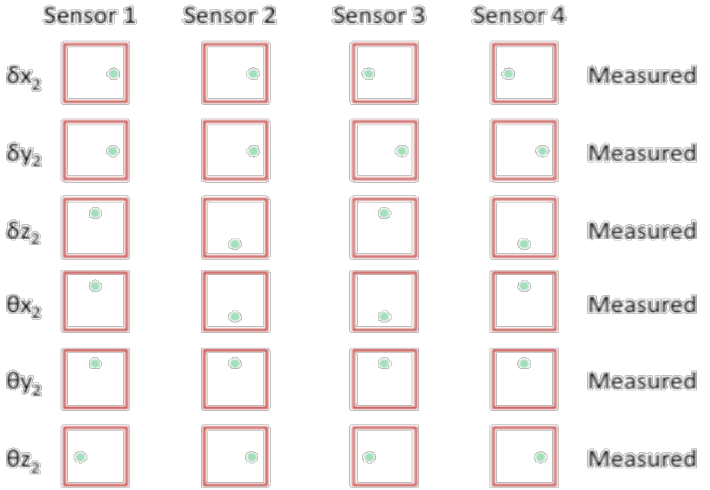

2 Sensor Pairs fully observe the 6 relative motions between 2 adjacent segments

- Each IDS sensor head has a projector and detector
  - Each sensor pair has 2 beams and 4 measurements
- Two sensor pairs are used for each segment-to-segment edge
- Angled configuration allows measurement of all 6 relative DOFs between 2 segments
- Each segment has multiple adjacent segments, and multiple measurements

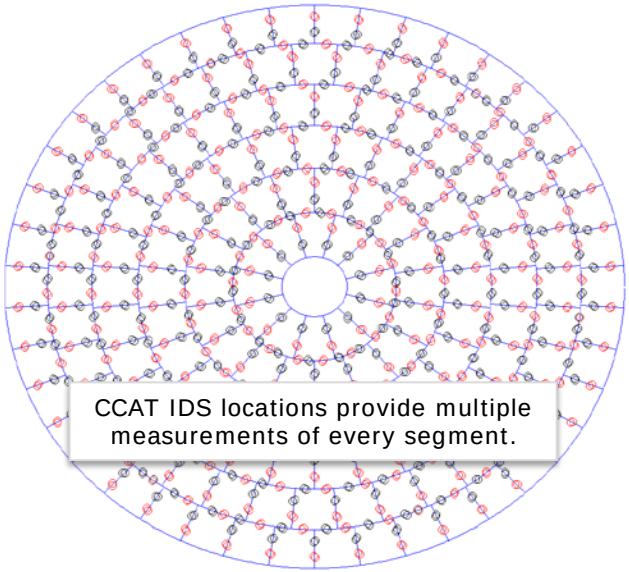

CCAT IDS locations provide multiple measurements of every segment.

Control Loops

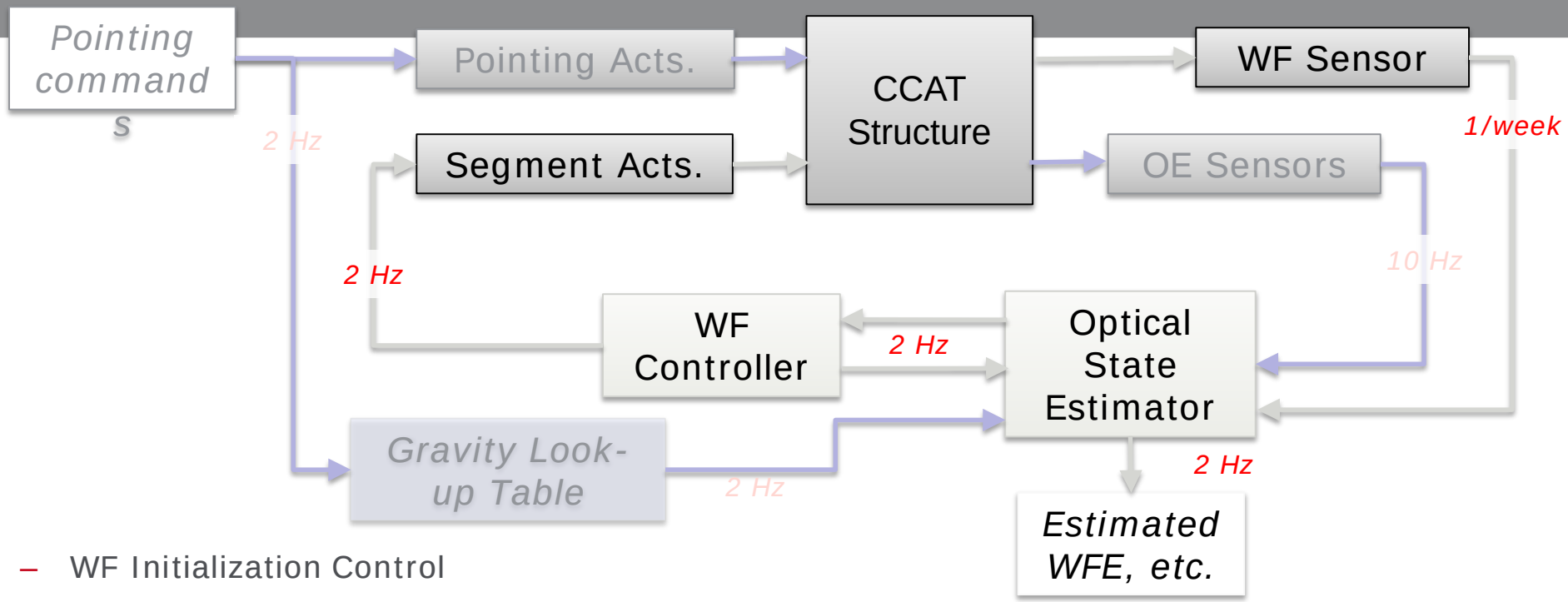

- WF Initialization Control
  - WF Sensing is conducted to directly measure the telescope WF to set initial figure
  - WF Sensing is repeated at intervals to reset WF Maintenance control errors

Control Loops

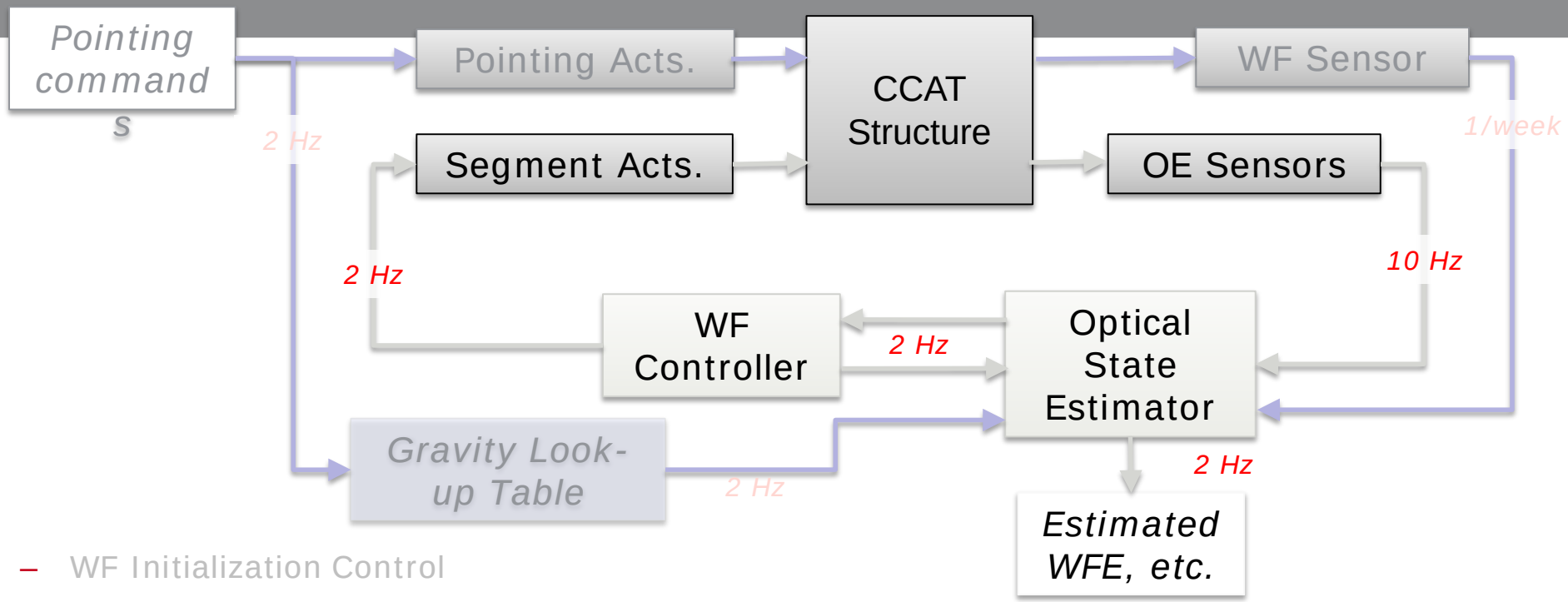

- WF Initialization Control
  - WF Sensing is conducted to directly measure the telescope WF to set initial figure
  - WF Sensing is repeated at intervals to reset WF Maintenance control errors
- WF Maintenance Control
  - Optical Edge Sensors are used to continuously estimate the WF error
  - WF Controller moves the PM segments to minimize WF error

Control Loops

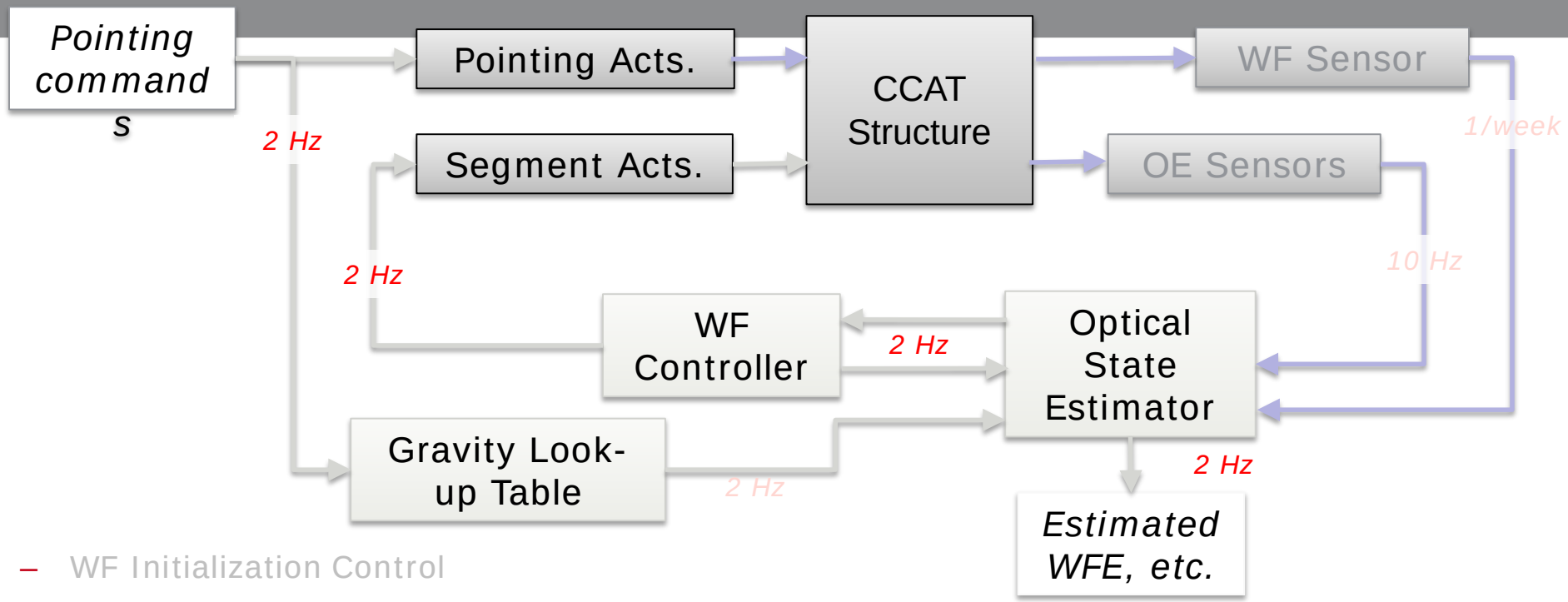

- WF Initialization Control
  - WF Sensing is conducted to directly measure the telescope WF to set initial figure
  - WF Sensing is repeated at intervals to reset WF Maintenance control errors
- WF Maintenance Control
  - Optical Edge Sensors are used to continuously estimate the WF error
  - WF Controller moves the PM segments to minimize WF error
- Gravity Look-up Table Feed-forward Control
  - Gravity direction wrt the telescope changes as the telescope pointing changes
  - Secondary Mirror position and angle are controlled open-loop to counter pointing errors

Linearized Model

- The optical state x_i: perturbations to the nominal position/orientation/figure of each optic
  - Subscript i indicates time step
- State x_i changes in time, driven by process noise ξ_i, quasi-static modes T_i, actuations u_i
- Wavefront output w_i
  - Wavefront $\boldsymbol{w}_i$ is affected by state changes $\boldsymbol{x}_i$ and actuation $\boldsymbol{u}_i$
- IDS optical edge sensor measurements l_i
  - Edge sensor measurements $\boldsymbol{l}_i$ are affected by state changes $\boldsymbol{x}_i$ and noise $\delta \boldsymbol{l}_i$
- Wavefront sensor measurements w_{mi}

x is the CCAT state vector: 6 rigid-body DOFs per optic

$$\boldsymbol{x}_{Opticj} = \left[\delta_x \delta_y \delta_z \theta_x \theta_y \theta_z\right]^T \qquad \boldsymbol{x} = \begin{bmatrix} \boldsymbol{x}_{Optic1} \\ \vdots \\ \boldsymbol{x}_{Opticn} \end{bmatrix}$$

State transition equation governs the evolution of the state with time

$$\boldsymbol{x}_i = \boldsymbol{x}_{i-1} + \frac{\partial \boldsymbol{x}}{\partial \boldsymbol{u}} \boldsymbol{u}_i + \frac{\partial \boldsymbol{x}}{\partial \boldsymbol{T}} \boldsymbol{T}_i + \xi_i$$

Wavefront is a function of the state

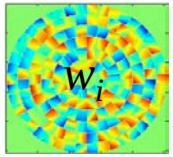

$$\boldsymbol{w}_i = \frac{\partial \boldsymbol{w}}{\partial \boldsymbol{x}} \boldsymbol{x}_i + \boldsymbol{w}_0$$

Optical edge sensor measurement

$$l_i = \frac{\partial l}{\partial x} x_i + l_0 + \delta l_i$$

Wavefront sensor measurement

$$\boldsymbol{w}_{mi} = \boldsymbol{w}_i + \delta \boldsymbol{w}_i$$

Control Approaches

- One approach is to control so that edge sensor measurements are driven to null
  - This approach nulls errors in the controlled DOFs only

- *Real objective is to minimize WF error*, while keeping control effort in balance
  - This can be done if WF is measured directly
  - It can also be accomplished using an "*Optical State Estimator*" to estimate WF from edge sensor measurements

- WF-based control...
  - *Compensates optical effects of all errors* by actuation of the controlled DOFs

A state-restoring control:

$$u_i = -pinv\left(\frac{\partial l}{\partial x}\frac{\partial x}{\partial u}, ptol\right) l_i$$

WF control cost function

$$\min_u \; J = w^T w + c_u u^T u$$

WF control control law and gain matrix

$$u_i = -G w_i$$

$$G = \left[c_u I + \left(\frac{\partial w}{\partial x}\frac{\partial x}{\partial u}\right)^T \frac{\partial w}{\partial x}\frac{\partial x}{\partial u} \right]^{-1} \left(\frac{\partial w}{\partial x}\frac{\partial x}{\partial u}\right)^T$$

WF control can be used with WF measurement w or WF estimate $\bar{w}$

$$u_i = -G \bar{w}_i$$

Optical State Estimator

- Kalman filter recursively estimates full state $\hat{x}_i$ from optical edge sensor measurement l_i , previous control u_{i-1}, and prior estimates $\hat{x}_{i-1}$, $\hat{x}_{i-2}$, $\hat{x}_{i-3}$, …
  - Balances measurement noise against error in prior estimates to produce optimal estimate
- Estimated state $\hat{x}_i$ used to estimate WF w_i for WF control
- Full-state controller feeds back $\bar{w}_i$ to minimize WFE
  - Observes 6DOF per segment, minus unobservable global tilt modes
  - Additional term c_u weights control effort, allows damping of response to avoid exciting structure and reduce noise sensitivity

Current state estimate computed from current measurement, prior state estimate, and prior actuation

$$\hat{x}_i = \left(I - K_i \frac{\partial l}{\partial x}\right)\hat{x}_{i-1} + \left(I - K_i \frac{\partial l}{\partial x}\right)\frac{\partial x}{\partial u} u_{i-1} + K_i l_i$$

Kalman gain weights contributions of data sources by their expected error

$$K_i = \mathrm{cov}\left(\hat{x}_i - x_i\right)\left(\frac{\partial l}{\partial x}\right)^T \mathrm{cov}\left(\frac{\partial l}{\partial x}\frac{\partial x}{\partial u} u_{i-1}^T + l_i\right)^{-1}$$

Kalman gain changes with time, as the state covariance evolves

$$\mathrm{cov}(\bar{x}_{i+1}) = \mathrm{cov}(\hat{x}_i - x_i) + \frac{\partial x}{\partial u}\mathrm{cov}(u_i)\left(\frac{\partial x}{\partial u}\right)^T + \mathrm{cov}(\delta x_i)$$

Estimated wavefront

$$\bar{w}_i = \frac{\partial w}{\partial x}\bar{x}_i$$

Wavefront Control

$$u_i = -G\bar{w}_i = -G\frac{\partial w}{\partial x}\hat{x}_i$$

$$G = \left[c_u I + \left(\frac{\partial w}{\partial x}\frac{\partial x}{\partial u}\right)^T \frac{\partial w}{\partial x}\frac{\partial x}{\partial u}\right]^{-1}\left(\frac{\partial w}{\partial x}\frac{\partial x}{\partial u}\right)^T$$

European Space Agency

Random IC Example

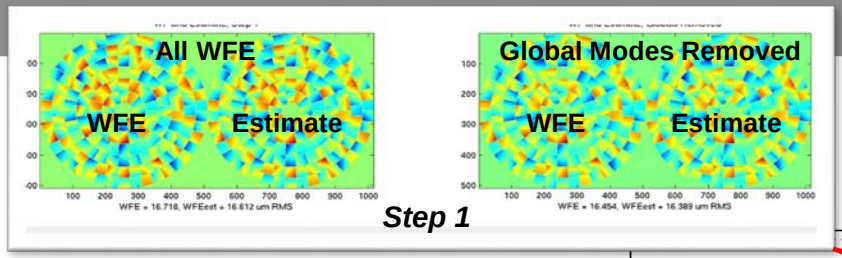

•Initial WFE due to random state errors

Random IC Response

- •Time-step control sim
- •No feed-forward
- •IDS at all steps
- •0.1 um IDS accuracy
- •WFC every third step
- •Full OSE Kalman filter
- •No cupping

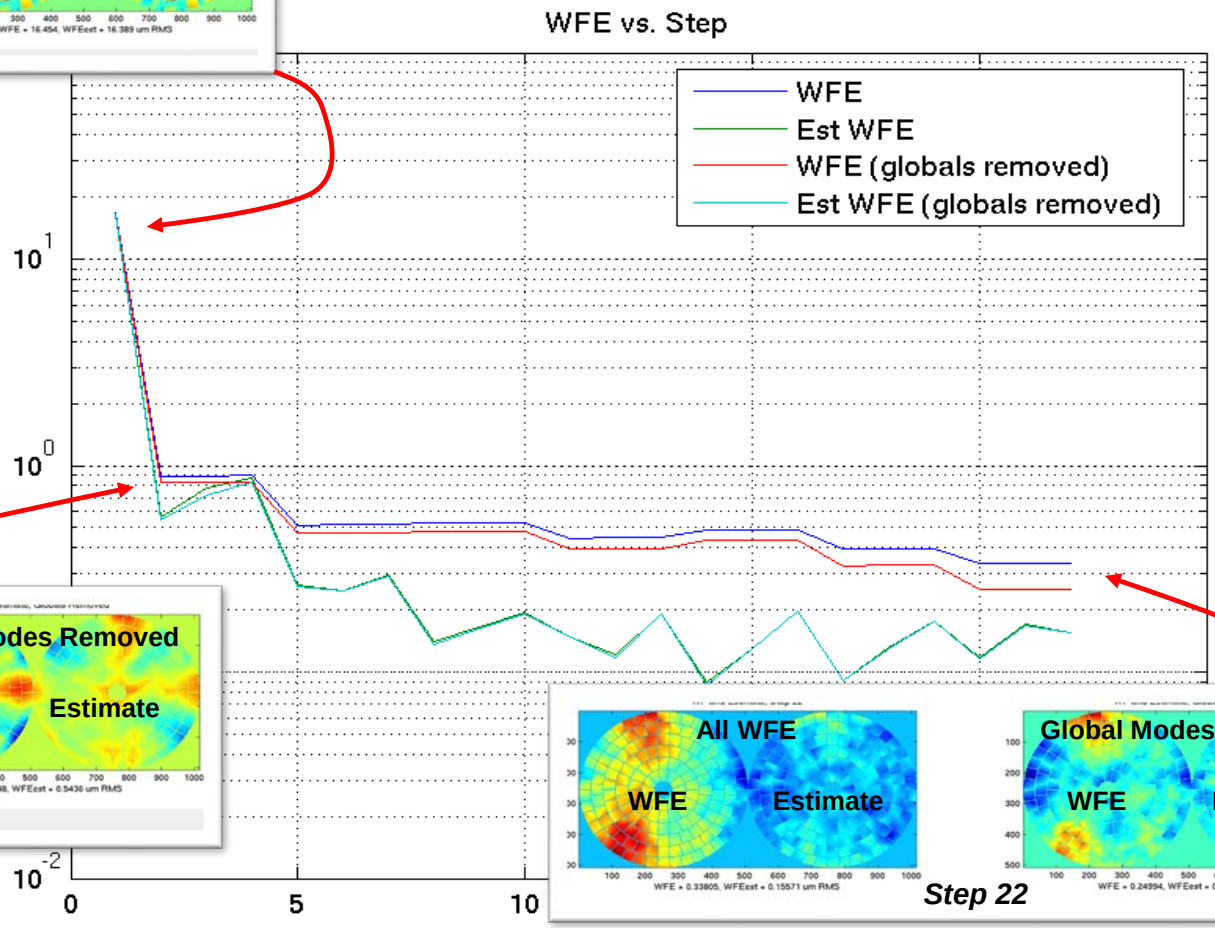

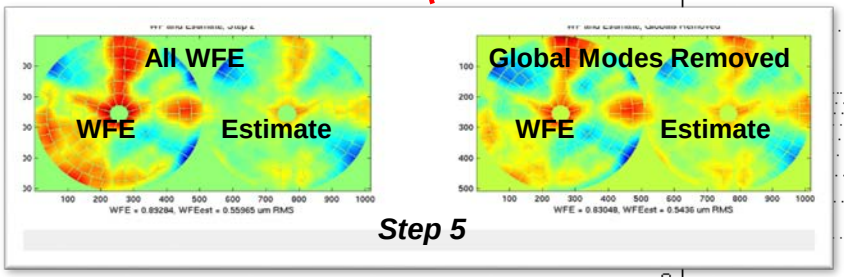

•WFE below 1 um after first step
•Estimates do not see global mode WFE

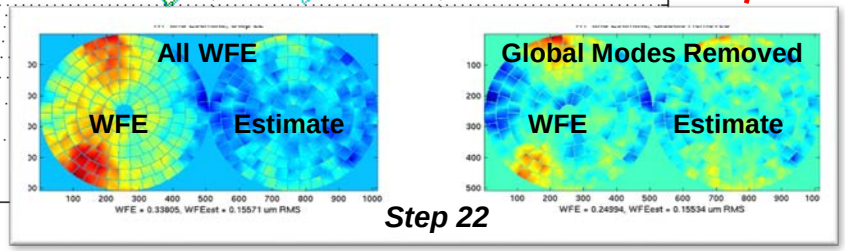

•WFE below 1/2 um, continuing to drop

Fixed-Gain Control

- ***Fixed-gain control with K_0:***

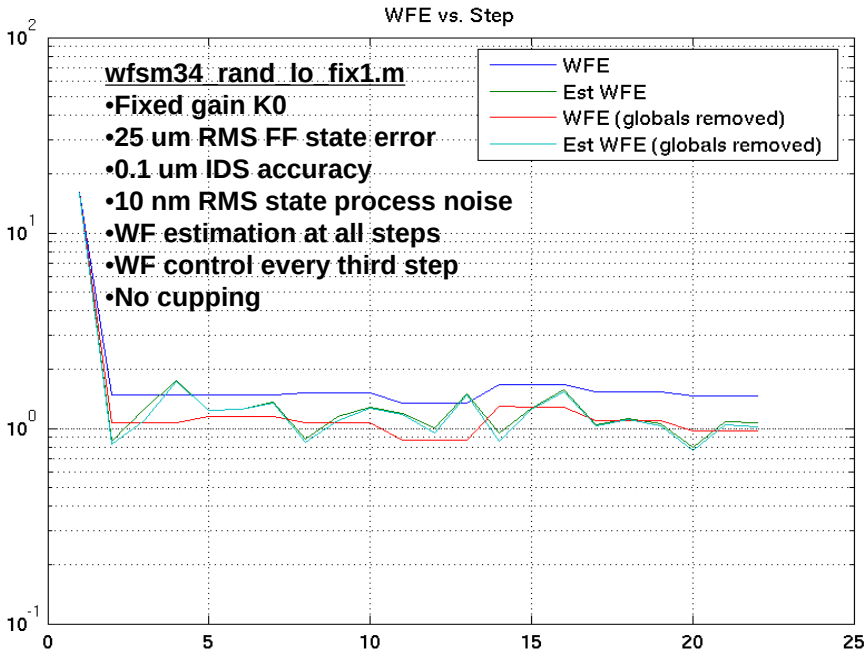

- ***Gain-scheduled control:***

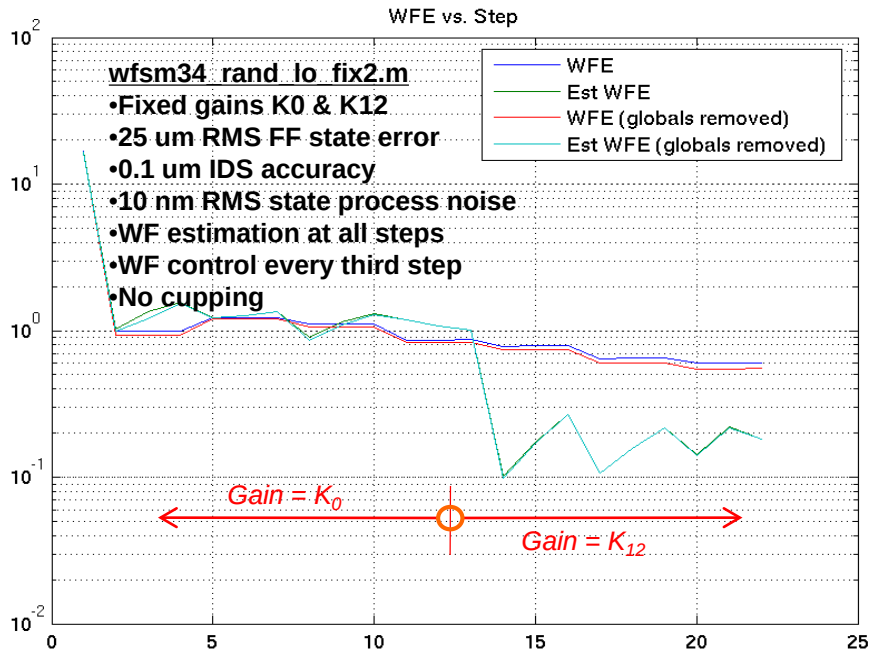

- Optimal OSE recomputes K_i every step
- Fixed-gain OSE is simpler
  - Performance can still be tailored to conditions by switching gain matrices
- CCAT performance analyses use conservative K_0 gains

Fixed-gain OSE does not recompute gains or covariances

$$\hat{x}_i = \left(I - K_0 \frac{\partial l}{\partial x}\right)\hat{x}_{i-1} + \left(I - K_0 \frac{\partial l}{\partial x}\right)\frac{\partial x}{\partial u}u_{i-1} + K_0 l_i$$

1G Disturbance Example

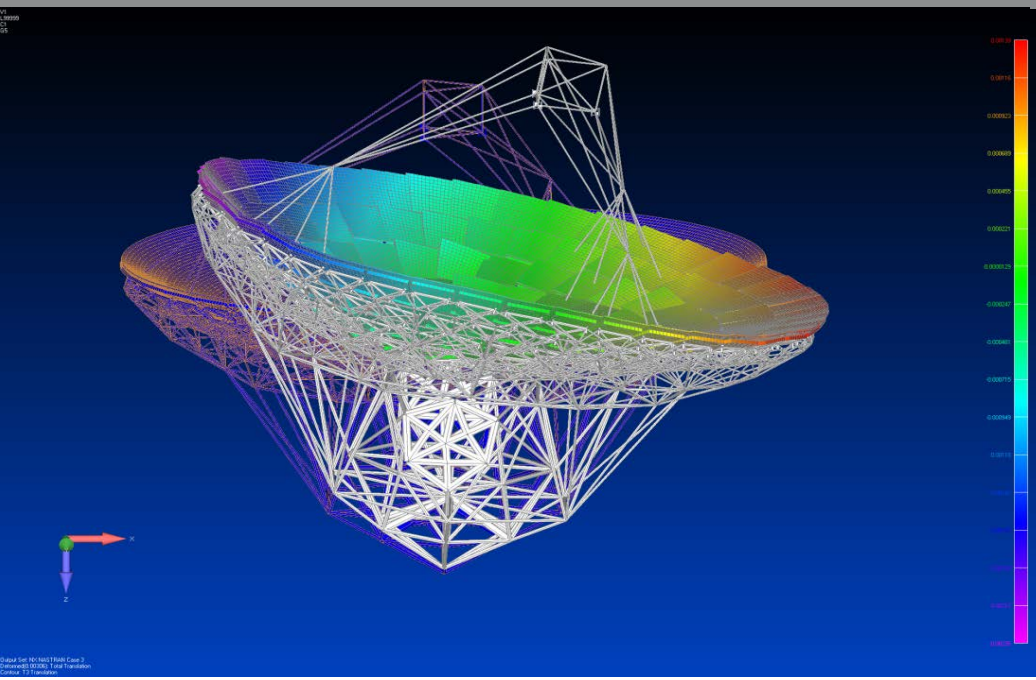

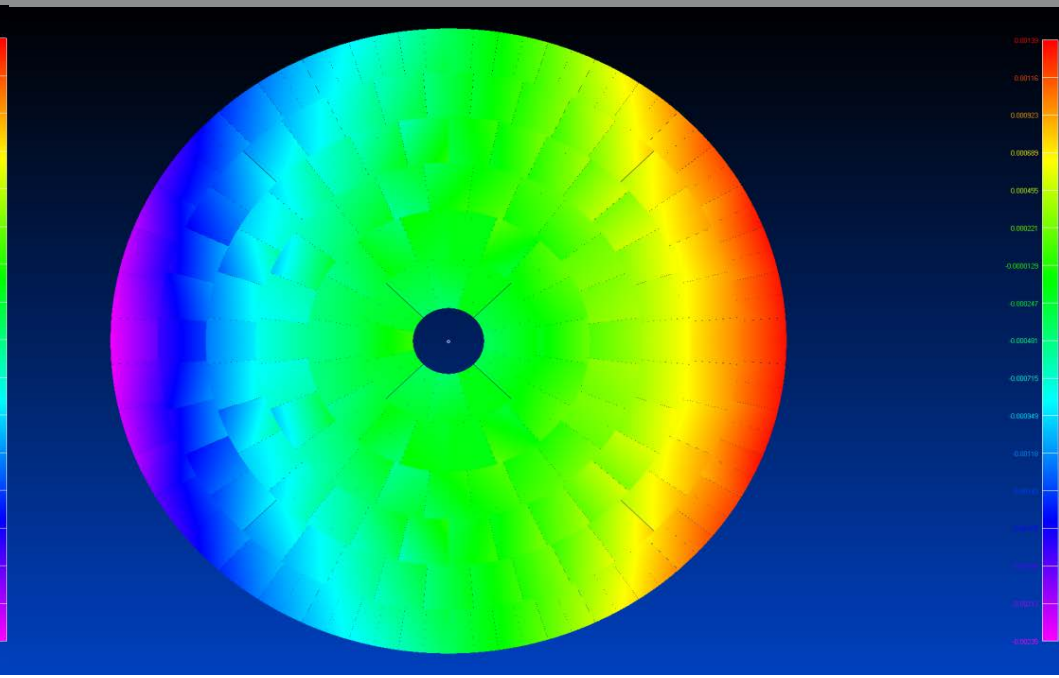

- Gravity sag deforms the PM and SM support structures as the telescope elevation axis changes
- This example shows the change incurred as the elevation axis moves from zenith to 45° pointing

WF Initialization Example

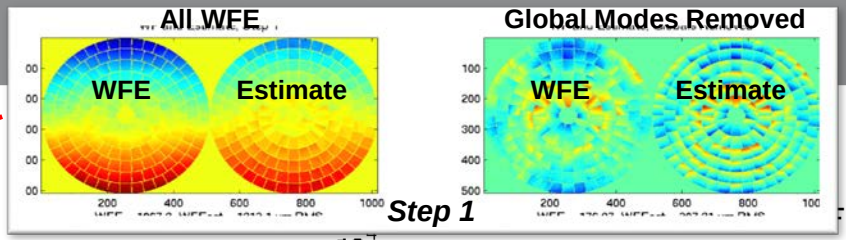

- Initial WFE due to gravity sag
- Initial WF estimate does not observe global WFE

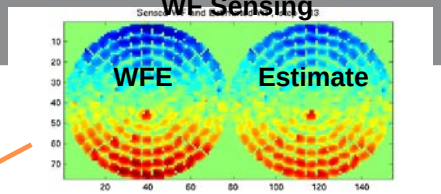

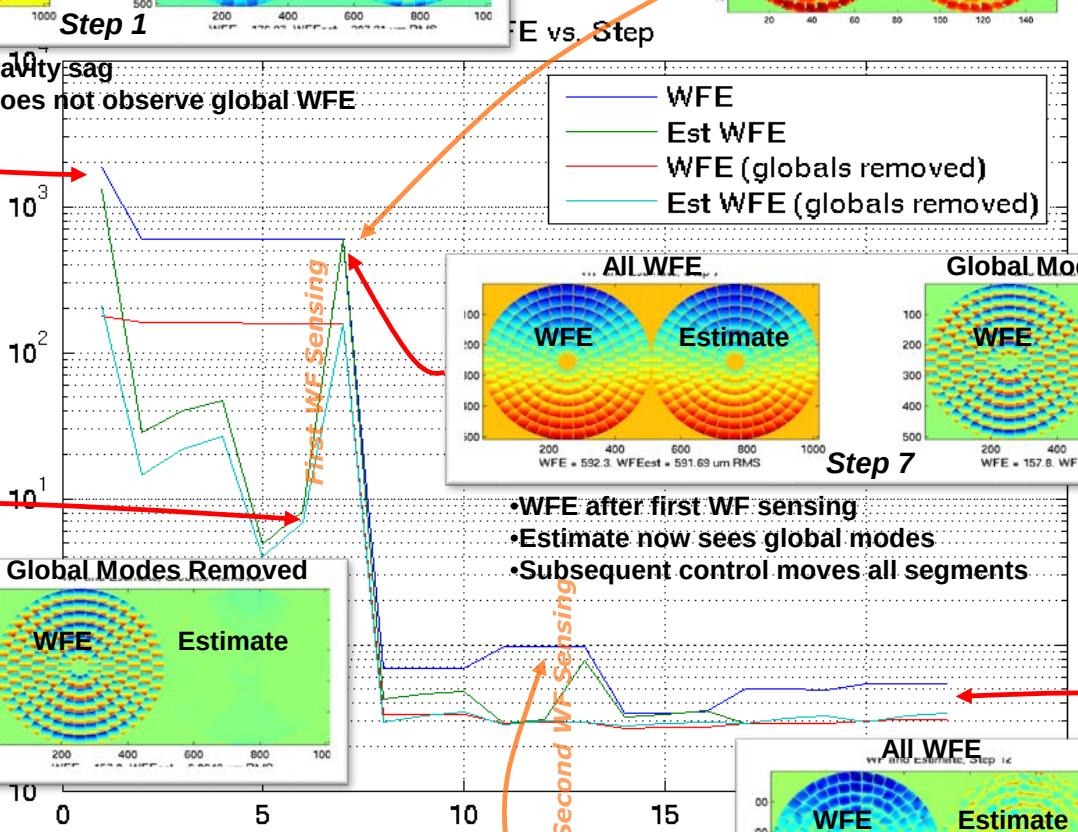

CCAT 1G Response

- Time-step control sim
- No feed-forward
- WFS at steps 7 and 13
- 80x80 WFS sampling
- 0.8 um WFS accuracy
- IDS at all steps
- 3 Fixed Points control
- 0.5 um IDS accuracy
- WFC every third step

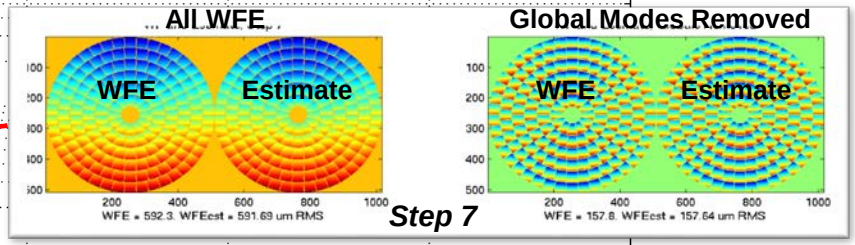

- WFE after first WF sensing
- Estimate now sees global modes
- Subsequent control moves all segments

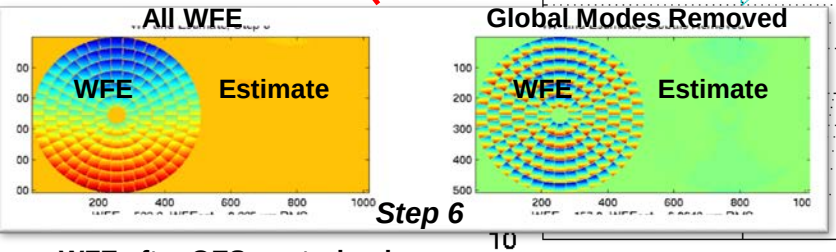

- WFE after OES control only
- Estimates do not see global mode WFE
- OES control only does not correct global mode WFE

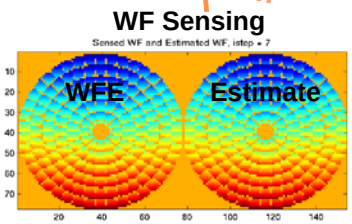

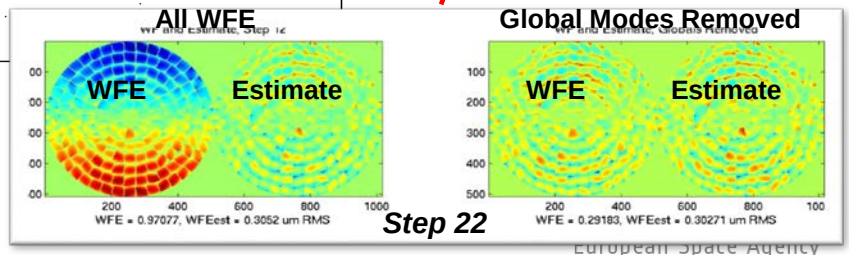

- Final WFE below 1 um, with long-term WFE growth driven by process, actuator and edge sensor noise

Performance Snapshot

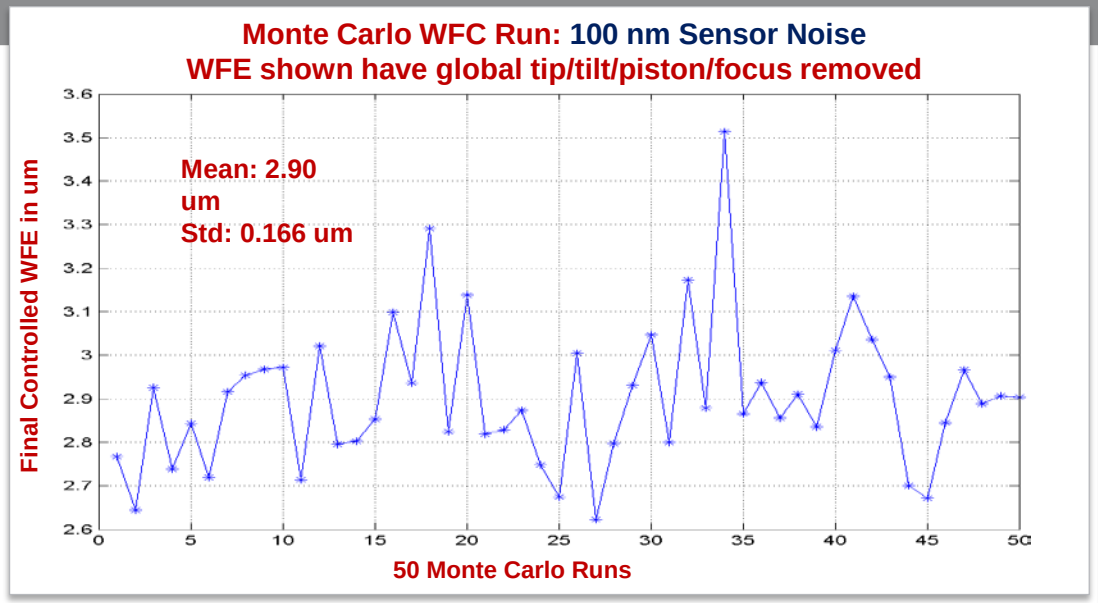

- Modeled performance better than CCAT WF Error Tree for the included component errors
  - 2.9 um vs. 5.3 um allocated
- This performance requires no heroic measures
  - Fixed-gain OSE
  - No estimation of thermal modes
  - No exotic components
  - No telescope collimation measurement

CCAT WFE Tree			
		Model only, with cupping	
System			System WFE (um RMS)
	Component	Component WFE (um RMS)	
1	Telescope Totals		5.32
	Secondary	0	
	Tertiary	0	
	Instrument	0	
	Mount	0	
	Design	0	
2	Primary		5.32
	Thermal Gradient	0.02	
	Actuator heating	0	
	Actuation error	0	
	Acceleration	0	
	Subframe	0.314	
	Truss	3.1	
	Tile	0	
3	Control		4.32
	Gravity	2.5	
	Thermal Gradient	1.38	
	Actuator heating	0	
	dCTE cupping	0	
	Sensor noise	0.7	
4	Estimation		3.16
	LUT error	3	
	Model error	0	
	Latency / Drift	1	

Global and Singular Modes

- ***Global modes: coordinated RB motions of the PM segments***

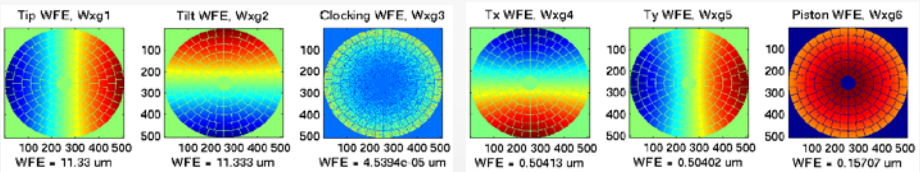

- *Global modes, TTP removed:*

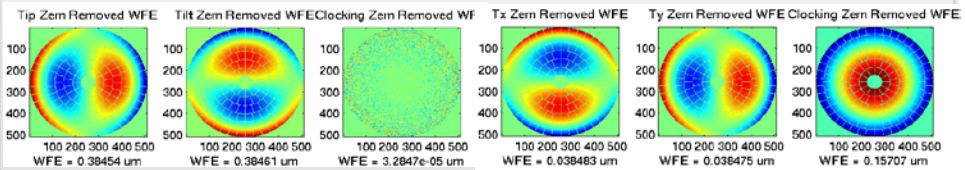

- ***Singular modes: linearly related to the global modes***

$$[U,S,V] = svd\left(\frac{\partial l}{\partial x}\right) \qquad w_{Gj} = \frac{\partial w}{\partial x} U_j$$

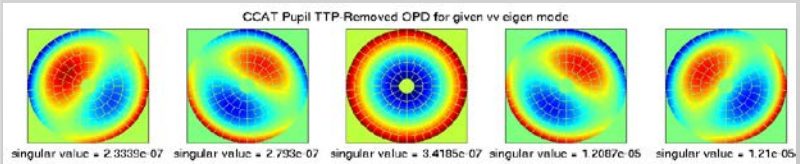

- ***The coma WFE in these modes occurs because PM RB motions decollimate the telescope***

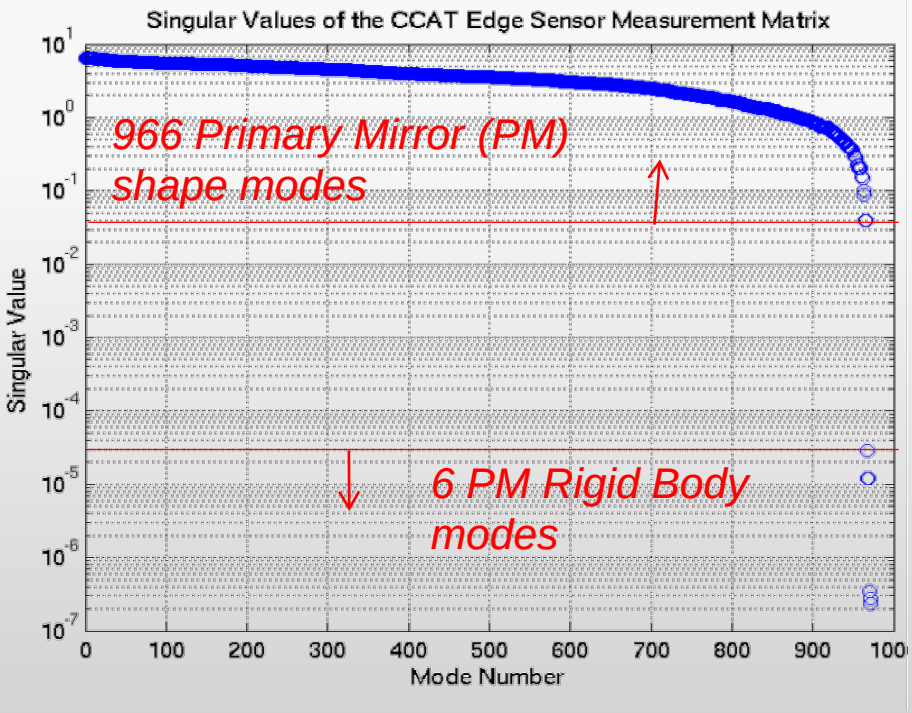

- The ratio of highest to lowest singular value is only 161 for the 966 PM shape modes, well within controller dynamic range
- Rigid body modes are not measurable – only relative segment motions are seen by the edge sensors

Bibliography – Wavefront Sensing and Control

35. Zhao, F., Rao, S., Ksendzov, A., “Swept-frequency laser ranging using a calibrated common-path heterodyne interferometer” Proc. ODIMAP V, Leganes, Spain (2-4 October 2006)
36. Zhao, F., “Development of high precision laser heterodyne metrology gauges,” Proc. SPIE, Vol. 5634, pp. 247-259, 2005.
37. D. Redding, P. Eisenhardt, G. Hickey, K. Stapelfeldt, W. Traub and M. Werner, “Active Optics for a 16-Meter Advanced Technology Large Aperture Space Telescope (ATLAST),” SPIE 7010 (2008).
38. D. Woody and D. Redding, “An Imaging Displacement Sensor with Nanometer Accuracy,” SPIE 8450 (2012). URS224395
39. D. Redding, J. Lou, A Kissil, K. Wallace, G. Serabyn, M. Bradford, S. Padin and D. Woody, “Model-Based Wavefront Control for CCAT,” SPIE (2011)
40. D. Redding, J. Lou, A Kissil, K. Wallace, G. Serabyn, M. Bradford, S. Padin and D. Woody, “CCAT Wavefront Control Interim Report,” CCAT TM-75, http://wiki.astro.cornell.edu/twiki/pub/CCAT/CCAT_Memos/WavefrontControl071411.pdf (2011). URS22560

Looking Ahead

NASA Path Ahead for Large Telescopes

- NASA has convened 4 Science and Technology Definition Teams, to prepare white papers for the 2020 Decadal Survey, which will determine which missions should be developed for the 2030s
- Three of these will likely benefit from active optics:
  - LUVOIR – a large UV/Optical/Near IR telescope for direct exoplanet imaging and spectrometry, and for a wide range of general astrophysics
    - Notionally 8-16 m aperture, segmented aperture, with a coronagraph
  - HABEX – the Habitable Exoplanet Imager, a Optical/Near IR large telescope for direct exoplanet imaging and spectrometry, that could do more limited general astrophysics
    - Notionally 4-8 m, aperture TBD, with a coronagraph
  - Far IR Surveyor – a cryogenic submillimeter-wave large telescope
    - Notionally a 4x6 m aperture telescope with 4K optics

LUVOIR, aka ATLAST, HDST, etc.

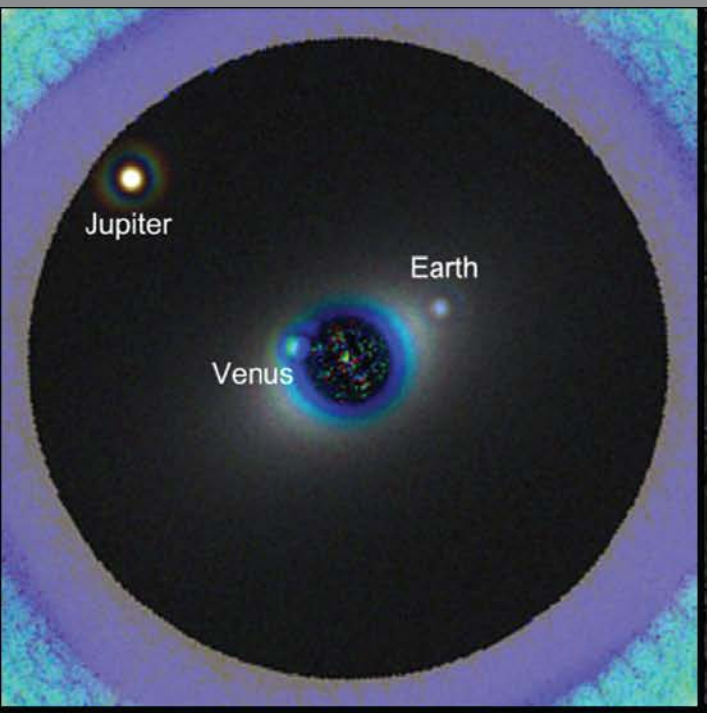

Binary anodized pupil coronagraph (L. Pueyo).

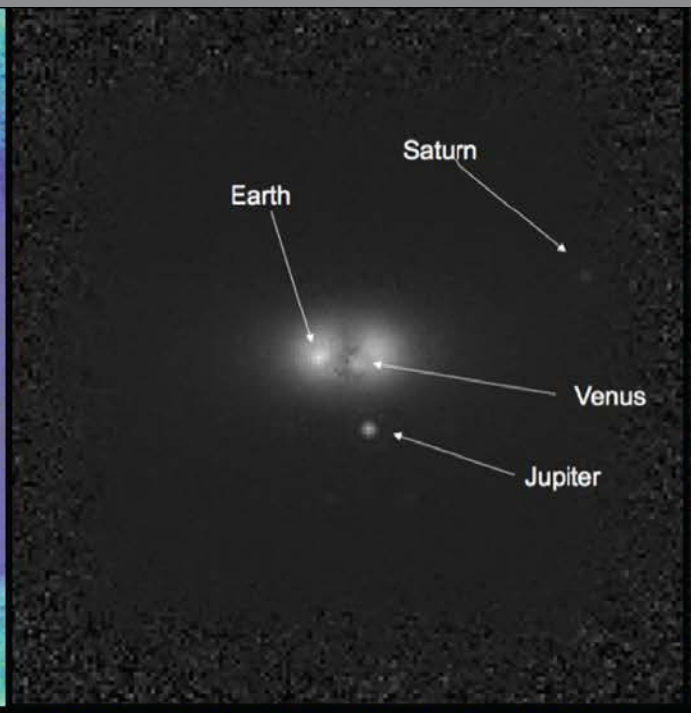

Phase-Induced Amplitude Apodization coronagraph with small IWA (Guyon).

Free-flying 100 m starshade (Kuchner).

- A 12-m class LUVOIR equipped with a coronagraph or starshade will provide direct imaging and spectrometry of hundreds of exoplanets, and dozens of exoEarth candidates
  - Imaging for discovery, spectroscopy for exoPlanet atmospheric chemistry, for the discovery of habitability, and of life

The NASA "ATLAST" Study

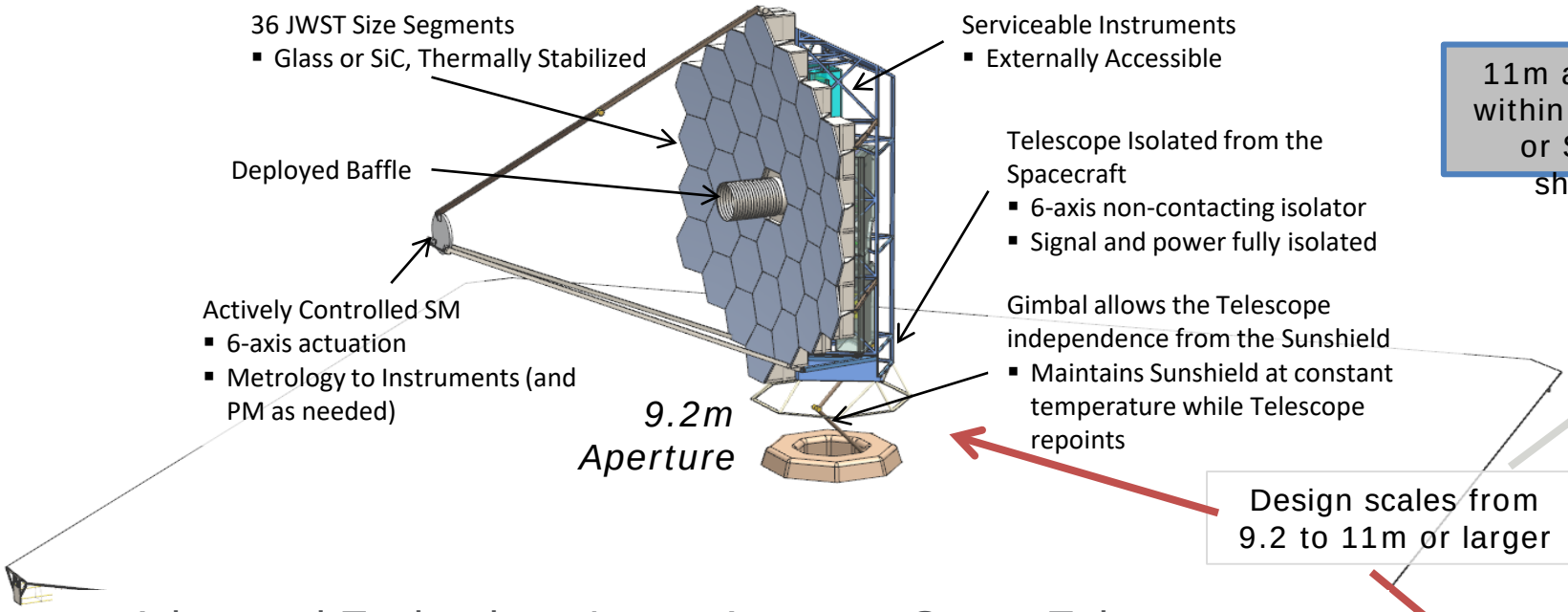

11m aperture within an EELV or SLS-1 shroud

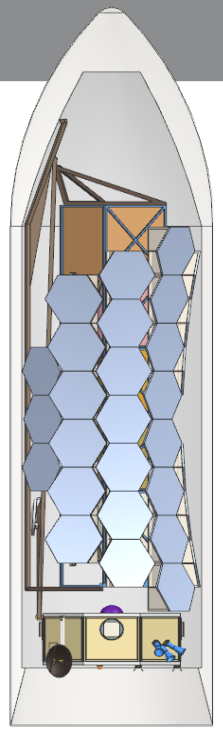

Design scales from 9.2 to 11m or larger

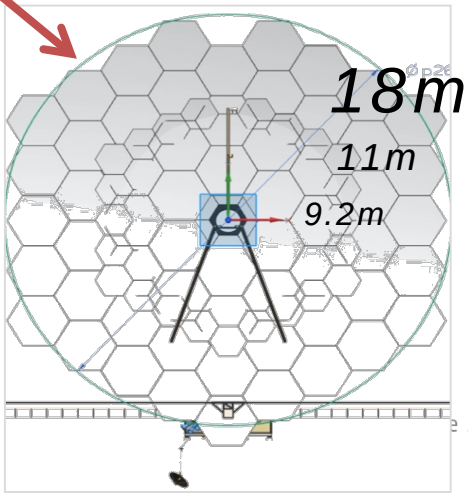

- Advanced Technology Large Aperture Space Telescope (ATLAST) is one approach to LUVOIR
  - An engineering reference design concept with JWST heritage: sunshield, deployment, passive thermal control, wavefront control, lessons learned
  - Other NASA heritage: starlight suppression, metrology
  - Non-NASA heritage: light-weight non-cryogenic optics, non-contacting isolation, detectors and electronics
  - Launch vehicle: EELV-class or SLS Block 1 to ~12 m aperture; SLS Block 2 for larger apertures

UV, Optical and Near IR Astrophysics

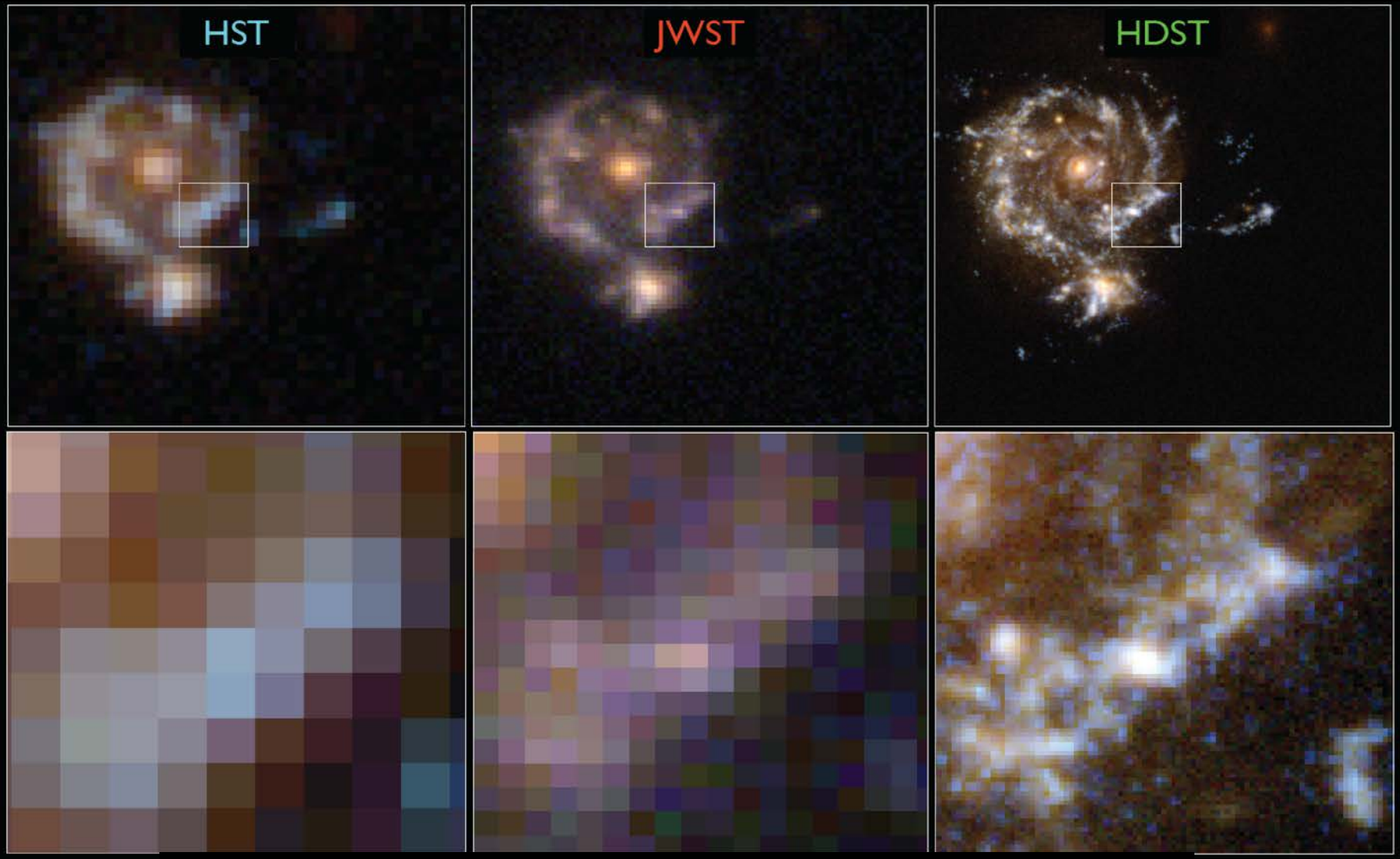

z = 2 Galaxy: Look-back time = 76% age of universe

Images simulated by Greg Snyder (STScI)

HDST will:

- *Resolve stellar populations in neighboring galaxies*
- *Detect the Main Sequence Turn-Off in galaxies up to 10 MPc away, to enable us to trace the Star Formation History in all major types of galaxies*
- *Resolve background QSOs for UV spectroscopic probes of gas around stars in neighboring galaxies, and of the IGM around more distant galaxies*
- *Probe the formation of galaxies and stars down to 100 parsec scales to the very edge of the observable Universe*

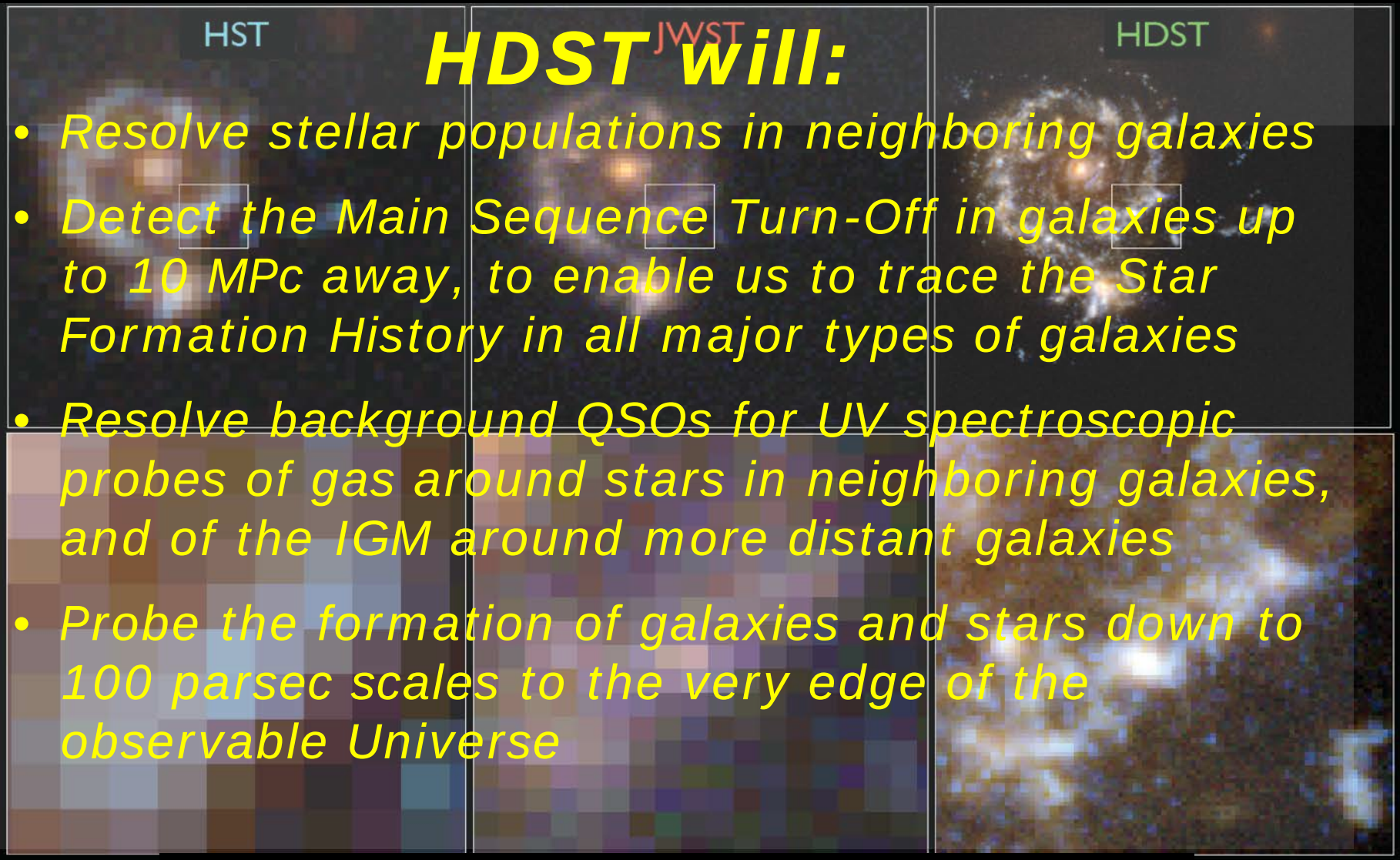

z = 2 Galaxy: Look-back time = 76% age of universe

Images simulated by Greg Snyder (STScI)

Conclusion

- We have presented particular solutions to the problems of active optics for large space telescopes
  - Wavefront sensing using science cameras and star images
  - Metrology and optical edge sensors
  - Movable and deformable mirrors, small and large
  - Monolithic and segmented active telescope architectures
- More particularly, we have described a mathematical and computational approach to active optical systems, one that is adaptable to a much wider range of devices and architectures than discussed here
  - Linearized ray-trace models
  - Control and estimation
  - Simulation
- These tools will help us meet the opportunities and challenges of the next generation of large space telescopes

Bibliography – NASA Path Ahead

44. NASA Astrophysics Division Roadmaphttp://science.nasa.gov/science-committee/subcommittees/nac-astrophysicssubcommittee/astrophysics-roadmap/, (2014).
45. Advanced Technology Large Aperture Space Telescope, Space Telescope Science Institute, http://www.stsci.edu/atlast (2015).
46. J. Dalcanton, S. Seager, S. Aigrain, S. Battel, D. Brandt, C. Conroy, L. Feinberg, S. Gezari, O. Guyon, W. Harris, C. Hirata, J. Mather, M. Postman, D. Redding, D. Schiminovich, H.P. Stahl, From Cosmic Birth to Living Earths, www.hdstvision.org, AURA (2015).

THANK YOU

David Redding
David.C.Redding@jpl.nasa.gov